2009

An investigation of active structural acoustic control in resonant enclosures

Christopher E. Whitmer
Iowa State University

An investigation of active structural acoustic control in resonant enclosures

by

Christopher Eldon Whitmer

A dissertation submitted to the graduate faculty

in partial fulfillment of the requirements for the degree of

DOCTOR OF PHILOSOPHY

Major: Mechanical Engineering

Program of Study Committee:
Atul G. Kelkar, Major Professor
James E. Bernard
J. Adin Mann III.
Partha P. Sarkar
Jerald M. Vogel

Iowa State University

Ames, Iowa

2009

TABLE OF CONTENTS

List of Tables

List of Figures

Acknowledgements

I would like to thank Dr. Atul G. Kelkar and the other members of my graduate committee for their guidance throughout this project. Dr. Mann was especially helpful as a sounding board for many aspects early in this project. There have a been a number of undergraduate students over the course of this project who have helped with the testing and construction of various laboratory setups. Specifically, I would like to thank Chris Ford, Frederick Thompson, and Tom Waite for their help and assistance. Thank you to my parents for their constant support and belief in the value of education. I want to thank my brother Jon for his help. Special thanks to my loving and supportive wife Karri who always knew the right thing to say or do. Thank you, all of you. I certainly could not have done any of this without you.

1 Introduction

Structureborne acoustic noise has been, and will continue to be, an active area for research and development in a number of fields. Excessive noise can affect the working and living of people, harming their hearing ability, decreasing the efficiency of their work, and it can even cause serious injury. With the development of modern industry, transportation and defense applications, noise and vibration control has attracted more and more attention. Noise mitigation techniques have numerous applications from reducing hearing loss and improving occupational safety to making quieter consumer devices that provide enhanced comfort and a competitive edge to the manufacturer. The approaches to mitigating structural noise can be classified as either passive noise control (PNC) or active noise control (ANC). Passive noise control (as its name implies) doesn't require the use of actuators or sensors to function. There are numerous approaches that can be considered passive including but not limited to: adding acoustically absorptive materials, using structural damping materials, adding mass and stiffness to a radiating structure, redesigning the structure to decrease its radiating capability, and using passive resonators to attenuate or block certain frequency bands. Typically passive noise control methods in structureborne noise problems are limited in their ability to attenuate in frequencies below 1000Hz. Absorbent acoustic materials require a significant quantity of material to be effective below this frequency, and the bulkiness of this solution sometimes doesn't permit its use. Other approaches like adding structural damping and redesigning the structure can be effective at decreasing structureborne noise below

1000Hz, but their successful application requires considerable knowledge and skill, and even then they don't usually yield broadband reductions.

Similarly there are several approaches to ANC. ANC uses actuators, sensors, and a control system to actively attenuate or cancel the effects of acoustic noise. For structure-borne noise there are a number of different ways to implement ANC including: using speakers or other additional acoustic sources along with sensor data to cancel or attenuate existing noise conditions, or targeting the structure with devices that are able to actively damp or cancel structural vibrations. Additionally there are two main paradigms for ANC; feedforward and feedback control. Both of these paradigms have some advantages and disadvantages. The majority of early works used the feedforward approach because instability issues due to feedback were hard to tackle. However, in light of significant advances made in the feedback control theory and robust feedback control in particular, the feedback methodology for ANC is again gaining popularity. Successful implementations of feedforward methods typically require the availability of reference signals with strong correlations to the noise sources and efficient adaptive schemes to tune the model. In addition, feedforward architecture has an inherent lack of robustness in the presence of uncertainties. On the other hand feedback methods can potentially destabilize the system as they alter the dynamics of the system. However, the problem of destabilization due to feedback can now be systematically addressed using robust control methods developed over the last two decades. An additional problem is that the dynamics of acoustic systems tend to be modally rich and do not roll-off at high frequencies, which poses difficult challenges for controller design. An ideal controller is the one that can achieve uniform noise reductions in space as well as in frequency. Existing ANC technology is not advanced enough to yield such a controller, but has considerable potential for doing so. ANC also has its limitations; for example, active noise control typically does not work well at higher frequencies above 1500Hz. There are several reasons for this including modeling uncertainties, the high order nature of these models, and the expense of using equipment that can sample, compute, and control high frequency noise.

Of these two methods PNC and ANC, PNC is far more common mostly due to its low cost and ease of application. However some applications like small acoustic enclosures can benefit by the size and performance improvements afforded by using an active approach. Ideally ANC control would be made as easy and effective in its application as passive noise control, but currently few approaches would be characterized as such. Additionally, to make enclosure structures quieter over the entire range of human hearing (0-20kHz) would require the use of both passive and active noise control. When using both of these methods together it would seem that both passive and active noise control approaches could be designed to explicitly complement each other. There have been some works that have begun to explore this that will be discussed in the following section. Most active structural acoustic control (ASAC) attempts to target and reduce the vibrations that are induced in a structure using additional input from actuators. While effective, these methods are rarely broadband, and rarely lead to spatially uniform reductions of acoustic noise. One interesting approach that might accomplish this is to target the fundamental parameters of a structure with active control rather than to reduce the existing vibrations. Such an approach is more of a semiactive control approach such as those that are often employed in semiactive suspensions.

The goal of both of these approaches (synergistic active and passive design, and active control of structural parameters) is to achieve spatially uniform reductions in enclosure acoustic noise. The questions then become: 1) is it possible to design the structure/passive treatments and active control scheme in such a way that they may complement each other, and even enhance the other?, and 2) is it possible to use novel active control approaches that target the mechanism of sound transmission rather than just the vibrational energy? The first question is a problem that is just beginning to be studied, and the second question is a logical extension of the first question where instead of a passive design the active control is itself attempting a "redesign". Both of these questions will remain topics for future effort in these types of structural acoustic problems. However there are several steps taken in this effort which lay the groundwork for future study problems.

1.0.1 The Problem and Approach

If the goal of spatially uniform noise reduction in acoustic enclosures is to be achieved through combined PNC and ANC design. It is then important to develop a passive redesign framework that will allow a structural response to be tailored for reducing and concentrating energy both in frequency and spatially. With such a methodology it becomes extremely important to develop MIMO (Multi-input Multi-output) control strategies that are stable, performing, and physically implementable.

1.0.1.1 The Problem Statement:

The problem statement of this dissertation is twofold: 1) Is it possible to develop a methodology for passive redesign of the plate structure that decreases acoustic-structure coupling and the sound level in the enclosure system? 2) Is it possible to develop and *implement* MIMO controllers that ensure some robustness but still have the necessary performance for meaningful reductions of SPL in the destination enclosure?

If these two problems can be tackled separately and a methodology developed, it will lay the groundwork for a combined multi-objective control/passive design optimization approach to the enclosure noise problem being studied (an all in one active-passive approach).

1.0.1.2 The Approach

This dissertation divides the problem into the following six steps:

1. Develop an analytical model of the enclosure-plate system and investigate the mechanisms of system coupling (to aid in both active and passive design efforts).

2. Develop a methodology for passive redesign and test it by experimentation.

3. Simulate different controller locations and strategies for MIMO control on the plate enclosure model.

4. Build hardware and setups for MIMO control.

5. Identify the system, develop strategies, and design controllers to achieve sound reduction.

6. Implement the designed controllers in physical hardware.

Each of these steps will now be discussed, and a brief description of the relevant tasks required to achieve each will be presented. The first step involves the construction of a combined computational and analytical model based on the modal interaction model [22]. Using BEM (boundary element) and FEM (finite element) methods the modal parameters of the system are solved, coupled, and then combined with sensor and actuator dynamics. Using this model the system is studied to determine what plate modes are of greatest importance to the acoustic response (essentially what plate modes couple with each acoustic mode).

The second step involves the development of a coupled finite element simulation with the above described model to interactively modify the eigenvector (modeshape) of a plate for decreased coupling by mass redistribution and stiffness redistribution. This is then experimentally validated both invacu and in the enclosure.

In the third step MIMO control approaches will be simulated with an emphasis on those methods which will be implementable on actual hardware. There are many existing approaches to robust control of acoustic structure systems. However, when it comes to implementation, the complexity of many of these advanced approaches becomes a liability. The real system is full of uncertainties, full of nonlinearities, full of input-output channels, and most importantly, full of dynamics. Most of these elegant methods produce very high order controllers that work marvelously in simulation and then either don't perform or are too large to permit implementation in hardware. This third step will attempt to address whether there are strategies for MIMO control that still impart robustness, allow performance, and are still implementable in hardware.

The fourth step involves creating the necessary hardware to study the highly MIMO control problem and ensure success. This means the judicious selection or design of actuators, sensors, and amplifiers/filters to yield systems that behave well from a control modeling and design perspective (and are better suited to feedback control).

The fifth step of this work involves the experimental identification, modeling, and controller design and simulation. This is a crucial step (especially in MIMO that are this modal dense): if inaccurate models are used for control design the results are disastrous. By far this comprises the greatest amount of time, skill, and effort in the control implementation process.

Finally the last step of this effort is to implement in hardware these control designs, refine them if necessary, and analyze the results.

In addition to studying this problem, several related efforts undertaken in the course of this study are presented. First of these is a possible approach for actively/directly affecting structural stiffness. Second is the application of the control methodologies investigated to a small 1-D tube apparatus (for the purpose of field testing/trouble shooting algorithms) before implementation in the more complicated MIMO system. Lastly several different plate concepts utilizing PVdF, and PZT as actuators were developed, identified and tested; however, it was found that these actuators either lacked the authority (PVdF) to affect the plate in a sizable way, or were not able to be formulated into a collocated arrangement and were thus less desirable than the eventual point force, point sensor arrangement.

1.0.2 Literature Review

This section will attempt to summarize some of the literature that relates to the research work in this dissertation. The works discussed are representative of the current state of the art in noise control, and illustrate the areas where contributions may be made.

1.0.2.1 Passive Design

There are numerous examples of research dealing with how to design acoustic properties into a material. Many of these approaches, like the use of absorptive layers and double panel construction, have become standard tools of the acoustic engineer and may be found in several intermediate, and introductory books on acoustics [83],[93],[59]. However, there have also been numerous approaches toward modifying or designing structures that exhibit desired radiation, transmission loss, or absorption. One example is the work conducted in a dissertation by Dan Kruger [62] in which BEM techniques and optimization methods were utilized to select the best locations for constrained layer damping and to minimize the amount of material used. In this work efforts were made to minimize the sound power radiated from a cube structure. His approach combined computational and experimental work, and it utilized structural intensity, and velocity constraints to optimize locations. These efforts were successful in producing measurable decreases in radiated sound power. Another important work by St. Pierre and Koopmann [107], attempted to modify the structure of flat plates to minimize radiation. This was done by the optimal placement of discrete masses at locations on the plate, and the optimization was conducted using BEM and FEM codes and sensitivity analysis. These efforts built upon earlier publications from Koopmann that outlined a general strategy for sound power minimization [2],[87]. This concept and work provided some guidance for the direction of this dissertation. Another work by Constans, Koopmann, and Belegundu [14] suggested the idea of modal tailoring of passive structures to minimize the radiated sound power of shells. Although the approach is somewhat different than the work of this thesis, the idea of using modal tailoring to passively achieve lower radiation was an effective one, and these efforts helped in the formulation of this concept. A final example dealing with passive design by structural modification is the work by Luo and Gea [76]. In this publication the sound level in a cube enclosure was lessened in simulation by placing optimal stiffeners for different loading conditions. Using the microstructure-based design domain method, ideal stiffener patches were place on the structure of the cube to deal with differing cases of tonal and wide band excitation.

The work in this dissertation attempts passive redesign by several modal tailoring methods. The approach taken in this dissertation is a sensitivity based optimization method much like that in [76]. Another approach attempted, which was unable to be implemented in practice, was an inverse eigenvalue approach for the directed redesign of stiffness and mass matrices based on desired mode shapes and modal frequencies. There are several references that describe the theory and methods for inverse eigenvalue problems [11], [89]. There has also been some work applying inverse eigenvalue problems to structural designs like in [64]. In Lai and Ananthasuresh a cantilevered beam was designed to have a desired first mode shape for microscope probe tip applications. This application benefits from analytic solutions, and fairly simple constitutive relationships. For the problem of this dissertation the inverse problem could be formulated but not solved. Additionally the literature and existing approaches typically only design for one mode and this work requires the design of multiple modes.

1.0.2.2 Modeling

There are two basic approaches to modeling acoustic enclosures that are broadly classified as either modal, or statistical. The decision as to whether to use a modal approach or a statistical approach depends on how densely packed the eigenmodes are in the desired frequency range. Essentially, when modeling the room or enclosure the size of the room will determine the Schroeder cut off frequency or the boundary line below which one can use a modal approach, and above which one needs to use a statistical approach. In smaller enclosures this frequency is much higher than in large rooms, hence the difference between modeling approaches between room and enclosure acoustics. The efforts of this dissertation focus on an enclosure with a Schroeder cut off that permits a modal approach. The desired frequency range of interest is from 0-800 Hz.

The modeling of this size of acoustic enclosure is specifically discussed in several publications. Two essential references for modeling acoustic noise are books by Frank Fahy [22] and Nelson and Elliott [88]. These books cover the approach for modeling both the enclosure acoustics and the plate by modal expansion. Additionally, Fahy discusses methods for developing coupled structural acoustic models, and was the source of an idea explored in this dissertation dealing with the design and control of this coupling. Other works that discuss enclosure modeling include [66],[90],[73] and deal primarily with small rectangular enclosures with simple boundary conditions and low cross-modal coupling. All of these methods essentially utilized the assumption of a rigid boundary condition for the acoustic enclosure and most assumed simply supported, or clamped-clamped plates. There are numerous works including those by Henry and Clark [40], and Fischer and Hayek [24] that discuss the approach for modeling the acoustic structure coupling in a variety of geometries and boundary conditions. All of these methods approached acoustic structure coupling from a standpoint of two independent systems that are gyrostatically coupled. There are also numerous references that discuss the modeling of other configurations besides enclosures and would prove useful for studying the behavior of radiating structures in larger rooms [79],[80].

A difference in the modeling efforts of this work and those mentioned above is that the efforts of this dissertation can model other acoustic boundary conditions, and arbitrary configurations of chamber and plate. The current efforts have the potential to solve for the coupled plate enclosure modes directly. To do this will require the use of coupled FEM and BEM methods for computationally modeling and designing the structure. There are numerous research works and commercial packages that are capable of this type of modeling, however. To allow for easier optimization, and design integration it was decided to use a combination of commercial and self written codes. There sources are a representative sample of the existing body of work. The boundary element method is a commonly employed method in acoustics and aerodynamics that is essentially an application of Green's Theorems to represent 3-D domain problems in terms of boundary integrals; in this case the Helmholz Integral Equation (HIE). In BEM these integrals are discretized and evaluated as the summation of boundary source solutions. With knowledge of boundary conditions these source strengths may be found as the solution of a linear system and used to reconstruct solutions in the 3-D domain. The advantage of these methods is that they are computationally less intensive than finite elements and can therefore be employed with greater accuracy. There are several references that describe the theory and methods for programming acoustic boundary element software to solve both interior and exterior problems. Two of these general references are books by Wu [111], and Brebbia [6]. Additionally the structural modeling is accomplished by finite element method (FEM). This is done through a variety of approaches, when considering a decoupled approach the FEM solution may be solved easily by commercial software like FEMLAB^{TM} or ANSYS^{TM}. In this work, it was more efficent to program a simple FEM solver for one type of plate element to optimize the structure and coupling with BEM. References by Moaveni [81] and Kwon [63] are representative of works that assist with this analysis and programming. These computational tools have been utilized in several relevant works. In papers by Cunefare and Koopmann [60], [61] BEM was utilized for the modeling, analysis, and design of both passive radiators and active noise control systems. In [17],[19] Dong and Edoa discuss coupled FEM-BEM modeling approaches for optimizing structural acoustics and designing better acoustic piezoelectric devices. The numerical methods employed in these works are nearly the same as the one developed in this thesis, and along with Brebbia [6] guided the development of the coupled FEM-BEM codes.

1.0.2.3 Active Structural Acoustic Control

Active structural acoustic control (ASAC) has recently been an active research area with many successful designs and important contributions being made. ASAC is a method for reducing the sound in coupled structural acoustic systems by actively controlling the structure with piezoelectric, magnetic, or servoelectric actuation. In two papers by Kessissoglou [56],[57] a ribbed plate was modeled and controlled using point force and moments. The radiation effects of the discontinuities from the rib structure were countered using active controllers and these controllers were optimized using the structural coincidence functions. In works by Gardonio [25] and by Kaiser [49] active structural acoustic control was applied to double panel configurations. In Kaiser systems are modeled by coupled modal expansions and are assembled into a state space model. These models were then validated by a laser vibrometer, and both feedback and feedforward controllers were designed to reduce sound being transmitted through the double pane window structure. In a paper by Tanaka [108] an approach called cluster control was utilized. In this approach it is desired to reduce the effects of spillover that can lead to destabilization of the control system. This was accomplished by refining a low authority method like direct velocity feedback to targeting clusters of resonant modes with similar properties. This interesting approach provides some of the inspiration and motivation for the passive and active redesign of modeshapes that was approached in this dissertation. There have been numerous works that explore the possibilities of using distributed actuators like single sheets of PVdF or PZT to control the transmission of acoustic energy through a structure [39], [16], [26], [27]. Additionally works by Elliott have explored the theory of using and controlling distributed sources [20]. There have also been many novel actuation approaches for ASAC that utilized smart materials. In Johnson and Fuller [44] an actuator was proposed that used a membrane and leg structure to amplify the acoustic emissions of PZT actuators. Another novel actuator proposed by Quanlu [97] utilizes both piezoelectric and electro-rheological materials.

Many works have sought to employ decentralized control with sensor and actuator arrays for use in the suppression of noise and vibration. A paper by Elliott, et. al. [21] investigated the effects of arrays of actuator and sensor connected only by local feedback loops. Large arrays, force actuators and velocity sensors were simulated, and a decentralized controller was shown to be unconditionally stable and to have significant reductions in both the kinetic energy and radiated sound power. This paper went on to propose that arrays of independent modular systems consisting of local feedback loops could be a simple and robust approach to broadband sound transmission. These efforts were then extended in three papers by Elliot, Bianchi, and Gardonio. This effort involved theoretical and experimental work for designing and testing a smart panel with decentralized units. The sensors and actuators were interconnected with velocity feedback controllers which created a kind of active damping. The simulations have showed that broadband reductions of the averaged kinetic energy or total sound power radiation can be achieved. In this work the decentralized units consisted of a collocated PZT patch and accelerometer with a single channel velocity feedback controller. Additionally a phase lag compensator was designed for each unit and the stability assessed. Testing demonstrating reductions of sound radiation were measured in all the third octave bands in the frequency range 0 to 5 kHz for shaker excitation, and with several bands showing

5 to 8 dB of reduction. The averaged vibration field was also shown to be highly damped (10 dB for all resonant modes) in the frequency range from 0 to 1 kHz. These exciting results show that novel approaches can be used to get around traditional ANC problems, and also illustrate the need for refinement of this decentralized approach to take advantage of passivity concepts. Other works [3],[113],[67] espouse similar approaches and benefits. These approaches and excellent results, however, are contingent on: 1) collocation of sensor actuator pairs, 2) no other dynamics in the system to produce non-minimum phase behavior(i.e. sensor and actuator are the same "type", or there are no dynamics from signal filters driver amps ect.). The types of collocated sensors and actuators used were found to lack the authority to control the noise levels experienced in the enclosure of this dissertation. Thus this dissertation focuses on a system that while collocated did not have perfect minimum phase behavior in each collocated channel (but did have enough authority to deal with the high noise level).

1.0.2.4 Enclosure Active Noise Control

The specific configuration investigated in this research work was ANC of resonant acoustic enclosures. The potential for application of ANC to such products as automobiles, washing machines, industrial machinery, and small rooms has made this particular topic a popular and active area of research [66]-[34]. In Lau and Tang [66], transmission control was explored using different measures for determining the basis of the control algorithms. Like the work of this dissertation, a rectangular enclosure with one flexible wall was considered. The impedance-mobility relations were developed for the control of sound transmission, and controllers were designed and compared using three different algorithms (based on potential energy, energy density, and squared pressure). Although not new, this work is very good at explaining the development of control optimization approaches. In Samejima [100] state feedback was utilized to redistribute the lower natural frequencies of a sound field. Using FEM a state-space model was derived and a model based controller was developed that located the closed loop poles at a desired frequency. This simulation was verified experimentally. There are several reasons that such a controller may be useful. One is to move the resonant modes to a region that is less effective at radiating or doesn't couple as well to the structure. Another purpose might be to move the modes to a region where PNC approaches can specifically deal with them. Often it is only possible or desired to control narrow band or tonal acoustic disturbances. Work by Sampath and Balachadran [101], used piezoactuators on an actively controlled structure to control several tones by a feedforward cancelation. Parkins used a feedforward approach to target both narrowband, and broadband noise. Like the work by [66] an energy density control method was utilized effectively. By contrast, Griffin [34] utilized a feedback approach with a state-space model of the radiation modes to minimize the amount of external noise that was radiated into an enclosed space. This was accomplished using only vibration sensors, and structural actuators, and did not require the use of control feedback microphones. Finally, there have been several important robust feedback control approaches by Kelkar et. al. [73],[51],[94] that have been successfully applied to 1-d, 2-d, and 3-d resonant enclosures. These works detail the modeling, control design, and stability analysis of ANC systems for several geometric configurations. But the limitations of most ASAC, and enclosure ANC methods motivates an investigation into so-called dissipative controllers. The controllers have been shown to have excellent performance and stability characteristics especially when paired with resonant mode controllers.

Passivity-based ANC methods (a special case of dissipative controllers) work on the principle of *energy dissipation* and hence are well suited for acoustic and vibration applications. Such controllers do not destabilize the system by exciting high frequency dynamics while controlling low frequency disturbances (which most other controllers tend to do as a result of what is called the 'waterbed effect'). Given a Lyapunov (energy) function $V(x)$ for a system (where x is the state of the system), then passivity-based controllers yield the control input $u(t)$ such that the $\dot{V}(x)$ is always negative definite along the system trajectories implying continuous dissipation of energy. It has been shown in [33], [51] that when passivity-based techniques are combined with resonant mode controller designs, the performance of the resulting controller is significantly enhanced. This is especially true for vibratory and acoustic systems which have resonant modes in their dynamics. Rigorous mathematical descriptions of passivity and a presentation of the resulting stability theorems are found in [55, 48, 75, 47]. The most significant property of passive systems is that they can be robustly stabilized by any passive controller. Furthermore this stability is guaranteed regardless of modeling inaccuracies and system uncertainty. These results involving the robust stability of passivity based controllers offer a powerful approach to robust controller synthesis. Many systems are not inherently passive and must first be passified using a suitable compensator, and then any strictly positive real controller (SPR) (as defined in [55, 48, 75, 47]) may be used to robustly stabilize the system. Examples of such passification methods are given in [52, 45]. There are several existing methodologies for synthesis of Positive Real (PR) (as defined in [55, 48, 75, 47]) controllers.

The current methods for synthesizing PR controllers for linear passive systems include, constant gain PR [52], LQG PR [74], and H_2/H_∞ controllers [37]. Constant gain PR controllers are limited by the design freedom they can offer due to a limited number of design variables. LQG PR controllers, while dynamic, are not truly optimal due to the dispassivity constraints that must be imposed on the weighting matrices of the LQG cost function. Another problem is that these controllers have the same order as the plant, and they are not minimal. Similar restrictions and high order controllers are also present in H_2/H_∞ controllers. Ongoing challenges in these approaches to control design are to reduce the conservatism imposed by PR constraints and to reduce the order of the controller. Several approaches to these problems involve the design of resonant mode and minimax LQG controllers [92, 95, 33].

1.0.2.5 Active Passive Noise Control

Collectively these feedforward and feedback methods for enclosures typically are only effective over narrow bands or for only a few resonant modes. Often times these limitations can be lessened though careful design, and novel actuation schemes, but to some degree there is always some limitations on the effectiveness. This motivates the concept of combined active and passive control design to achieve larger reductions than either approach alone could.

Recently there have been several works that have sought to combine active and passive materials, or to tailor active and passive design properties to complement each other. In Smith, et. al [103] and Yuan [112] a broadband hybrid absorption system which composed of absorbing foam and a control speaker were tested inside an impedance tube. By using the speaker to impose desired boundary conditions in a cavity behind the foam layer the absorption of the combined foam/speaker system was enhanced. These efforts were repeated in Cobo [13] where a micro-perforated panel was separated by a small air gap from a piezoelectric piston actuator (for imposing the rear boundary condition). In a Lee [68] specially selected absorbent materials were laminated to panels and then both active vibration control and piezoelectric shunt damping were used to suppress lower frequency noise. Another interesting paper is by Cabell and Gibbs [8] where constrained layer damping and feedback control where designed together. In this way constrained layer damping attacked the high frequencies and a simple adaptive controller was used to attenuate sound radiation at low frequencies. Another added benefit of the damping material was that it was found to smooth phase transitions and to promote robustness in the presence of shifts in the natural frequencies. There have also been numerous other combinations of active and passive designs [35], [65], and [98]. The most interesting feature of these applications is that by Guo who utilized noise barriers and active noise control to create quiet zones at the top edge of the barrier lessening noise due to edge diffraction. This dissertation seeks to first tackle the passive noise control problem by developing a framework for computational optimization and then by developing a MIMO strategy for active control. Thus the two parts of the problem are currently separated. However these efforts lay the groundwork for a combined optimization of the structure and control.

1.0.2.6 Acoustic Parameter/Mechanism Control

One direction initially explored in the work of this thesis was to develop a mechanism to allow active control of structural parameters to reduce sound transmission and radiation. This is a relatively untouched topic although there are some useful works whose efforts can be instructional. In Samejima [99], an electro-acoustic diaphragm had its electrical parameters modified actively to control the impedance of the device. In this approach model based controllers (specifically LQG) were designed to produce the desired acoustic impedance. In Kim and Kim [58], a similar approach was used in a piezo embedded panel. In this work a controllable electric circuit was attached to the piezoelectric devices and the piezo was configured as a semi-active dissipator. In Zhu, et. al. [116] the acoustic parameters known as the absorption, reflection, and transmission coefficient were actively controlled using flat panel speakers. This paper doesn't represent a new technology so much as a new approach to ASAC. The difference is a shift from attempting to control and suppress vibration (indirectly affecting the coefficients of absorption, reflection, and transmission) to controlling these coefficients directly. The effort utilized a feedforward controller, and was demonstrated to reduce broadband sound transmission.

In this dissertation one of the guiding mechanisms for intuitively designing controllers to reduce sound level involved studying the coupling coefficient and redesigning or suppressing those modes that factor into the transmission sound from one chamber to another (effectively reducing the coupling coefficient). The idea behind targeting this mechanism is that although it may not make the source enclosure quieter or even decrease the total plate vibration it should prevent noise that is generated inside or outside a fully enclosed space from being transmitted outside or inside the enclosure, respectively.

1.0.3 Statement of Contribution

Even with this extensive background of passive and active noise control literature, there is still a considerable amount of research that must still be done. Specifically there are four major deficiencies in existing knowledge that I hope to make new contributions to:

First is that there is no existing work to my knowledge that attempts to directly target the vibroacoustic coupling by passive redesign or through active control. Most other efforts have attempted to affect the absorption or transmission characteristics directly, and have often targeted structural vibrations for suppression (this is a significant difference).

Second there has recently been research into combined active-passive control of acoustic noise. However, these efforts have focused on simply using passive materials in high frequency, and active approaches at low frequency. In this dissertation, a directed design approach of the passive structure lays the groundwork for simplifications of the active control system and improvements in its performance. Although the concept is not new, the existing work surrounding it is incomplete and mostly ad hoc'. The design methodology also allows a combined controller structure optimization to be formulated.

There has been some past work modeling and controlling 3-D enclosures but these have been confined to smaller one sided enclosures and there has been little to no results for a two enclosure barrier plate setup like the one considered here. There are especially few experimental results. Dealing with the analytical modeling, control design modeling, and control of a larger modally rich enclosure is a significant contribution.

Fourth, most approaches to active MIMO ANC are difficult to implement in practice due to uncertainties, the large size of the controller, and hardware limitations. In this thesis passivity based approaches were explored to develop simpler, stable, and performing controllers.

STATEMENT OF CONTRIBUTION:

This dissertation contributes to the existing knowledge in the field of noise control in the following four areas:

1. Exploration of active and passive control of the acoustic structure coupling.

2. Demonstration of an approach to passive tailoring allowing integration with control design

3. Development of a flexible modeling approach to the enclosure. acoustics problem, and development of approaches to identifying and constructing the MIMO control design model.

4. Investigation of several novel approaches to robust and implementable active noise control using passivity, clustering, and resonant mode filters.

Additionally, smaller original contributions include: A)Development and implementation of an LMI formulation for a passive LQG design (using relaxed Riccati equation solution); B) Design, simulation, and implementation an improved proof mass actuator; C) Development of a proof of concept active stiffness control prototype using rheological fluid.

The organization of the dissertation is discussed in the following section.

1.0.4 Dissertation Organization

The organization of the remainder of this dissertation is broken down into seven chapters. In chapter 2 a detailed background of the acoustic, modeling, measurement, and control theory is presented. First in this chapter is a discussion of the acoustic relations of the enclosure, acoustic quantities of interest, methods for measurement of them, and computational simulation approaches (BEM). Next the basics of plate vibration and modeling are discussed along with the specifics of the FEM method developed for this work. Then the approaches for constructing a coupled state model are presented. Next the actuator modeling efforts are discussed, and passive structural design approaches presented. Finally active control techniques, and theory are presented.

Chapter 3 explores the actual creation of the MIMO model of the acoustic enclosure and the possibility of exploiting acoustic structure coupling to reduce the sound transmitted through the panel into and out of a resonant enclosure. A plate redesign strategy is presented in chapter 4 and then the redesigned plates are then experimentally validated. Chapter 5 explores several active control strategies in simulation to gage their effectiveness for control. Chapter 6 discusses the development of the experimental hardware needed to conduct the MIMO active control investigation. Chapter 7 discusses the experimental ID, control design, and implementation for two systems: first a SISO 1-D tube (to develop and work the bugs out of algorithms) and then for the 3-D enclosure separated by an actively controlled plate. Each of the control designs, and the successful results are discussed. Finally chapter 8 summarizes the efforts and contributions of this work, and discusses additional avenues of future study. A brief overview of the potential applications of this work is also given.

2 Theoretical Preliminaries for Structural Acoustics Modeling and Control

This section will discuss the background theory used to derive the models and control designs for the analytical portion of this work. Before continuing further, the limitations of the models used these investigations will be discussed. First the analytical and computational models developed here are restricted to be linear and are based on modal expansions. This assumption for the most part is extremely representative of this type of structural acoustic system at low frequency. However there are several notable exceptions. One is when the enclosure boundaries are very absorptive and lack resonances. In such a situation modeling the acoustic system dynamics with a modal expansion is less appropriate than considering only a direct propagation of the waves from the sources to the plate and from the plate directly to the microphones. A second notable situation is when the enclosures modeled are so large as to make the resonant modes indistinguishable from one another. In this case the model approach used in this work will be very difficult to use, as will be shown later in this dissertation. Yet another exception is in the modeling of the sensors and actuators in this thesis. While sensors like accelerometers are fairly accurate and free from nonlinear effects over their operating range, piezoelectric devices (sensors and actuators) are known to have some degree of hysteresis nonlinearity associated with them. Additionally the finite supply amplifiers used to drive these devices and the finite bit converters used to sample them were not considered and would represent saturation and quantization nonlinearities. Lastly the voice coil inertial actuators considered have several possible nonlinearities not considered including magnetic hysteresis, static friction deadband, and non-idealities field concentration in and near the coil gap. Despite these issues the models developed in this work are useful at quickly validating or invalidating possible control designs and providing insights into the system.

2.1 Enclosure Acoustics

In this section acoustic relations are presented then the acoustics of an enclosure are developed. The efforts of this work are concerned only with linear acoustics for which the governing partial differential equation is given in Eqn. 2.1

$$\rho_o \nabla \frac{\partial \dot{\vec{u}}}{\partial t} = -\nabla^2 p \tag{2.1}$$

Additionally with the relation $\rho_o \frac{\partial \vec{u}}{\partial t} = -\nabla p$ and the equation of state Eqn. 2.1 may be rewritten as in Eqn. 2.2.

$$\nabla^2 p = \frac{1}{c^2} \frac{\partial^2 p}{\partial t^2} \tag{2.2}$$

In these relations c is the speed of sound in the acoustic medium, ρ_o is the equilibrium density of the fluid, p is the acoustic pressure, and $\vec{u}$ is the particle velocity of the fluid. Before going further, the velocity potential q_a will be defined.

$$\vec{u} = \nabla q_a \tag{2.3}$$

This quantity is sometimes more convenient to use than the acoustic velocity as we will see later. In the case that the acoustic variables are functions of three spatial coordinates the waves that are generated are known as spherical waves. Those waves that diverge from a point source are known as harmonic with frequency ω and are represented in complex form (with amplitude A, $\vec{r} = \sqrt{x^2 + y^2 + z^2}$, and $k = \frac{\omega}{c}$ as follows.

$$p = \frac{A}{r} e^{j(\omega t - kr)} \tag{2.4}$$

Next, several common acoustic quantities are defined including the acoustic impedance, acoustic intensity, the sound power, the reflection coefficient, and the transmission coefficient. The convention from this point forward will be to indicate a complex quantity with an underbar (i.e. complex pressure is $\underline{\mathrm{p}}$. The first quantity presented is the complex acoustic impedance, and it is defined as in Eqn. 2.5

$$\underline{\mathrm{Z}} = \frac{\underline{\mathrm{p}}}{\underline{\mathrm{u}}} \tag{2.5}$$

The complex acoustic intensity is a vector quantity defined as (where $(\cdot)^*$ indicates complex conjugate):

$$\underline{\vec{I}} = \frac{1}{2}\underline{\mathrm{p}}(\vec{r},t)\underline{\mathrm{u}}^*(\vec{r},t) = \vec{I}(\vec{r}) + j\vec{Q}(\vec{r}) \tag{2.6}$$

In Eqn. 2.7 $\vec{I}$ and $\vec{Q}$ are known as the active and reactive intensities respectively. With this definition the sound power W is defined:

$$W = \int\int \underline{\vec{I}} \cdot \hat{n}\, dS \tag{2.7}$$

The transmission coefficient τ is defined as transmitted pressure amplitude over incident pressure amplitude, and reflection confident $\mathcal{R}$ is the reflected pressure amplitude over the incident pressure amplitude.

With these basics out of the way we are ready to begin describing the modeling of enclosure acoustics. Beginning with the homogeneous wave equation for the enclosure:

$$\nabla^2 p - \frac{1}{c_o^2}\frac{\partial^2 p}{\partial t^2} = 0 \tag{2.8}$$

With the application of boundary constraints this boundary value problem's solution may be expressed as an eigenfunction expansion of the pressure in terms of these mode shapes and modal coordinates $p(t) = \sum_i \Phi_{a_i}\mathcal{P}_i(t)$. Now consider the inhomogeneous Helmholtz equation.

$$\nabla^2 p - \frac{1}{c_o^2}\frac{\partial^2 p}{\partial t^2} = -\rho_o\frac{\partial q(t)}{\partial t} \tag{2.9}$$

Using the homogenous expansion solution results in an infinite sum of eigenfunctions. In practice these sums are truncated to yield a finite dimensional linearized model that can be represented by the following vector matrix differential equation:

$$\ddot{\mathcal{P}}(t) + \tilde{\mathcal{C}}_a \dot{\mathcal{P}}(t) + \Omega_a \mathcal{P}(t) = \rho c^2 (\Lambda_a)^{-1} \dot{Q(t)} \tag{2.10}$$

where, Λ_a is a diagonal matrix where the diagonal entries are $\Lambda_{a_{ii}} = \int_V \Phi_{a_i}^2 dV$ and Q(t) is the generalized volume source strength vector whose rows are given by $Q_i(t) = \int_V q(r_o)\Phi_{a_i}(r_o)dV$ where $q(r_o)$ is the source term. This is rewritten in terms of the velocity potential q_a, by noticing $p(t) = -\rho\dot{q}_a(t)$ and $q_a = \sum_i \Phi_{a_i} \mathsf{q}_{ai}(t)$, then substituting into Eqn. 2.10, and integrating.

$$\ddot{\mathsf{q}}_a(t) + \tilde{\mathcal{C}}_a \dot{\mathsf{q}}_a(t) + \Omega_a \mathsf{q}_a(t) = -c^2 (\Lambda_a)^{-1} Q(t) \tag{2.11}$$

In this equation $\mathcal{C}_a$ is a general acoustic mode damping term, and Ω_a is a diagonal matrix of acoustic eigenvalues. All that remains to use these expressions is the homogenous eigenfunction expansion. For the case of a perfectly rigid/reflective enclosure this ends up being fairly simple to solve analytically. However this is one of the only boundary conditions where a "nice" solution is possible. A rigid enclosure is an idealization and if the enclosure has flexible walls, absorptive walls, or perforated walls (all very "real world" situations) this approach may lead to inaccuracies. Technically to utilize an eigenfunction expansion only requires two things: 1) the functions are solutions to the homogeneous equation, and 2) the functions are orthogonal to one another. Therefore if one was able to find these orthogonal functions they could be used to construct the solution. The next section describes a numerical method by which these eigenfunctions may be found.

2.2 Boundary Element Method

Beginning from the wave equation the (HIE) given in Eqn. (2.12) may be derived [6],[22]. This equation expresses the solution for the acoustic field in terms of known and unknown quantities on the boundaries.

$$\hat{p}(\vec{r}) = \frac{1}{\alpha(\vec{r})}\int_{S_i} \hat{p}(\vec{r_s})\frac{\partial G(\vec{r},\vec{r_s})}{\partial n} + j\omega\rho\hat{v}(\vec{r_s})G(\vec{r},\vec{r_s})dS_i$$
$$+j\omega\rho\int_V q(\vec{r_o})G(\vec{r},\vec{r_o})dV \tag{2.12}$$

where $G(\vec{r},\vec{r_o}) = \frac{e^{jk(\vec{r}-\vec{r_o})}}{4\pi(\vec{r}-\vec{r_o})}$ is the Green's function (in this case the free space Green's function but this choice is somewhat arbitrary as long as it is a fundamental solution to the wave equation). The other quantities are a geometry dependent coefficient $\alpha(\vec{r})$, the complex pressure $\hat{p}(\vec{r})$, the complex velocity $\hat{v}(\vec{r_s})$, a source term $q(\vec{r_o})$, and the boundary surfaces S_i with $(i = 1, 2, 3...., n)$. Essentially the boundary element method seeks to evaluate this HIE numerically to determine the solution for $\hat{p}(\vec{r})$. This process requires that the surface first be discretized, and like terms collected. Without going into details (if interested these details may be found in a number of texts and papers [111],[6]) the discretized HIE equation essentially becomes a linear system of equations in terms of the boundary variables like those in Eqn. (2.13).

$$[H]\vec{p} = [G]\vec{v} \tag{2.13}$$

In this problem, for each equation either p_i, v_i, or the ratio of p_i to v_i is a known and thus the linear system may be solved for the remaining boundary terms and then a form of Eqn. (2.12) may be used to express interior points as combinations of these boundary source solutions.

A method similar to this that uses linear elements, and is capable of handling the more general robin boundary condition was used to solve for the acoustic mode shapes and frequencies. First the boundary conditions (rigid) were specified, and the problem was solved with a monochromatic point source for a desired vector of frequencies. For each frequency the field solutions were evaluated at a point close to this excitation point. Then the eigenfrequencies are determined from the maxima of the frequency response function developed in the previous step. This process is repeated for numerous source and measurement locations then the eigenmodes are found by finding the internal solution at a desired spatial grid for the identified eigenfrequencies. When possible, several solutions are generated and used to remove the distortion in the field solution that occurs near the source point location. This method was used to generate the acoustic modal frequencies and mode shapes for this dissertation and the BEM result was nearly identical to the analytical result that exists for this specific problem.

2.3 Finite Element Method

This chapter is focused on the development of a mathematical model for the acoustic-structure system. This model will be used later for the controller design and passive tailoring. First, an underlying modeling methodology is presented for a generic flexible structure system. Flexible structures represent infinite dimensional systems; however, for control design purposes, one often needs to obtain a finite dimensional approximation of an infinite dimensional system. Infinite dimensional systems are also computationally intractable. There are several approximate modeling methods that can be used to model flexible structures. Essentially, each method represents a scheme to discretize a continuous system into a number of discrete elements (thus transforming an infinite dimensional description into a finite dimensional one). A general group of methods used in this thesis are known collectively as modal space methods. They represent the solution in the form of a finite sum of the product of two functions, one of which is a spatial function, and the other is a function of time.

A finite dimensional approximation of infinite dimensional flexible structure often leads to an eigenvalue problem of the following form:

Determine matrix Φ and matrix Λ which satisfy

$$M^{-1}K\Phi = \Lambda\Phi \tag{2.14}$$

where, M is the inertial (mass) matrix of the system, K is the stiffness matrix, Φ is matrix of eigenvectors and Λ is a diagonal matrix of eigenvalues (both of which have a special meaning to be discussed later). There are different approaches to solving the eigenvalue problem and constructing the solution of the governing differential equation. The three most commonly known methods are the Rayleigh-Ritz method, the method of weighted residuals, and the finite element method. Given next is a brief overview of these methods.

2.3.1 The Rayleigh-Ritz Method

The procedure in this method is based on the theorem of minimum potential energy. By restricting a set of admissible basis functions for approximating the eigenvector to a particularly simple subset (like the space of linear combinations of n independent basis functions) an approximate eigenvector of the eigenvalue problem is expressed as:

$$u(s) = \sum_{i=1}^{n} v_i u_i(s) \tag{2.15}$$

where v_i are real coefficient, and u_i are the basis functions (often called the comparison functions)

Suppose ϕ and λ is an eigenpair which satisfy the operator eigenvalue problem:

$$K\phi = M\lambda\phi \tag{2.16}$$

Taking the inner product of both sides with respect to ϕ yields

$$\lambda = \frac{<\phi, A\phi>}{<\sqrt{m}\phi, \sqrt{m}\phi>} \tag{2.17}$$

Replacing ϕ with the u in Eqn. (2.15), the relationship in Eqn. (2.17) doesn't hold. However by forming this Rayleigh quotient with the approximation as in Eqn. (2.18) it is possible to find the best approximation to the eigenvector ϕ.

$$R(\bar{v}) = \frac{\langle \sum_1^n v_i u_i, \sum_1^n v_i A u_i \rangle}{\langle \sqrt{m} \sum_1^n v_i u_i, \sqrt{m} \sum_i^n v_i u_i \rangle} \tag{2.18}$$

This is done by minimizing $\partial R / \partial \bar{v}$, where $\bar{v} = (v1, v2, \ldots)^T$. The approximate eigenpairs found using this approach can then be used in modeling of the system.

For flexible structures, a specific application of the Rayleigh-Ritz method known as the assumed modes method is used. In this method, a solution is assumed to have the following form:

$$u(s,t) = \sum_{i=1}^{n} \psi_i(s) \eta_i(t) \tag{2.19}$$

In this instance, ψ_i represents a best guess of the mode-shape functions, and η_i are time dependent generalized spatial coordinates. The kinetic and potential energy equations are expressed in terms of ψ and η resulting in the following form:

$$M\ddot{\eta} + K\eta = 0 \tag{2.20}$$

This set of differential equations can then be recast as an algebraic eigenvalue problem. Furthermore, if the mode shapes ϕ_i represent the eigenvectors and the square of the natural frequencies ω_i^2 represent the eigenvalues λ_i, then the eigenvectors are orthogonal with respect to M. This means that

$$\phi_i^T M \phi_j = 0 \text{ if } i \neq j \tag{2.21}$$

When ϕ_i are mass normalized such that $\phi_i^T M \phi_i = 1$. For

$$\Phi = [\phi_1, \phi_2, \ldots, \phi_n], \text{ and } \Lambda = \text{diag}[\omega_1^2, \omega_2^2, \ldots, \omega_n^2] \tag{2.22}$$

It holds that

$$\Phi^T M \Phi = I \text{ and } \Phi^T K \Phi = \Lambda \tag{2.23}$$

Transforming the generalized coordinates to modal coordinates $\eta(t) = \Phi q(t)$ produces the following set of decoupled second order ODE's:

$$\ddot{q}_i + \lambda_i q_i = 0 \qquad (i = 1, 2, \ldots, n) \tag{2.24}$$

2.3.2 Method of Weighted Residuals

The method of weighted residuals is more general than the Rayleigh-Ritz method. In this method, an approximate eigenvector is assumed as in Eqn. (2.15), and the residual of the eigenvalue equation is defined as:

$$R(u, s) = Au(s) - \lambda m(s)u(s) \tag{2.25}$$

Let $\psi_i(i = 1, 2, \ldots, n)$ represent a set of basis functions. For a given n, the goal is to find $\psi_i(i = 1, 2, \ldots, n)$, all of which are orthogonal to R. This condition minimizes R and achieves the best approximation of ϕ. This again results in an algebraic eigenvalue problem $(K - \lambda M)\bar{v} = 0$ where M and K are generally not symmetric. Depending on the choice of $\{\psi_i\}$, a variety of methods for solution can be obtained. If A is self-adjoint, the resulting algebraic eigenvalue problem is equivalent to that obtained by the Rayleigh-Ritz method.

2.3.3 Thin Plate Model

The plate structure developed later in this work was modeled using the finite element method. There are numerous advantages in using finite element method (FEM), including the ease with which parametric optimizations can be formulated and conducted, and handling boundary conditions for which there are no closed form analytical solutions (like the clamped clamped plate). Many effective FEM packages are readily available for obtaining mathematical models of structural systems. The basic idea of the FEM is to divide a continuous system into a number of discrete elements. The points of intersection of the dividing lines are referred to as the "nodes". For a particular problem type the relevant PDEs are then approximated and solved over these discretized regions.

An FEM model of a clamped, square plate was developed using two different finite element packages. Using ANSYS and FEMLAB the eigenfrequency and mode shape data was obtained. After a reasonable degree of confidence was achieved in the model FEMLAB was chosen to do the remainder of the structural modeling. The reason for this selection was to allow Matlab coupled optimizations and simulations to be run with relative ease. FEMLAB [**?**], is a Matlab-based toolbox that allows the user to work directly with the partial differential equations governing each structural element. When constraints are applied and the element PDE's are linearized, these equations reduce to a generalized eigenvalue problem of the form :

$$\begin{bmatrix} K & N^T \\ N & 0 \end{bmatrix} \begin{bmatrix} V \\ Y \end{bmatrix} = \lambda \begin{bmatrix} M & 0 \\ 0 & 0 \end{bmatrix} \begin{bmatrix} V \\ Y \end{bmatrix} \tag{2.26}$$

Since the elements are assumed to have a governing PDE the matrices K,N,and M (which are constructed from the PDE coefficients and constraints) are already known. In this case, the linear solver in Matlab transforms this problem (by Gaussian elimination) to the standard algebraic eigenvalue problem which can be solved using a method similar to the Rayleigh-Ritz method.

2.3.3.1 Mindlin Plate Model

A Mindlin plate is based on the following engineering assumption: a plane originally perpendicular to the mid surface remains planar after loading, but not necessarily perpendicular to the deformed mid surface. The change in angle accounts for the transverse shear deformation. The dependent variables for this plate formulation are the z displacement w and the rotations Θ_x and Θ_y. The governing equations for shear stress and moment are given 2.27. The element implementation used in FEMLAB is a six nodes twelve degrees of freedom Reissner-Mindlin triangle.

$$
\begin{aligned}
M_{xx} &= D(\frac{\partial \Theta_x}{\partial x} + \nu \frac{\partial \Theta_y}{\partial y}) \\
M_{yy} &= D(\frac{\partial \Theta_y}{\partial y} + \nu \frac{\partial \Theta_x}{\partial x}) \\
M_{xy} &= \frac{(1-\nu)D}{2}(\frac{\partial \Theta_x}{\partial y} + \frac{\partial \Theta_y}{\partial x}) \\
S_x &= \kappa^2 Gt(\Theta_x + \frac{\partial w}{\partial x}) \\
S_y &= \kappa^2 Gt(\Theta_y + \frac{\partial w}{\partial y})
\end{aligned}
\tag{2.27}
$$

With the plate stiffness D and shear modulus G given by $D = \frac{Et^3}{12(1-\nu^2)}$ and $G = \frac{E}{2(1+\nu)}$, and $\kappa = \frac{5}{6}$ as the shear correction factor.

2.3.3.2 The finite dimensional model for the plate

The first and second modal solutions appear in Fig. 3.1 and Fig. 3.2. A finite dimensional linearized model of the plate can be represented by the following vector matrix differential equation:

$$
M\ddot{\eta}(t) + \mathcal{C}\dot{\eta}(t) + K\eta(t) = f(t) \tag{2.28}
$$

where, $\eta(t)$ is $n \times 1$ normal displacement vector, $f(t)$ is force input from an actuator, and M, $\mathcal{C}$, and K are symmetric $n \times n$ mass, damping, and stiffness matrices, respectively. Equation (2.28) can be rewritten in the modal form as in Eqn. 3.1, and constructed using mode shape and frequency information from ANSYS:

$$
\ddot{q}_p(t) + \tilde{\mathcal{C}}_p \dot{q}_p(t) + \Omega_p q_p(t) = \Phi_p^T f(t) \tag{2.29}
$$

where, Φ_p is the mass normalized mode shape matrix of the plate, $q_p(t)$ are the modal coordinates, $\eta(t) = [\Phi_p]\{q_p(t)\}$, $\Phi_p^T M \Phi_p = I$, $\Phi_p^T \mathcal{C} \Phi_p = \tilde{\mathcal{C}}_p$, and $\Phi_p^T K \Phi_p = \Omega_p$. These may then be transformed to a standard state space form by selection of a state variable description. The obvious choice of q_{p_n}'s and $\dot{q_{p_n}}$'s is a convenient and useful description.

2.4 Structural-Acoustic Modeling

The fluid structure coupling method utilized in this paper is known as the modal interaction model [22]. Begin by considering a fluid loading of the plate expressed in terms of the generalized acoustic modal coordinates. The fluid loading in 2.30 is expressed as a summation of the acoustic eigenfunctions for the pressure multiplied by the element area S and the coupling matrix Π that indicates how each acoustic mode couples to each structural mode. With this additional term the system of structural equations become:

$$\ddot{q}_p(t) + \tilde{\mathcal{C}}_p \dot{q}_p(t) + \Omega_p q_p(t) = \Phi_p^T f(t) - S\rho_a \Pi^T \dot{q}_a(t) \tag{2.30}$$

Where $\Pi_{mn} = \frac{1}{S}\int_S \Phi_{a_m}(r_s)\Phi_{p_n}(r_s)dS$ defines the coupling term. The expression of the structures effect on the fluid may be similarly expressed as the modal velocities of the plate multiplied by the coupling matrix Π, c, S, and the inverse acoustic mass matrix Λ_a. With this new term the system of acoustic equations becomes:

$$\ddot{q}_a(t) + \tilde{\mathcal{C}}_a \dot{q}_a(t) + \Omega_a q_a(t) = -c^2\Lambda_a^{-1}Q(t) + c^2 S * \Lambda_a^{-1}\Pi\dot{q}_p(t) \tag{2.31}$$

As one might expect this type of coupling between the two systems manifests itself as a damping term in each differential equation. However unlike viscous damping these terms do not dissipate energy they merely transfer it to either the structural or acoustic system in a lossless fashion. Future efforts will improve upon this model by considering loss in this transference of energy.

2.4.1 State Space Model

Now, considering the specific system of this work (two identical enclosures separated by the flexible plate) Equations (2.30) and (2.31) can now be formulated into a $2 * N$ dimensional state space representation (with N equal to the combined number of structural (n) and acoustic (m for each enclosure) modes in the finite dimensional model). This has the form shown in equation (2.32). In this expression, the matrix $A = A_{coup} + A_{dec}$ and a_s and a_d indicate the source and destination enclosures.

$$\begin{aligned} \dot{x}(t) &= Ax(t) + B[u(t), s(t)]^T \\ y(t) &= Cx(t) \end{aligned} \tag{2.32}$$

$$\begin{aligned} A_{dec} = \mathrm{diag}(&\begin{bmatrix} 0 & 1 \\ -\omega_{p1}^2 & -2\zeta_{p1}\omega_{p1} \end{bmatrix}, \cdots, \begin{bmatrix} 0 & 1 \\ -\omega_{pn}^2 & -2\zeta_{pn}\omega_{pn} \end{bmatrix} \\ &, \begin{bmatrix} 0 & 1 \\ -\omega_{a_s1}^2 & -2\zeta_{a_s1}\omega_{a_s1} \end{bmatrix}, \cdots, \begin{bmatrix} 0 & 1 \\ -\omega_{a_sm}^2 & -2\zeta_{a_sm}\omega_{a_sm} \end{bmatrix} \\ &, \begin{bmatrix} 0 & 1 \\ -\omega_{a_d1}^2 & -2\zeta_{a_d1}\omega_{a_d1} \end{bmatrix}, \cdots, \begin{bmatrix} 0 & 1 \\ -\omega_{a_dm}^2 & -2\zeta_{a_dm}\omega_{a_dm} \end{bmatrix}) \end{aligned} \tag{2.33}$$

$$\begin{aligned} A_{coup} &= \begin{bmatrix} [0]_{2\cdot p_n \times 2\cdot p_n} & C_{a_s2p} & -Ca_{d2p} \\ C_{p2a_s} & [0]_{2\cdot a_s n \times 2\cdot a_s n} & [0]_{2\cdot a_s n \times 2\cdot a_d n} \\ -C_{p2a_d} & [0]_{2\cdot a_d n \times 2\cdot a_s n} & [0]_{2\cdot a_d n \times 2\cdot a_d n} \end{bmatrix} \\ C_{a_s2p} = C_{a_d2p} &= -\rho_a S \begin{bmatrix} 0 & 0 & 0 & 0 & 0 \\ 0 & \Pi_{1,1}^T & \cdots & 0 & \Pi_{1,m}^T \\ \vdots & \vdots & \vdots & \vdots & \vdots \\ 0 & 0 & 0 & 0 & 0 \\ 0 & \Pi_{n,1}^T & \cdots & 0 & \Pi_{n,m}^T \end{bmatrix} \\ C_{p2a_s} = C_{p2a_d} &= -c^2 S \begin{bmatrix} 0 & 0 & 0 & 0 & 0 \\ 0 & (\Lambda_a^{-1}\Pi)_{1,1} & \cdots & 0 & (\Lambda_a^{-1}\Pi)_{1,n} \\ \vdots & \vdots & \vdots & \vdots & \vdots \\ 0 & 0 & \cdots & 0 & 0 \\ 0 & (\Lambda_a^{-1}\Pi)_{m,1} & \cdots & 0 & (\Lambda_a^{-1}\Pi)_{m,n} \end{bmatrix} \end{aligned} \tag{2.34}$$

$$
B = \begin{bmatrix}
0 & 0 \\
(\tilde{\Phi}_{p_1}|_{actlocs})^T & 0 \\
\vdots & \vdots \\
0 & 0 \\
(\tilde{\Phi}_{p_n}|_{actlocs})^T & 0 \\
0 & 0 \\
0 & (\tilde{\Phi}_{as_1}|_{actlocs})^T \\
\vdots & \vdots \\
0 & 0 \\
0 & (\tilde{\Phi}_{as_m}|_{actlocs})^T \\
\vdots & \vdots
\end{bmatrix};
$$

$$
C = \begin{bmatrix}
\hat{\Phi}_{p_1}|_{senslocs} & 0 & \cdots & \hat{\Phi}_{p_n}|_{senslocs} & 0 & \cdots & 0 & 0 & \cdots & 0 & 0 \\
0 & 0 & \cdots & 0 & 0 & \cdots & 0 & -\rho_o\hat{\Phi}_{ad_1}|_{senslocs} & \cdots & 0 & -\rho_o\hat{\Phi}_{ad_m}|_{senslocs}
\end{bmatrix} \tag{2.35}
$$

With desired outputs being the positions at a series of points on the plate and the measurement of pressure at specific enclosure locations, the structural and acoustic modeshape matrices are evaluated at this subset of discrete sensor points. Similarly the structural forcing locations and the acoustic source locations are also extracted from the mode shape matrix. Together these sets of modeshape data form a map from forces in real coordinate space to modal coordinate space for the inputs and outputs and the B and C matrices are given by equations 2.35.

Where, in the C matrix $\hat{\Phi}_{p_n}$ corresponds to the n^{th} modeshape evaluated at the location of the position sensor and $\hat{\Phi}_{ad_m}$ similarly corresponds to the location of the microphone on the destination side. If one desires the output to be plate velocity instead of position the $\hat{\Phi}_{p_n}$ terms are moved over one position to the right in the C matrix. In the B matrix the $\tilde{\Phi}_{p_n}$ terms correspond to the n^{th} modeshape of the plate evaluated at each force (actuator) input location. $\tilde{\Phi}_{as_m}$ terms correspond to the m^{th} modeshape of the acoustics evaluated at each acoustic source location. These equations may be further modified to include the effects of sensor and actuator dynamics these details are further discussed in section 3.1.3.3.

2.5 Active Noise Control Methodologies

2.5.1 Model Based Control (LQG)

2.5.1.1 LQG Regulator Design

The LQG regulator or LQR controller is part of the dual problem of optimal observer and controller design for an LQG controller. Because of the separation principle the observer and controller portions of the LQG design may be separately tackled. A Linear Quadratic Gaussian (LQG) design involves a solution for an optimal control input that will minimize a given quadratic cost function. In this particular instance, this cost function reflects an effort to penalize the states and control energy for the system's worst-case performance criteria. For the LQG regulator the cost function to be minimized was considered to be:

$$J(x,u) = \frac{1}{2}E\left\{\lim_{T\to\infty}\int_0^T (\left\{\begin{array}{c} x \end{array}\right\}^T Q_c \left\{\begin{array}{c} x \end{array}\right\} + u^T R_c u)dt\right\} \tag{2.36}$$

where $Q_c = Q_c^T \geq 0$ and $R_c = R_c^T > 0$ are the design parameters reflecting state weighting and control weighting matrices, and u is the control input. With u as defined in Eqn. (2.37) the state feedback gains are determined optimally in the same computation.

$$u = -[K_x]\left\{\begin{array}{c} \hat{x} \end{array}\right\}^T \tag{2.37}$$

$$[K_x] = -R_c^{-1}B_u^T P_c \tag{2.38}$$

where, $P_c = P_c^T \geq 0$ is the solution of the following (steady-state) algebraic Riccati equation (ARE):

$$\tilde{A}^T P_c + P_c\tilde{A} - P_c\tilde{B}_u R_c^{-1}\tilde{B}_u{}^T P_c + Q_c = 0 \tag{2.39}$$

2.5.1.2 LQG Observer (Kalman Filter) Design

The LQG (Linear Quadratic Gaussian) controller is essentially the combination of a regulator and a Kalman filter (an optimal observer). For a design of the Kalman filter, a state-space model of the plate-enclosure system with random disturbance inputs and sensor noise is considered. Both of these random signals are assumed to be stationary, uncorrelated, and zero mean white noise processes. The system model can be represented as follows:

$$\begin{aligned} \dot{x} &= Ax + B_u u + B_u \gamma + B_d d \\ \tilde{y} &= C_{\tilde{y}} x + D_u u + D_d d \xi \end{aligned} \tag{2.40}$$

where, γ and ξ are the actuator and sensor noise with covariances Q_e and R_e, respectively. Since the values of Q_e and R_e for realistic disturbances are not known a priori, Q_e and R_e are treated as the design parameters and are chosen so that the observer is stable and converges quickly. The observer dynamics are given by

$$\dot{\hat{x}} = [A - LC_y - B_u K_x - LD_u K_x]\,\hat{x} - Ly \tag{2.41}$$

where, the Kalman estimator gain L is given by $L = P_e C_m^T R_e^{-1}$ and P_e is the solution of filter Riccati equation:

$$P_e A^T + AP_e - P_e C_y^T R_e^{-1} C_y P_e + B_u Q_e^{-1} B_u^T = 0 \tag{2.42}$$

where, $Q_e = Q_e^T \geq 0$ and $R_e = R_e^T > 0$. The control signal u is then given by

$$u = -K_x \hat{x} \tag{2.43}$$

The closed-loop system is the combination of the regulator and estimator given by Eqn. (2.44).

$$\begin{aligned} \begin{Bmatrix} \dot{x} \\ \dot{\hat{x}} \end{Bmatrix} &= \begin{bmatrix} A & -B_u K_x \\ LC_y & A - LC_y - B_u K_x - LDuK_x \end{bmatrix} \begin{Bmatrix} x \\ \hat{x} \end{Bmatrix} \\ &\quad + \begin{bmatrix} B_d^T & 0 \end{bmatrix}^T d(t) \\ y_{pf} &= \begin{bmatrix} C_y & 0 \end{bmatrix} \begin{Bmatrix} x^T & \hat{x}^T \end{Bmatrix}^T + D_d d \end{aligned} \tag{2.44}$$

In this work there were several approaches to the design of LQG controllers. When possible state models of the plant including both plate and enclosure dynamics were used. When this became untenable (in the high order MIMO systems) only the plate state description was used. In simulation the continuous formulation of the controller and observer equations were utilized (what was presented here). However, when dealing with high frequency control and models were the dynamics are lightly damped, straight conversion of the continuous controller to z-domain can cause problems. First, the algorithm doesn't consider the finite sampling rate effects of the model. While if extremely oversampled this is not a problem, it does lead to performance issues when this is not the case. Second, if the controller is not structured/balanced/scaled properly in the continuous to discrete conversion, rounding error in the filter coefficients introduces uncertainty to the pole and zero locations (a disaster when there are so many poles so close to the unit circle). One way to avoid this problem is to use the discrete time formulation of the regulator and observer design problems. This is what was done in this work. In all cases the LQG controller was reduced in order before implementation

2.5.2 Passivity Based Control

2.5.2.1 Theoretical Preliminaries

Before further discussion of these efforts the results of several theorems developed and presented in [**?**, **?**, **?**, **?**] some definitions must be made. First the $\mathcal{L}_p$ and $\mathcal{L}_{pe}$ spaces are defined.

Definition 1 *Let the $\mathcal{L}_p$ - norm of a signal u(t) beginning at t=0 be given as*

$$\|u(t)\|_{\mathcal{L}_p} \doteq \left(\int_0^\infty \|u(t)\|^p dt\right)^{\frac{1}{p}} \tag{2.45}$$

then the $\mathcal{L}_p$ space is the space containing all signals that have a finite $\mathcal{L}_p$-norm. The $\mathcal{L}_{pe}$ space is the space of all signals that when truncated at time T have a finite $\mathcal{L}_p$-norm.

For example $\mathcal{L}_2$ is the space of finite square integrable signals. This also corresponds to space of bounded energy signals. Also for $\mathcal{L}_2$ there is an inner product $\langle u, v \rangle$ defined on it and the $\mathcal{L}_2$-norm can be written as $\sqrt{\langle u, u \rangle}$. Thus this is an infinite dimensional Hilbert Space. Next is a general definition of dissipativity. Simply said dissipativity parallels the concepts of energy loss and dissipation in physical systems [?].

Definition 2 *The supply rate is a function $w(t) = w(u(t), y(t))$ with $u(t) \in \mathcal{L}_{pe}$ and $y(t) \in \mathcal{L}_{pe}$ (where u and y may be vector valued). Such that $w(t)$ is locally integrable.*

Definition 3 *A system is said to be internally dissipative with respect to $w(u, y)$ if there exists a function of the state x known as the storage function E that satisfies the following "dissipation inequality"*

$$E(x(0)) + \int_0^T w(u(t), y(t))dt \geq E(x(T)) \tag{2.46}$$

$\forall T \geq 0$ *and for all measurable real valued states.*

Definition 4 *A system is said to be input output dissipative with respect to $w(u, y)$ if there exists a β such that*

$$\int_0^T w(u(t), y(t))dt + \beta \geq 0 \tag{2.47}$$

$\forall T \geq 0$

Now if one considers a system that is zero state observable and reachable [?] then input-output dissipativity and internal dissipativity are the same. Furthermore if the supply rate function is quadratic with

$$w(y, u) = [y^T u^T] \begin{bmatrix} Q & S \\ S^T & R \end{bmatrix} \begin{bmatrix} y \\ u \end{bmatrix} \tag{2.48}$$

Then one may define what is known as passivity [?].

Definition 5 *a passive system is a subset of the class of dissipative systems where the number of inputs and outputs are equal and the supply rate function $w(u, y)$ is quadratic. The following forms of passivity are defined in the input output sense*

A system is **passive** *if $Q = 0$, $R = 0$, and $S = \frac{1}{2}I$ and there exists a β so that $w(y, u) + \beta = \langle y, u\rangle_T + \beta \geq 0$ for all $T \geq 0$.*

A system is **input strictly passive** *if $Q = 0$, $R = -\epsilon I$, and $S = \frac{1}{2}I$ and $\exists$ a β such that $\langle y, u\rangle_T + \beta \geq \epsilon\|u_T\|_2^2$ for all $T \geq 0$, and $\epsilon \geq 0$.*

A system is **output strictly passive** *if $Q = -\delta I$, $R = 0$, and $S = \frac{1}{2}I$ and $\exists$ a β such that $\langle y, u\rangle_T + \beta \geq \delta\|y_T\|_2^2$ for all $T \geq 0$, and $\delta \geq 0$.*

One additional definition is needed to describe situations where the system has a state variable description with state $x(t)$.

Definition 6 *A system is* **state strictly passive** *if $\exists$ a $V(x) \geq 0$ such that $\langle y, u\rangle_T \geq \dot{V} + \psi(x)$ for all $T \geq 0$ and $\psi(x) \geq 0$.*

The concept of passivity is a useful one in the analysis and control of dynamic systems. A large class of physical systems can be classified as being naturally passive (i.e. have Lyapunov functions $V(x)$ for which $\dot{V} < 0$). A very important property of a passive system is that it can be robustly stabilized by any strictly passive controller, despite unmodeled dynamics and parametric uncertainties. For finite-dimensional linear, time-invariant (LTI) systems, passivity is equivalent to the "positive realness" of the transfer function.

Let $G(s)$ denote a $m \times m$ matrix whose elements are proper rational functions of the complex variable. $G(s)$ is said to be stable if all its elements are analytic in $\Re(s) > 0$. Let the conjugate-transpose of a complex matrix H be denoted by H^*.

Definition 7 *An $m \times m$ rational matrix $G(s)$ is said to be positive real (PR) if*

1. *all elements of $G(s)$ are analytic in Re(s) $>$ 0;*

2. *$G(s) + G^*(s) \geq 0$ in Re(s) $>$ 0; or equivalently,*

   Poles on the imaginary axis are simple and have nonnegative-definite residues, and $G(j\omega) + G^*(j\omega) \geq 0$ for $\omega \in (-\infty, \infty)$

Definition 8 *An $m \times m$ rational matrix $G(s)$ is said to be marginally strictly positive real (MSPR) if it is positive real, and $G(j\omega) + G^*(j\omega) > 0$ for $\omega \in (-\infty, \infty)$*

The following established theorems about the passivity of interconnections of passive systems are now presented without proof.

Theorem 1 *The closed-loop system consisting of negative feedback interconnection of $G_1(s)$ and $G_2(s)$ is globally asymptotically stable if $G_1(s)$ is PR, $G_2(s)$ is MSPR, and none of the purely imaginary poles of $G_2(s)$ are transmission zeros of $G_1(s)$. If $G_1(s)$ and $G_2(s)$ are interchanged this theorem still holds.*

Theorem 2 *The parallel interconnection of two strictly passive systems $G_1(s)$ and $G_2(s)$ is itself a passive system.*

2.5.2.2 Sensor blending for Passification

With the storage function of $G(s)$ defined as $V(x) = \frac{1}{2}x^T Px \qquad P > 0$ one can write the dissipativity condition of Definition 6 as:

$$x^T(PA + A^TP)x + 2x^TPBu - x^TC^Tu = \tag{2.49}$$

$$\begin{bmatrix} x \\ u \end{bmatrix}^T \begin{bmatrix} A^TP + PA & -C^T + PB \\ -C + B^TP & -(D + D^T) \end{bmatrix} \begin{bmatrix} x \\ u \end{bmatrix} \leq 0 \tag{2.50}$$

and this may be expressed as the following LMI for which a P must be found:

$$\begin{bmatrix} A^TP + PA & -C^T + PB \\ -C + B^TP & -(D + D^T) \end{bmatrix} \leq 0 \tag{2.51}$$

In the situation where there are more sensor inputs available than control outputs in the system it may be possible to blend these sensor signals such that the resultant combination does yield a passive system. This problem becomes one of finding a matrix M such that the state space system (A, B, MC, MD) is passive. This problem then becomes one of finding M and P matrices such that

$$\begin{bmatrix} A^TP + PA & -(MC)^T + PB \\ -MC + B^TP & -(MD + (MD)^T) \end{bmatrix} \leq 0 \tag{2.52}$$

Additionally the resultant system should retain a certain threshold of observability. Thus the following set of LMI's are added for further constraint using the observability grammian Q_o.

$$\begin{bmatrix} A^TQ_o + Q_oA & (MC)^T \\ MC & -I \end{bmatrix} \leq 0 \tag{2.53}$$

$$Q_o > \epsilon_o I \tag{2.54}$$

Here ϵ_o is chosen to set a lower bound on the observability of the system. This approach to passification was utilized in the both the simulation and experimentation section.

2.5.2.3 Actuator blending for Passification

The dual problem to sensor blending the actuator blending or allocation problem. In this case the number of actuators available (r) is greater than the number of sensors

(q) and the goal is to find a combination of actuators that will passify the system and achieve a desired level of observability. Beginning again with condition Eqn. 2.51 the goal is to find blending matrix N, such that the state space system (A, BN, C, DN) is passive this boils down to a similar LMI constraint.

$$\begin{bmatrix} AP + PA^T & -PC^T + BN \\ -CP + N^T B^T & -(DN + (DN)^T) \end{bmatrix} \leq 0 \tag{2.55}$$

Like in the sensor the LMI system is further constrained with a lower bound on the controllability grammian of the system. This ensures that the solution of this LMI system for N yields an actuator blending that leaves the system controllable. This constraint equation is:

$$\begin{bmatrix} AQ_c + Q_c A^T & BN \\ N^T B^T & -I \end{bmatrix} \leq 0 \tag{2.56}$$

$$Q_c > \epsilon_c I \tag{2.57}$$

The solution is to find a $P \geq 0$, $Q_c > \epsilon_c I$, and $N \in \Re_{r \times q}$ so that the system is passive and controllable.

2.5.2.4 Passivity Based LQG

Reconsider the following state space system of the LQG design problem.

$$\begin{aligned} \dot{x} &= Ax + B_u u + B_u \gamma + B_d d \\ \tilde{y} &= C_{\tilde{y}} x + D_u u + D_d d\xi \end{aligned} \tag{2.58}$$

Again with the observer dynamics are given by equation 2.59 and Kalman estimator gain L given by $L = P_e C_m^T R_e^{-1}$, and the control gain K_x given by a similar Riccati solution.

$$\dot{\hat{x}} = [A - LC_y - B_u K_x - LD_u K_x]\,\hat{x} - Ly \tag{2.59}$$

$$u = -K_x \hat{x} \tag{2.60}$$

With this formulation for the LQG controller there is no guarantee of the passivity of the controller even if the system from which the observer is derived is passive. However it is possible as shown in [74] to judiciously select Q_e ,Q ,R, and R_e such that the resultant solution for the controller is passive. However this controller may lack the performance as the noise and covariance matrices utilize no longer free for the user to choose. In many cases this may be fine but there is some definite benefit to having greater flexibility in the selection of the weighting matrices. Next a method is proposed and described by which this may be done using an LMI framework. Begin with the equations for the LQG controller dynamics and the LMI formulation of the passivity condition given in equations 2.59 and 2.51 respectively. By substituting the controller A,B,C,D into the 2.51 you arrive at the following necessary sufficient condition for the passivity of the controller.

$$\begin{bmatrix} A_c^T P + PA_c & -C_c^T + PB_c \\ -C_c + B_c^T P & -(D_c + D_c^T) \end{bmatrix} =$$
$$\begin{bmatrix} [A - LC_y - B_u K_x - LD_u K_x]^T P + P[A - LC_y - B_u K_x - LD_u K_x] & K_x^T + PL \\ K_x + L^T P & 0 \end{bmatrix} \leq 0 \tag{2.61}$$

Again it should be noted that in practice the LMI solution converges better when there is a small nonzero element on the 22 of the matrix above. Even though it is not in the controller formulation a small addition of a "D" term doesn't adversely affect controller performance.

Now lets examine the solution for the optimal LQG observer in greater detail. In the traditional optimal observer design P_e is found by the solution of the Algebraic Riccati Equation (ARE).

$$P_e A^T + AP_e - P_e C_y^T R_e^{-1} C_y P_e + B_u Q_e^{-1} B_u^T = 0 \tag{2.62}$$

Note that in the above equation it is assumed that the input matrix for the process noise is the same as the control input matrix if this is not the case a more general G matrix can be used in its place and substituted in the subsequent equations. However this strict equality is more of a liability in the proposed multi-objective H_2 design (optimal observer and passive controller). This is because this formulation doesn't lend itself to solution as an LMI. What would be helpful is if the strict equality of this ARE could be relaxed and molded into an LMI framework. It can be shown and was in [71] that this can be done an that the solution of the general Riccati ($A^TP + PA^T + C^TC - PBB^TP = 0$) may be found by relaxing the problem to the following LMI's given in equation 2.63

$$\begin{bmatrix} AY + YA^T - BB^T & YC^T \\ CY & -I \end{bmatrix} < 0 \qquad \begin{bmatrix} Y & I \\ I & Q \end{bmatrix} > 0 \qquad Tr(Q_\epsilon) < \epsilon \tag{2.63}$$

For this particular ARE this becomes

$$\begin{bmatrix} AY + YA^T - C_y^T R_e^{-1} C_y & YB_u Q_e^{\frac{1}{2}} \\ Q_e^{\frac{1}{2}} B^T Y & -I \end{bmatrix} < 0 \qquad \begin{bmatrix} Y & I \\ I & Q \end{bmatrix} > 0 \qquad Tr(Q_\epsilon) < \epsilon \tag{2.64}$$

where $Y = P_e^{-1}$. Now rewriting equation 2.61 in terms of Y using the definition of L provided above yields:

$$\begin{bmatrix} [A^T - K_x^T B_u^T - (C_y^T R_e^{-1} C_y - C_y^T R_e^{-1} D_u K_x)^T Y^{-1}]P + P[A - B_u K_x - Y^{-1}(C_y^T R_e^{-1} C_y - C_y^T R_e^{-1} D_u K_x)] & K_x^T + PY^{-1} C_y^T R_e^{-1} \\ K_x + (C_y^T R_e^{-1})^T Y^{-1} P & \delta I \end{bmatrix} \leq 0 \tag{2.65}$$

$$P > 0 \tag{2.66}$$

Similarly the relaxed ARE for the controller is given by 2.67

$$\begin{bmatrix} AY_c + Y_c A^T - B_u R_c^{-1} B_u & Y_c (Q_c^{\frac{1}{2}})^T \\ Q_c^{\frac{1}{2}} Y_c & -I \end{bmatrix} < 0 \qquad \begin{bmatrix} Y_c & I \\ I & Q_\gamma \end{bmatrix} > 0 \qquad Tr(Q_\gamma) < \gamma \tag{2.67}$$

where $Y_c = P_c^{-1}$ is the inverse of the solution of the control optimal state feedback ARE. This result allows for the substitution for $K_x = R_c^{-1} B_u^T P_c = R_c^{-1} B_u^T Y_c^{-1}$ into 2.61 (not shown for brevity).

Efforts are ongoing in formulating a bandlimited version of this approach. This will be accomplished with a series of weights that are incorporated into a new system of LMI's capturing the passivity and small gain objectives respectively. Although preliminary, the results show promise for melding the small gain and passivity based approaches to the robust control problem for certain types of structured H_2 control.

2.5.3 Model and Controller Reduction

After modeling the system either computationally or using blackbox system ID techniques, the first problem that usually arises is that realization of the system is both non-minimal (as a artifact of it's construction) and high order. This becomes more problematic when working with highly MIMO systems, larger and larger frequency ranges, and high order controllers. When it comes to the practical implementation of these designs, simpler (smaller) designs are a must. There are two methods used to reduce the order of the model and the controller for simulation and implementation. First of these is by finding a minimum realization and the second is by using a balanced residualization. The procedure for finding a minimum realization by Kalman decomposition is presented in any variety of introductory linear systems texts. The concept behind a balanced residualization is different though. Given a state space system with controllability and observability grammians Q_c and Q_o. The balanced grammian is found by finding a state transformation T for which $TQ_cT^T = T^{-T}Q_oT^{-1} = Q_b$. The matrix Q_b is diagonal and the same size as the transformed state description. Furthermore, under this state description Q_b's entries are descending and give a direct measure of how important a particular state is to the input-output response. This provides a convenient approach for reducing the number of states in the model while preserving the input-output response as best as possible.

3 Modeling of the Plate and Enclosure System

Past efforts in active structural acoustic control have exposed the major difficulties with using a MIMO approach to ASAC. The difficulty; how is the best way to synthesize the controller? When using a MIMO design a control designer is has fewer techniques at their disposal including model based controllers (like LQG), resonant mode controllers, H_∞ based designs, passivity based designs, and frequency weighted or constant gain position,velocity, or acceleration based feedback designs. Although this list is by no means complete it represents most of the major approaches to MIMO design for ASAC. A second difficultly is also related to control design and that is, the modeling process. In the modeling process, it is quite common that some of the dynamics are left unmodeled. If unaccounted for or neglected in the control design and analysis, these unmodeled dynamics will lead to spillover or worse instability in the presence of the control action. Third, while in SISO it is possible to maintain collocation of sensor and actuator (in order to avoid RHP zeros and their detrimental effects on performance), MIMO systems will generally not have perfect collocation of sensors and actuators for all channel combinations. This means that spatially induced delays will produce RHP zeros unless special care is taken to passify the system. A final problem experienced in the MIMO ASAC problem is the large size of the system models. Often as many as a 60-70 state model may be required to effectively capture the system dynamics over a 1000Hz range and this is in simulation where the basic form of the system model is known. When experimentally identified models are generated it becomes even more difficult to construct low order models. This presents a problem for both design and implementation. Higher order models, containing at best 60-70 states, make the using model based controllers more difficult in practice. This is because the order of the controller will in the best case be the same order as the plant (without model reduction) and for some controllers (like H_∞) the order will be even greater. If you computer is sufficiently fast this may not present a problem for simulation of controllers for MIMO ASAC problems but when one attempts to implement these controllers on real hardware in real time this will present a whole host of problems. This is further compounded by the fact MIMO ASAC systems must be sampled at a high enough rate (on many channels in this case up to 25) so that discrete sampling effects do not present a limitation in the performance of the controller. A general rule of thumb is that if it is desired to control a frequency range up to 1000Hz then one needs to sample at least 10 times faster than this or up to 10000Hz. Collectively the necessary digital filters, the high sampling rate, the MIMO system, and the high system order work together to limit the size of controller that can be practically implemented. This in part helped to motivate the control architecture investigation in this dissertation.

In order to explore approaches to control that were more implementable in MIMO ASAC systems, the following qualities were required: 1) reasonable (¡40) controller state size, 2) a design methodology that lends itself well to highly MIMO systems (more than just 2x2), and 3) a control approach that is inherently robust. To achieve these qualities several ideas were explored. First was passive redesign of the system by plate mode shape optimization. Next the concepts and intuition gained in this investigation were applied to active control. Lastly other approaches to passifying (mathematically speaking) the system used in active structural acoustic control were investigated (passifying filter/controllers, and sensors blending). For all of these approaches what is first needed is an analytical control design model. In the following section the specific development of a coupled model of two enclosures separated by a plate will be discussed. Then the simulation efforts to redesign the structure of the plate for reduced noise transmission through the plate are discussed in section 4. Then in section 5 control simulation on this analytical model are conducted to evaluate various control approaches.

3.1 The Computational Models of the Plate Enclosure System

This effort makes use of the theory and analytical developments of section 2 to construct a computationally based state space model of the 2 enclosure plate system. This process begins with the construction and solution of both a finite element method (FEM) model of the plate and a boundary element model (BEM) of the enclosures.

3.1.0.1 Acoustic Model

The BEM acoustic model used a uniformly discretized model of the interior surfaces of the enclosure (containing approximately 20,000 tessellated triangle mesh elements of an average of 1 square inch). Rigid boundary conditions for the enclosure were imposed. Both enclosures considered have interior dimensions of 96 in by 41.5 in by 41.5 in. A random sampling of 10 monochromatic point source locations was utilized to generate the source strength solution at the boundary. Then this boundary source distribution was represented at 10 random locations inside the enclosure. Next the monochromatic sources were swept through a range of frequencies, and in this way, simulated frequency response functions (frf's) were generated for each internal evaluation point. At this point, these frf's were imported into a model fitting tool (SOCIT) that uses the eigensystem realization algorithm (ERA) to fit a series of second order systems to the data in a least squares sense for a desired order of model. After running each of these 10 frfs through the algorithm using approximately 50 modes for the system order of each fit. The fitted model's eigenfrequencies were tabulated and a consolidated listing of all the fitted modes was produced. This tabulated list was then reduced by careful manual inspection to the first 63 modes (a time consuming approach). The first consensus mode starting at low frequency (69Hz) and moving to high frequency modes (723Hz). With this information the BEM was again called to generate the acoustic mode shapes for these frequencies by evaluating solutions for each of the point source locations (10 total) at a evenly spaced grid of internal points (to generate the acoustic modeshape for each modal frequency). These 10 different evaluations of the were then normalized and combined to eliminate the local effects of the point source in the solution (by first removing the region around the source from the solutions and then using the averaged result of the remaining nine instances at those locations. The end result was a composite modeshape and a modal frequency that matched very closely to the analytically predicted shapes (especially at low frequency). Table 3.1 shows a comparison of the first 10 eigenfrequencies of this approach to the analytical solution. Although this method was not absolutely needed for generating the model of the enclosures for a rigid rectangular box it is necessary if you desire to relax the boundary condition to an impedance boundary condition.

Table 3.1 Decoupled acoustic modal frequencies of each acoustic enclosure

Mode	**BEM Freq. (Hz)**	**Analytic Freq. (Hz)**	**Damping**
1	68.86	69.72	0.01
2	136.11	139.43	0.01
3	159.97	163.33	0.01
4	161.23	163.33	0.01
5	176.01	177.59	0.01
6	178.27	177.59	0.01
7	206.32	209.15	0.01
8	215.11	214.75	0.01
.		.	.
60	685.15	692.96	0.01
61	687.76	696.46	0.01
62	695.44	706.85	0.01
63	714.89	723.84	0.01

Using the modes and modeshapes of the enclosure an eigenfunction expansion of the pressure in terms of these modeshapes and modal coordinates $p(t) = \sum_i \Phi_{a_i} \mathcal{P}_i(t)$ is constructed. A finite dimensional linearized model of the plate can be represented by the equation 2.10.

3.1.1 The Plate Model

An FEM model of a clamped, square plate was developed first in ANSYS and then in FEMLAB. In both cases the plate was modeled as a Mindlin plate, in which the thin plate experiences bending, twisting, and transverse shear deformation. The plate considered is 0.515 m by 0.515 m and is approximately 0.0016 m thick. The material of the plate model is assumed to be steel with at density of 7850 kg/m^3 and an elastic modulus of 2.06e11 Pa. In the initial model (the baseline) there is only one square domain and this domain is meshed using a Delaunay triangularization (as seen superimposed in Fig. 3.1). The boundary conditions applied to edges of the plate are clamped boundary condition(s) meaning that both deflection and rotation degrees of freedom are fixed to zero. To begin the modeling process, a constrained eigenvalue problem was posed in FEMLAB and the first 20 eigenpairs were solved for. Next the mass matrix was extracted and the modeshapes from the eigensolution were mass normalized $(\Phi_p = \Phi_{p_{old}}(\Phi_{p_{old}}^T M \Phi_{p_{old}})^{-.5}$ using the extracted mass matrix. The first and second modal solutions appear in Fig. 3.1 and Fig. 3.2. A finite dimensional linearized model of the plate, written in the

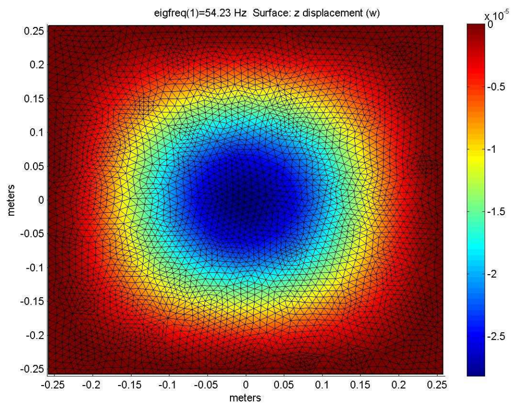

Figure 3.1 Flexible mode 1 for the plate

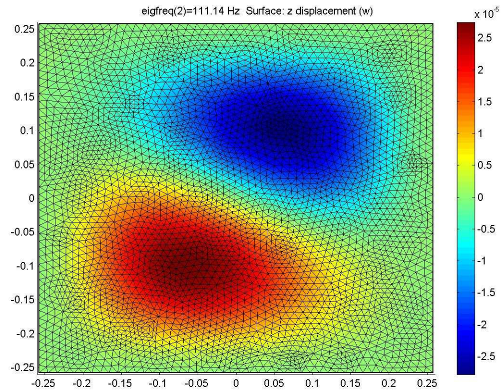

Figure 3.2 Flexible mode 2 for the plate

form of Eqn. (3.1) can be rewritten in the modal form as in Eqn. 3.1. This form can be constructed using mode shape and frequency information from the FEM solution:

$$\ddot{q}_p(t) + \tilde{\mathcal{C}}_p \dot{q}_p(t) + \Omega_p q_p(t) = \Phi_p^T f(t) \tag{3.1}$$

where, Φ_p is the mass normalized mode shape matrix of the plate, $q_p(t)$ are the modal coordinates, $\eta(t) = [\Phi_p]\{q_p(t)\}$, $\Phi_p^T M \Phi_p = I$, $\Phi_p^T \mathcal{C} \Phi_p = \tilde{\mathcal{C}}_p$, and $\Phi_p^T K \Phi_p = \Omega_p$. For the sake of this investigation the finite dimensional model was limited to first 10 modes as the modes 11 to 20 did not contribute significantly to the simulated structural response. These first ten modes are listed in table 3.2.

3.1.2 Coupling Acoustics and Structure

As mentioned in the background information in section 2, the fluid structure coupling method utilized in this work is known as the modal interaction model. The fluid loading in Eqn. 2.30 is expressed as a summation of the normalized acoustic eigenfunctions for the pressure multiplied by the element area S and the coupling matrix Π that indicates how each acoustic mode couples to each structural mode. Where the term $\Pi_{mn} = \frac{1}{S}\int_S \Phi_{a_m}(r_s)\Phi_{p_n}(r_s)dS$ defines the coupling term. The expression of the structure's affect on the fluid may be similarly expressed as the modal velocities of the plate multiplied by

Table 3.2 Modal frequencies of steel plate

Mode	**Freq. (Hz)**	**Damping**
1	54.2	0.01
2	111.1	0.01
3	111.1	0.01
4	164.5	0.01
5	200.8	0.01
6	200.8	0.01
7	252.9	0.01
8	252.9	0.01
9	323.6	0.01
10	325.6	0.01

the coupling matrix Π, c, S, and the inverse acoustic mass matrix Λ_a. To compute both of these terms the portion of the acoustic mode shape corresponding to the two dimensional domain of the plate is extracted from the acoustic eigenfrequency data. Then both the acoustic modeshape and the plate modeshape are interpolated on a regular grid. Next, a two dimensional Simpson quadrature integration is carried out on the product of the modeshapes at the plate interface. This coupling formulation shows directly that it should be possible to decouple portions of the dynamics of the structure and acoustics simply by redesigning (passive approach) or actively (suppressing) the vibration pattern of the modeshape. However the difficulty lies in how a redesign to target one mode, causes unintentional and undesired effects on the other modes (passive case) or energy from controlling one mode adversely excites other modes. After investigating the coupled acoustic and structural models using these methods, it was found that it is extremely important to include enough modes to accurately model the coupling phenomenon. For example, the region of interest for this analytical modeling is only from zero to 400 Hz. However, if you allow the number of acoustic modes considered in the coupled model to extend beyond 400 Hz (say up to 700 Hz as in model 1) then the frequency response is significantly different than if you only consider modes up to the 400 Hz range (as in model 2). In an uncoupled model truncating higher frequency modes will only affect the frequency response significantly if the modal frequencies are in close proximity to the region of interest. This is because the coupling induced by viscous damping decreases significantly farther away from the mode (in frequency). However, this gyrostatic coupling of the acoustic and structural modes doesn't behave in the same way. This indicates that one needs to be very careful when limiting or selecting the number of modes that are included as it could drastically affect the frequency response. Due to the nature of the coupling integration, the spatial distributions of higher order modes, and the inherent damping of the uncoupled modes this effect should diminish as you go farther out in frequency (just not as intuitively as in the uncoupled case). For the final formulation of the statespace that will now be described, appropriate accuracy was determined by investigations to be a model consisting of the first 10 structural modes and the first 26 acoustic modes.

3.1.3 Construction of State Space Model

In order to construct the state space model given in section 2.4.1 sensor and actuator type, dynamics, and location need to be defined. The equations for the plate and the enclosures can now be formulated into a $2 * n$ dimensional state space representation (with n equal to the combined number of structural and acoustic modes in the finite dimensional model plus the states for actuator and sensor dynamics). As stated previously there are 10 structural modes and 26 acoustic modes for each enclosure meaning that there are 124 states in the model –actuator and sensor dynamics not withstanding. This has the form shown in equation (2.32). In this previously supplied expression, the matrix $A = A_{coup} + A_{dec}$ and a_s and a_d indicate the source and destination enclosures.

3.1.3.1 Sensor Types and Location

There were four types of sensors considered in this model. The first was a control (button) microphone and its associated analog filters and gains. These microphones are used exclusively in close proximity to the plate in simulation, and always in the same number as the number of actuators (so as to yield a square plant).

The second type was a performance microphone (PCB) with its conditioning electronics. In this simulation model these were used as a measurement of the specific SPL at a user desired point, if the sound level at a specific point was a metric of interest. More commonly these sensor types were used in great numbers 50-100 in each enclosure total to determine the average sound level in the enclosures. These 50 to 100 points were randomly distributed in each of the chambers exactly as is shown in Figs. 3.3 and 3.4 Another type of sensor was the piezo patch which translates local strain of the

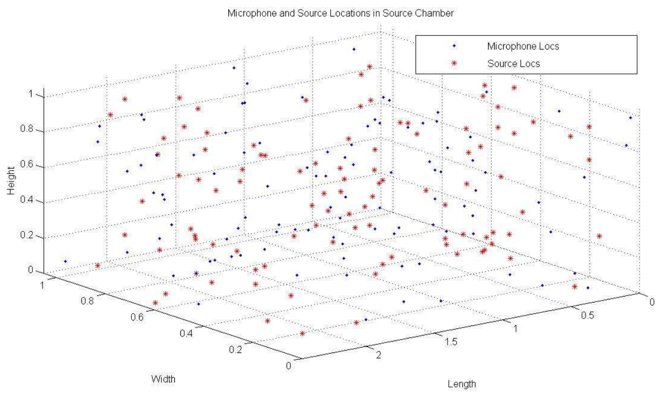

Figure 3.3 The microphone and simulated source locations on the source side

plate under the patch to a voltage signal. In this sensor configuration the current in the circuit is directly proportional to the velocity furthermore by using an actuator of the same size as the sensor patch this perfect co-location yields a passive combination.

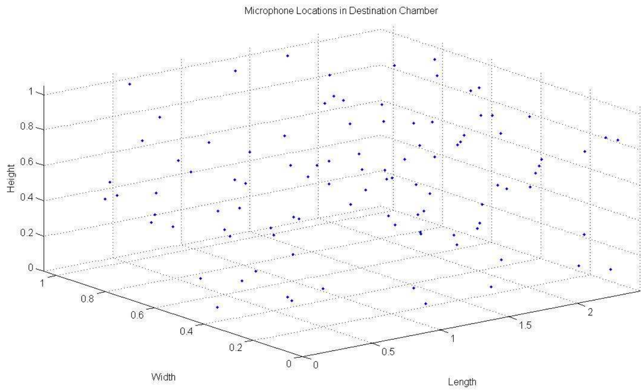

Figure 3.4 The microphone locations on the destination side

The last type were accelerometers that could then be integrated to yield velocity or position output signal. Along with the sensors were their associated filter and conditioning electronics.

3.1.3.2 Actuator Types and Location

In the analytical models there were three types of actuator descriptions utilized. The first was a simple point acoustic noise source for generating the disturbance to the model. Many of these sources were randomly distributed throughout the source enclosure and the source levels adjusted to give approximately 100dBA SPL in the source enclosure. More complicated models, considering source dynamics and spatial directivity, were not considered as the goal was merely to achieve desired sound levels in the enclosure. After initially using 50 sources, a smaller number of about 15 was found sufficient to excite all the dynamics of the enclosure model and achieve the 100dBA SPL. The second type of actuator considered was a structural point force actuators and their associated dynamics (these are in essence the inertial shakers developed for experimental work). These actuator types were used in varying numbers from 1-16 across the plate in simulation although the final number used for experiment was 5. The other type of simulated actuator considered was a Piezo actuator and the associated dynamics.

These were also used in numbers ranging from 1-16 and in varying sizes. Piezo actuator behavior is described by the following equations. As stated earlier piezoelectric devices respond to the presence of an electric field by deformation in one or more of their crystal planes. For the shear type actuators used in this investigation the electrical to mechanical stain coefficient is d_{31} the electric field between the two contact plates is given by $E = V_a/t_a$ where V_a is the voltage across the contacts and t_a is their separation. Thus the associated strain-voltage relationship is

$$\epsilon = \frac{d_{31}}{t_a} V_a \tag{3.2}$$

with elastic modulus of the piezo E_a the expression for the stress is

$$\sigma(x,t) = \frac{E_a d_{31}}{t_a} V_a(x,t) \tag{3.3}$$

Then the associated induced bending moment is give by where K_a is a lumped constant incorporating geometric parameters, and material quantities, and loss factors due to bonding non-idealities.

$$M_a = \int_{\frac{t_p}{2}}^{\frac{t_p}{2}+t_a} K_{loss}\sigma(x,t) w y dy = K_a V_a(t) \tag{3.4}$$

3.1.3.3 Actuator and Sensor Dynamics

The model development thus far has considered only a plate and acoustic states with direct forces, pressures, or moment applications and direct measurement of position, velocity, or pressure entering into the state space description. This is without regard for any actuator or sensor gains or dynamics. However this is somewhat inaccurate and a better description would be to describe the dynamics relating voltages to forces or moments in the actuators and pressures,accelerations, velocities, and positions to outputted sensor voltage. Consider the block diagram in Fig. 3.5. In this block diagram the plate-enclosure dynamics are represented by $G_{plant}(s)$, the actuator dynamics are represented by $G_{act}(s)$, and the sensor dynamics are represented by G_{sens}. Also the new

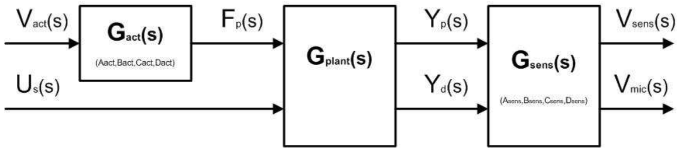

Figure 3.5 Block Diagram of Actuator/Sensor and Acoustic-Structure Dynamics

signal $\vec{v}(t)$ is the input that drives the actuators to produce a force/or moment which is still applied at the nodes. The state space representation of the system with actuator dynamics (neglecting disturbance input at the sources) is given in Eqn. (3.5) and this is then used to add the sensor dynamics in Eqn. (3.6). This general form of model was used for simulation, passive tailoring, and control design investigations.

$$\begin{bmatrix} \dot{\vec{x_p}}(t) \\ \dot{\vec{x_s}}(t) \\ \dot{\vec{x_d}}(t) \\ \dot{\vec{x_{act}}}(t) \end{bmatrix} = \underbrace{\begin{bmatrix} A_p & C_{a_{s2p}} & -C_{a_{d2p}} & B_p C_{act} \\ C_{p2a_s} & A_s & 0 & 0 \\ -C_{p2a_d} & 0 & A_d & 0 \\ 0 & 0 & 0 & A_{act} \end{bmatrix}}_{\tilde{A}} \begin{bmatrix} \vec{x_p}(t) \\ \vec{x_s}(t) \\ \vec{x_d}(t) \\ \vec{x_{act}}(t) \end{bmatrix} + \underbrace{\begin{bmatrix} 0 & 0 \\ 0 & B_s \\ 0 & 0 \\ B_{act} & 0 \end{bmatrix}}_{\tilde{B}} \begin{bmatrix} \vec{v_{act}}(t) \\ \vec{u_s}(t) \end{bmatrix}$$

$$\begin{bmatrix} \vec{y_p}(t) \\ \vec{y_d}(t) \end{bmatrix} = \underbrace{\begin{bmatrix} C_p & 0 & 0 & 0 \\ 0 & 0 & C_d & 0 \end{bmatrix}}_{\tilde{C}} \begin{bmatrix} \vec{x_p}(t) \\ \vec{x_s}(t) \\ \vec{x_d}(t) \\ \vec{x_{act}}(t) \end{bmatrix} + [0] \begin{bmatrix} \vec{v_{act}}(t) \\ \vec{u_s}(t) \end{bmatrix} \quad (3.5)$$

$$\begin{bmatrix} \dot{\vec{x}}(t) \\ \dot{\vec{x_{Sens}}}(t) \end{bmatrix} = \begin{bmatrix} \tilde{A} & 0 \\ B_{Sens}\tilde{C} & A_{Sens} \end{bmatrix} \begin{bmatrix} \vec{x}(t) \\ \vec{x_{Sens}}(t) \end{bmatrix} + \begin{bmatrix} \tilde{B} \\ 0 \end{bmatrix} \begin{bmatrix} \vec{v_{act}}(t) \\ \vec{u_s}(t) \end{bmatrix}$$

$$\begin{bmatrix} \vec{v_{sen}}(t) \\ \vec{v_{mic}}(t) \end{bmatrix} = \begin{bmatrix} D_{Sens}\tilde{C} & C_{Sens} \end{bmatrix} \begin{bmatrix} \vec{x}(t) \\ \vec{x_{Sens}}(t) \end{bmatrix} \quad (3.6)$$

Piezo and Amplifier Dynamics: The form of the diagonal entries into the diagonal NxN actuator transfer matrix depends on the type of actuator and the gain of the driving amplifier. For the piezo actuator this form is that of a high pass filter (due mostly to the amplifier dynamics) with a high frequency gain equal to $K_a K_{amp}$ from Eqn. 3.4 and a cut in frequency of $f_c = 100Hz$. For this investigation the specific values necessary to calculate K_a are: $d_{31} = 23e - 12$m/V, $t_a = 100e - 6$m, $E_a = 2e9$N$/m^2$, $K_{loss} = .5$,and a length and width of .10 m. The identified amplifier gain K_{amp} was nearly 50 times. These values were utilized to calculate voltage dependent moments at discrete locations. These were then multiplied into mode shape components corresponding to the Θ_x and Θ_y DOF's to get the forcing term on the structural equations from this couple.

Point Source and Amplifier Dynamics: The form of these diagonal entries for a point source inertial driver was that of a moderately damped second order system driven by a force nearly proportional to the voltage in the coil (actually this is a 2nd order system coupled with an series RL circuit but at lower frequencies $< 2000Hz$ the voltage current relationship is dominated by the resistance). This transfer function for position of the reciprocating mass relative the base of the second order system can then be twice differentiated and multiplied by mass to yield the force load on the structure in terms of the applied coil voltage as is shown in equation 3.7. The properties of the system modeled, were a cut in frequency of around 20Hz (i.e. $f = \sqrt{\frac{K}{(2\pi)^2 m}}$), and a damping of $C_{damp} = 2\pi f 2(\zeta)$ with $\zeta = .1$. The experimentally determined values of $K_{coil} = 0.0942$ and $K_{pAmp} = 33$.

$$F(s) = \frac{K_{pAmp} K_{coil} s^2}{s^2 + \frac{C_d amp}{m} s + \frac{K}{m}} V_{act}(t) \tag{3.7}$$

Sensor and Signal Filter Dynamics: The sensors considered in our study all have associated sensor gains (which will vary somewhat in implementation), and also active low pass and high pass filters. The low pass was 4th order with a break frequency at 5000Hz, and the high pass was a 2nd order with a break frequency at 10Hz. Initially the gains of the devices and amps were not considered since the simulated sensors were simply assumed to have calibration constants of 1.

3.2 Resultant Models

There were two main types of models that were generated for control studies and those were co-located point force point sensor models and co-located piezo patch piezo sensor models. There are numerous variations on each of these models where sensors and actuators are intermingled in various combinations. However, there are too many variations to display here so for brevity only the two types mentioned above are shown. The following are relevant response plots and model details of the specific models constructed for the simulation work.

3.2.1 Point Force Actuated Point and Point Sensed Plate and Enclosure System

This model was developed using the methodology described above for 9 collocated plate sensor and actuator locations. The sensors were assumed to be accelerometers that were once integrated to give velocity. Other variations on this model include position sensors, and true acceleration sensors which were implemented by an approximate proper transfer function implementation of a derivative (since an actual derivative is problematic both in real life and in simulation/control design.) Figure 3.6 shows the bode plots of the plate sensors and actuators superimposed (as velocity is the output signal the collocated diagonal entries in the transfer matrix are passive combinations (as is evident also by the phase response). However the cross channels do not have this property as would be expected of non-spatially coincident sensors and actuators. Figure 3.7 shows the maximum singular value of the 100 source locations to the 100 microphone locations on the destination side. The were two primary reasons for using so many locations for sound sources first was to make sure that all the acoustic modes were excited and excited as uniformly as possible, the second is that it is a relic from some fully coupled FEM-BEM work that was conducted in support of this work. The maximum singular value response

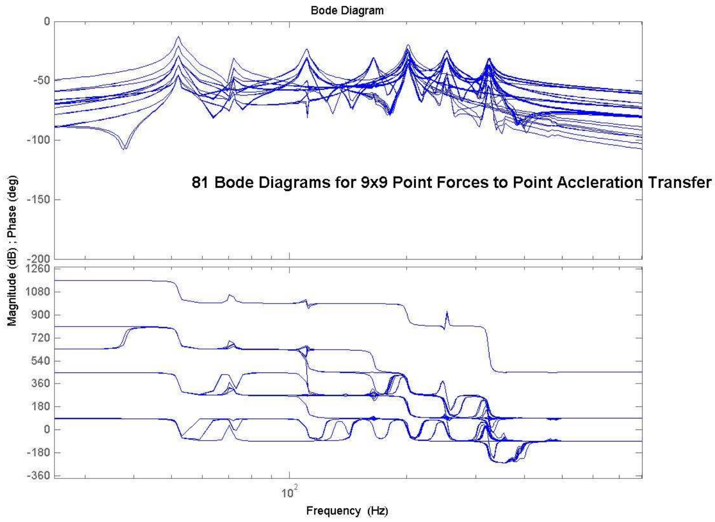

Figure 3.6 The 81 bode diagrams overlayed for the 9x9 actuator accelerometer matrix

may be thought of as a magnitude plot for a MIMO system wherein the plot indicates the maximum gain in any input direction and is a more compact and meaningful way of representing a system with so many inputs and outputs than plotting all the responses. The next two figure (3.8, and 3.9 show the maximum singular values of the cross term portions of the transfer matrix that is to say the response from structural inputs to microphone outputs and the responses from sound source inputs to structural sensors.

3.2.2 PVdF Patch Actuated and Sensed Plate and Enclosure System

The actuators were assumed to be piezo patches. The sensors in this were now assumed to be piezo patches that were once differentiated integrated to give velocity. Other variations on this model include piezo position sensors, and piezo acceleration sensors. Again all derivatives were implemented by an approximate proper transfer function of the derivative. One major difference from the last sensor and actuator is that these patch sensors/actuators are not sensing or actuating at a discrete point but

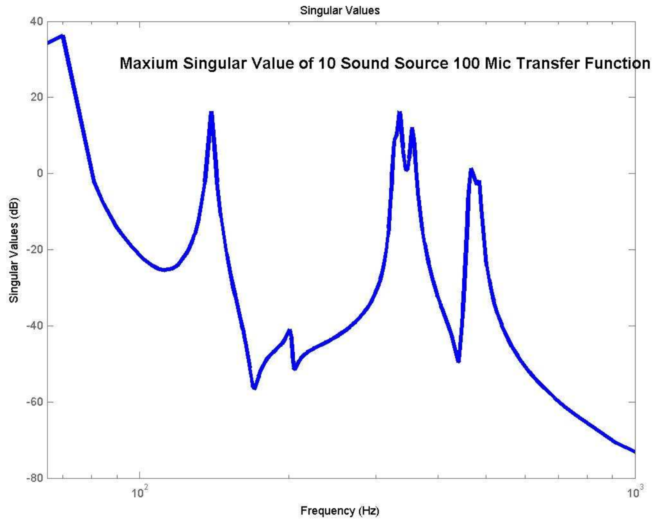

Figure 3.7 The maximum singular value from the sound source locations to the mic locations on the destination side

instead are sensing or actuating in a spatially averaged way over the 4x4 inch squares of the patch actuators. This means that this approach will avoid some of the problems with introducing a local deformation in the plate effect due to the actuation that might be expected in the point force actuators, it also means that it may be possible to capture a better picture of the local plate deformation and thus a more complete picture of the coupling and radiation properties of a small portion of plate using just one sensor. However there are a couple of drawbacks to this approach. First, the actuators are not as strong as their point force counterpoints and must be driven much harder. Second at higher frequencies this spatial averaging of the plate motion properties will tend to filter out the vibratory signal of modes that are on the same length scale as the patch and this could be a major problem. Figure 3.10 shows the bode responses of the piezo actuators to piezo sensors. Again since the responses are analogous to applied moment actuation to and measured rate of bending sensing on the plate the pair constitutes a passive combination when located at the same spatial location (i.e. the diagonal terms of the transfer matrix). The maximum singular value of the 100 source locations

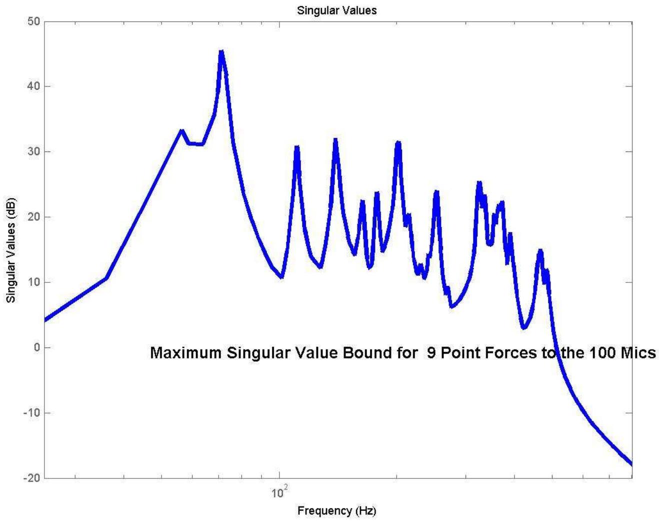

Figure 3.8 The maximum singular value of the point force actuators to the performance microphones

to the 100 microphone locations on the destination side is unchanged by the new plate configuration (in this simulation at least due to the assumption that the addition of the actuators has not changed the passive properties of the plate). This response is still give by figure 3.7.

The next two figure (3.11, and 3.12 show the maximum singular values of the cross term portions of the transfer matrix that is to say the response from structural piezo inputs to microphone outputs and the responses from sound source inputs to structural piezo sensors. All in all the responses have the same general characteristics but there are some small difference in some couplings that in the point force and point sensor case.

3.3 Concluding Remarks

In this section a computational model was developed from using the outline of section 2. FEM and BEM models were produced and then relevant information was extracted

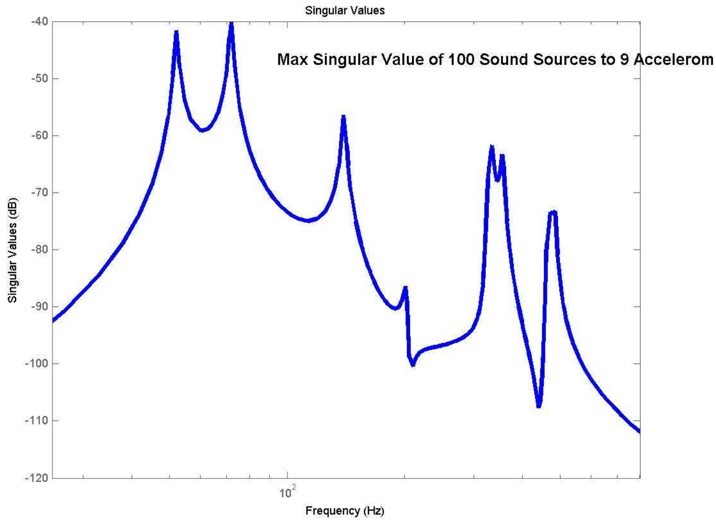

Figure 3.9 The maximum singular value of the acoustic inputs to the structural sensors

and further processed to produce coupled model of the acoustic enclosure and plate system. In the process of generating this model information was gleaned as to what plate and acoustic modes are most responsible for transmission of sound in these resonant enclosures. Even if the modal interaction model mechanism doesn't perfectly replicate the experimentally observed responses it is a good place to start as the next level of complexity would be the solution of a fully coupled FEM-BEM model of the system (a time consuming and computationally costly approach). This simpler coupled acoustic structure model still gives insights into system behavior and can now be applied to study both parts of the active passive control design problem in the subsequent sections.

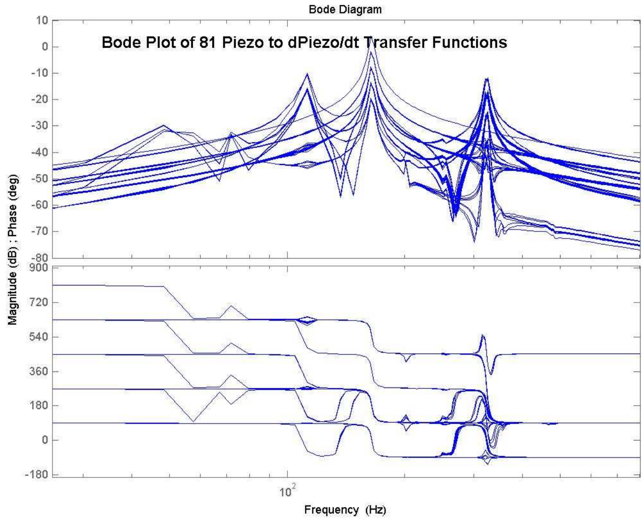

Figure 3.10 The 81 overlaid bode plots of the piezo to piezo transfer functions of the transfer matrix

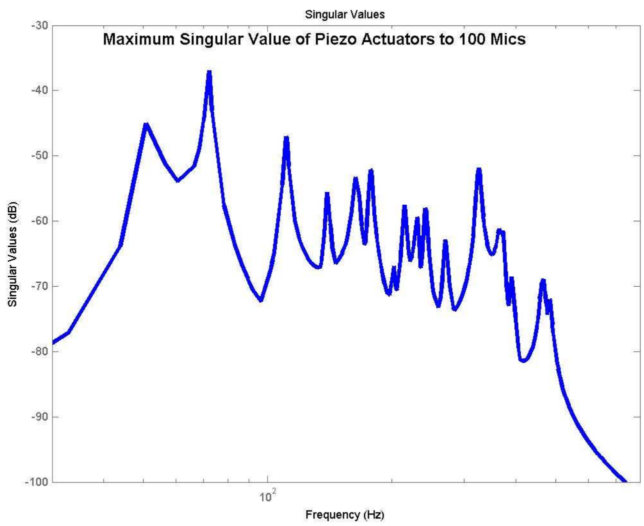

Figure 3.11 The maximum singular value of the piezo actuators to the performance microphones

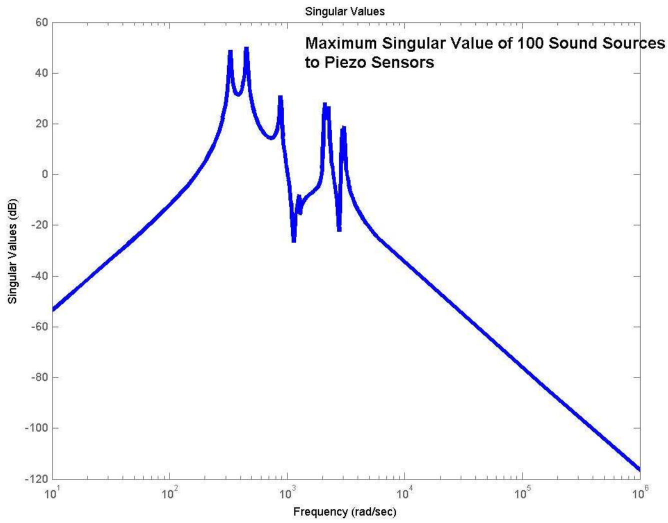

Figure 3.12 The maximum singular value of the acoustic inputs to the piezo sensors

4 Passive Redesign of Plate Structure

This section will address the first half of the central question: *Is it possible to develop a methodology for passive redesign of the plate structure that decreases coupling and the sound level in the enclosure system?* While there are undoubtedly many ways to attack this problem, the approach selected here is chosen for its high speed of implementation. This is a must for eventual integration into a combined control–structure optimizer. These approaches are also attractive for their potential to be posed in the same context as many different control optimization problems. This is discussed further in the conclusions and future work section 8).

4.1 Passive Redesign

Active noise control in MIMO structural acoustic systems, like the ones modeled above, is fraught with challenges. First, these systems are modally rich, meaning that unless high order models are utilized for system models the controllers designed will be plagued with robustness issues due to unmodeled dynamics and control spillover. Second, there are RHP zeros introduced in the cross terms due to a lack of spatial collocation, from the sensor and actuator in these terms. These have disastrous implications for the stability and performance of your controller. Third, the high order of the required control design models and the highly MIMO character means that control design techniques are more limited. It is more difficult to design weights and gains, and the controllers become high order and thus difficult to implement experimentally. Lastly, most controllers designed for the ASAC problem do not reduce energy everywhere in space. In fact, these controllers typically fail to reduce energy across a broad range of frequencies due to coupling of modes, RHP zeroes, and waterbed effects.

One of the goals in this dissertation is the exploration of techniques that yield stable, performing controllers that can be realized in both simulations and physical systems. Several approaches were explored to this end, such as: collocation and passivity based controllers, passive design inspired control approaches, spatial filtering with resonant mode control, and coupled structural redesign and control (redesign of the structure to concentrate energy and make control more effective). A central premise of this work is that no matter what the active control approach, the best way to yield a truly robust, broadband reduction requires also utilizing a passive design or redesign approach. This effort then will provide both intuition for active control design and the framework for a combined active passive control optimization in the future.

With the goal of noise reduction from source to destination enclosures, several investigations were conducted where the plate structure was passively redesigned. Numerous studies have conducted such redesigns. In a work by Koopman [59] discrete masses were placed on the surface of a plate to reduce its radiated acoustic energy. In Koopman's investigation the spatially integrated velocity of the modeshapes (the volume velocity) is as close to zero as possible. This causes the plate to radiate sound poorly at low frequencies.

In this work, a similar approach is presented, along with a redesign method based on the tailoring of the plate stiffness. Additionally an alternate (but similar) target was explored. Namely, reducing the coupling terms in the above mentioned acoustic structure coupling developed in section 2.4. Additionally, these results are explored and discussed for several different sizes of enclosure model.

4.1.1 Conceptual Approach

Traditionally a structural redesign is conducted with target performance objective of a reduction in radiated sound power. Sound power radiated from a plate mode can be generally written as $P = \frac{1}{2}\rho_o c\sigma S\langle v_N^2\rangle$, where ρ_o and c are fluid density and sound speed, σ is the radiation efficiency, S is the area, and v_N is the modal normal velocity. The radiation efficiency σ is a wavenumber ($k = \omega/c$) dependent quantity which will cause the power radiated from a particular modal velocity pattern to change with both the spatial scale of the pattern and with frequency. This is similar in behavior to a number of simple point sources located at the maxima and minima of the modeshape. At low dimensionless wavenumbers kd, where d is the source separation distance, these sources exhibit a canceling effect, and the radiated sound power is effectively the sum of these signed sources. However, at larger kd this is no longer the case and an expression for σ must be developed. The modal volume velocity is defined as the spatially integrated normal modal velocity. Volume velocity is an accurate measure of how well a particular structural mode will radiate, but only at low frequencies. This is because the integration is a parallel the summation of the discrete sources at low wave number, just as with the discrete sources the high frequency behavior is dependent on σ and the absolute value of the normal velocity. This means that approaches like those in [59] (which seek to balance velocity such that volume velocity source and radiation are minimized), are only effective for low kd. This is completely acceptable for low frequency noise; however a better target for all frequencies is to minimize the square of the normal velocity distribution. Minimization of the sound power without regard to the volume velocity is even more preferable.

Additionally, the redesign of plate the structure such that the coupling between acoustics and structure are lessened is investigated. This approach is limited only by the validity and accuracy of the coupled acoustic structure model. However, the modal interaction model is only meant to be accurate in low frequencies where the density of acoustic and structural modes is low. Coupling may be reduced either by decreasing the value of the individual coupling coefficients, or by weighting their summation into a particular modal equation. In this work, a combination of these approaches was used. First, the most important coupling coefficients were reduced. Other coupling terms are then optimized for a given design space such that when multiplied into their respective states and summed, the response from source side to destination side is minimized. This redesign was accomplished in two ways. In one the mass on a plate was redistributed optimally among nine locations and the rest of the plate. In the second the plate was strategically stiffened without changing the mass distribution.

4.1.2 Implementation in Simulation

Both the mass redistribution and the stiffening investigations were conducted in FEMLAB^{TM}. FEMLAB^{TM} is a finite element package whose commands and parameters are fully accessible from Matab^{TM}. In fact a model can be developed and solved in the FEMLAB^{TM} GUI and then the command sequences can be output to a Matlab^{TM} mfile. This makes it very easy to conduct parametric investigations and optimizations on finite element models. For these simulations two finite element mfiles were created; one which accepted an argument for changing the mass distribution and the other which accepted an argument for the placement and design of several stiffeners. Then a plausible design space was selected for the variable parameters and the mfile FEM model was modified to search over it and find the minimum.

4.1.2.1 Coupling Analysis

Before undertaking further analysis it is desirable to gain better intuition for which coupling terms are of greatest importance in noise propagation between chambers. To do this each of the individual coupling terms were changed one at a time by 10% and the resultant change in the averaged predicted response was plotted for each of the terms entering into a particular structural mode. Several of these plots appear in figures 4.1,4.2,4.3.

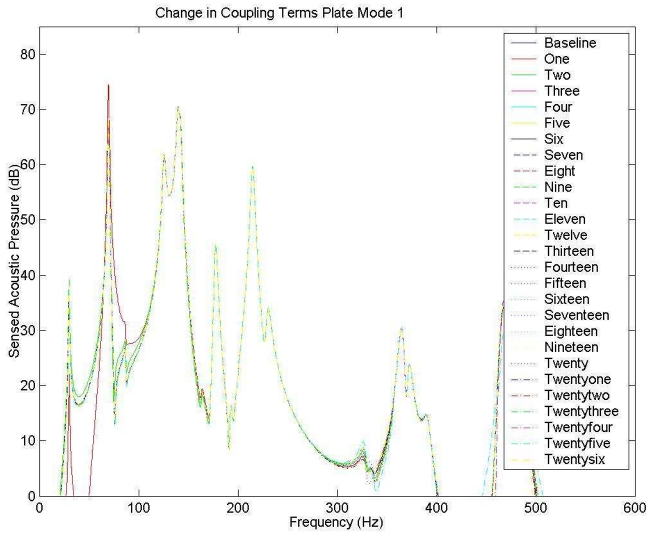

Figure 4.1 Plots of Effects of coupling terms involving plate mode 1.

4.1.2.2 Sensitivity Analysis

The first step in this investigation was to create a two parimetrically defined FEM models of the plate, then link this into the above coupled acoustic structural model (with microphones and sound sources) to allow for evaluation of the sensitivity of acoustic energy to changes in the plate. The first FEM model utilized the same base plate as the one described earlier, modified to have 625 equally spaced domains. When exported to m-file code from the FEMLAB GUI a sensitivity analysis routine was integrated directly in to the geometry, material definition, and mass and stiffness matrix assembly routines of the Mindlin plate FEM model. The basic approach is to independently perturb the thickness of each domain of the panel by a small increment, and then extract the complete structural modal expansion from the new mass and stiffness matrices. It should be noted

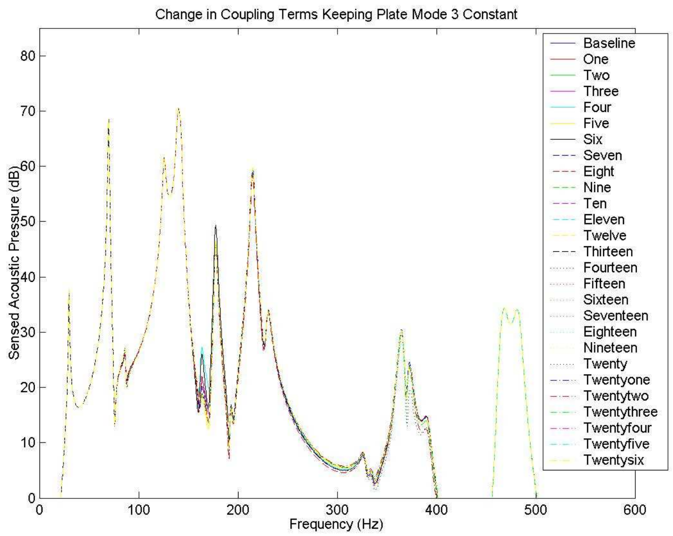

Figure 4.2 Plots of Effects of coupling terms involving plate mode 3.

that these changes have no appreciable effect on global stiffness. From these matrices a new coupled structural acoustic model with microphones and sound sources is generated. Next the 100 simulated sources were excited with a white noise excitation signal and the simulated 100 microphones measured then FRF of these signals were calculated and averaged over all the spatial locations and integrated to determine a good estimate for the average acoustic signal energy in the destination enclosure. This energy was then compared to the nominal case and the difference (ΔE_s) was divided by the thickness perturbation (Δt_p) to yield an rough estimate of the sensitivity to this change after doing this for each of the 625 domains the absolute value of the results normalized to the range from zero to one and distributed into a set of discrete bins (10 total). This process is repeated for several different seed meshes, and thicknesses Δt_p to determine and minimize mesh effects and nonlinearities in the energy thickness relation. A color coded plot of the average normalized sensitivities to mass changes is presented in figure 4.4. This plot indicates several regions as being excellent candidates for mass changes, and helps form the basis for the subsequent mass distribution optimization.

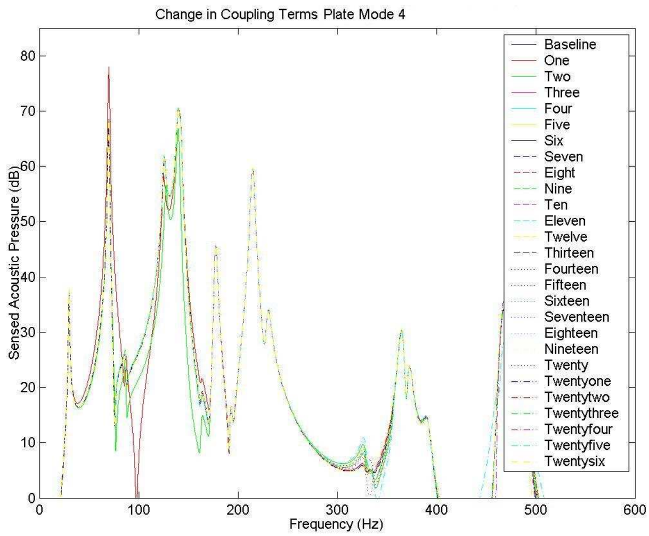

Figure 4.3 Plots of Effects of coupling terms involving plate mode 4.

4.1.2.3 Mass Redistribution

A basic statement of this problem is to modify the mass normalized structural modeshape and thus the coupling coefficients through the subtraction of plate mass from some areas and the addition of plate mass to others. This is accomplished by parametrically defining the thickness of the Mindlin plate model over the 10 subdomains shown in figure 4.5. These regions are based on those spots indicated by the sensitivity analysis. Changing the thickness over domain 1 also changes the stiffness of the panel. However this stiffness change was a secondary factor, and the primary mechanism for modification was the redistribution of mass to the concentrated locations 2 through 10. In fact similar results were obtained with only the addition of discrete masses; however it was not clear whether the change occurred due to the redesigned modeshapes or due to the overall increase in the plate's mass. Therefore, this investigation allowed the subtraction of mass elsewhere such that the total mass added is kept to a small percentage of the original value. Starting with the nominal uniform plate (whose properties are given

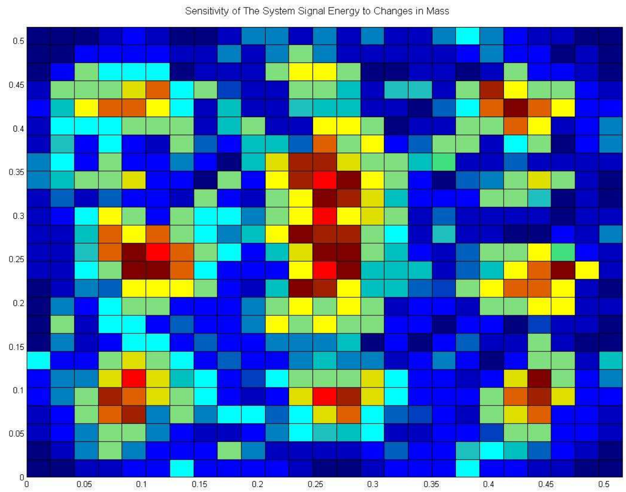

Figure 4.4 The sensitivity of plate domains to changes in mass.

above) which is clamped on its boundary, mass is added to or subtracted from all of the numbered subdomains subject to the following constraints:

- Total mass stays within 15% of original value
- The mass of subdomain 6 should account for less than 30% of the total mass
- The combined mass of subdomains 3,5,7,and 9 should account for less than 15% of the total mass
- The combined mass of subdomains 2,4,8,and 10 should account for less than 35% of the total mass.

After constraining the design parameters, minima were found on the design space. For this space, the performance metric of spatially averaged signal energy displayed a non-convex behavior and the result of this optimization was likely suboptimal. To possibly improve upon this result the solution was perturbed several times (in a simulated annealing approach) in an iterative fashion until either a maximum number of iterations were reached, or until the optimization converged consistently to the same values. The

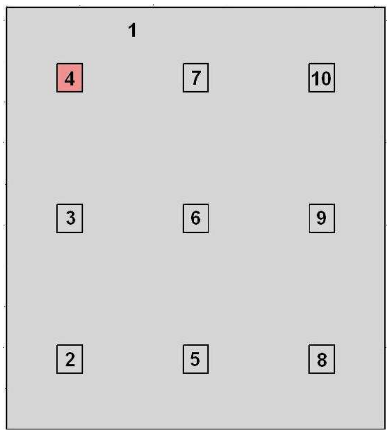

Figure 4.5 Subdomains for mass redistribution.

initial design target was the largest mode for the coupled acoustic structure system—this occurred at 70 Hz, corresponding strongly to the first acoustic mode. The optimization approach was then applied to the 10 domains above to redesign of the structural modes coupled to this first acoustic mode to be directly targeted. The thickness parameters over each of the subdomains were then optimized.

4.1.2.4 Sensitivity to Stiffness

As in the previous case, a parametrically defined FEM model of the plate was developed and inserted into our enclosure structure model. In this case, instead of modifying the mass of individual elements, the stiffness of the elements is modified (while keeping area mass constant). The same procedure of optimization is then followed as with the mass sensitivity analysis. Unfortunately, the result shown in figure 4.6 was not at all helpful except to indicate that islands of stiffness do not have an appreciable effect on the overall stiffness of the plate. Thus there is little to no effect on the signal energy of microphones from modifying single elements. The domains which have greatest effect from modified stiffness are closest to the boundary where the change effectively stiffens the plate as a whole. This indicates that boundaries may be a good starting point for structural stiffening, but to have a large effect a global patterning approach is necessary.

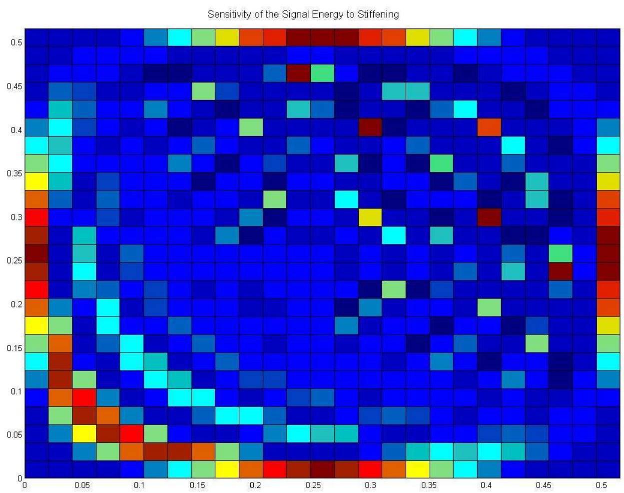

Figure 4.6 The sensitivity of plate domains to changes in stiffness.

4.1.2.5 Plate Stiffening

Two plate stiffening patterns were initially investigated for achieving a desired structural modeshape while keeping the eigenfrequencies close to their original values. The first pattern consisted of four stiffening ribs arranged in a pound sign and lying closer to the edges of the plate. This pattern was more effective at keeping the eigenfrequencies similar to original values, but it was not as effective at imposing a desired mode shape. For this reason the second pattern shown in Fig. 4.7 was selected for the stiffness design for minimal coupling.

The massless (from an area mass perspective) stiffening ribs were specified as follows in subdomains 1, 2, 3, and 4 the parameters remain unchanged from the nominal model. In subdomain 5 the thickness is multiplied by a factor, while the density is divided by the same factor. The reasoning behind this is that any change in the model will predominantly be the effect of stiffening without being the result of the added mass of a stiffener (since the total mass of the plate will then remain unchanged). This is only a crude approximation meant to gauge the effect of stiffening. The thickness multiplier was allowed to vary from 1 (nominal case) to 7.850 (7.850 times the plate thickness and the density of water). Then the value of this parameter that yields the minimum "coupledness" of the structural modes to the primary acoustic mode was found by searching over the design space. This value will balance the reduction in the SPL at this mode with the increased responses elsewhere. Because of this design trade off the optimizing parameter value can actually exist inside the design space rather than just on the boundary of the space as might be expected.

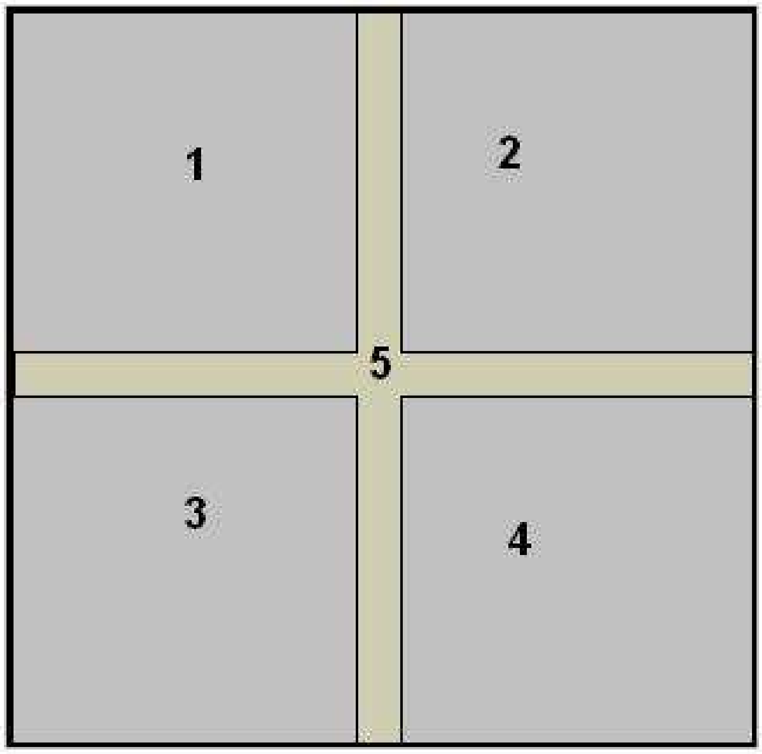

Figure 4.7 Subdomains for plate stiffening investigation

4.1.2.6 Simulation Result

Optimized thickness values of each subdomain subject to the above constraints are shown in table 4.4. Figure 4.8 shows the resultant frequency response of the mass

Table 4.1 Redistributed Subdomain Masses

Subdomain	**Thickness (m)**	**Mass (kg)**
1	0.0012	2.398
2	0.0165	0.153
3	0.0055	0.051
4	0.0165	0.153
5	0.0055	0.051
6	0.0650	0.601
7	0.0055	0.051
8	0.0165	0.153
9	0.0055	0.051
10	0.0165	0.153

redistributed system. From this it is clear that the strength of the major radiating mode is significantly reduced. This coincides with a reduction of approximately 35% in each of the key coupling terms, and a reduction or increase in the rest such that the summation of the structural state coupling terms is minimized. The signal energy (for the range from 0 to 500 Hz) for spatially averaged microphone measurements (200 random locations in the chamber) has been decreased to less than 3% of its original value. Also clearly visible is one of the biggest limitations of the passive redesign technique—it is not possible even with optimization to redesign the structure targeting all coupling terms. This means that the redesign for one or two strongly radiating modes can and usually does adversely affect the radiation of other modes. The only sizable reduction was in the mode at 70 Hz and the other reductions were mainly due to the small increase in the total mass of the plate.

In the stiffness investigation the optimized value of the stiffening parameter was determined to be approximately 5 times the nominal thickness of the plate. Figure

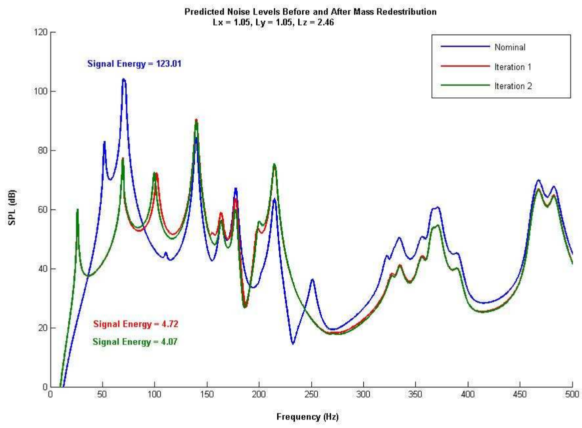

Figure 4.8 Mass Redistribution Optimization for an Small Enclosure

4.9 shows the resultant frequency response of the stiffened system. Again the major radiating mode has been reduced significantly. It should be noted that this method is even more difficult to apply to multiple modeshapes and thus the effect really only works on coupling terms relating to this one modeshape target. Additionally, this approach doesn't translate as easily to an active control scheme (although these possibilities will be discussed later). The first modeshape of this stiffened structure is shown in figure 4.10.

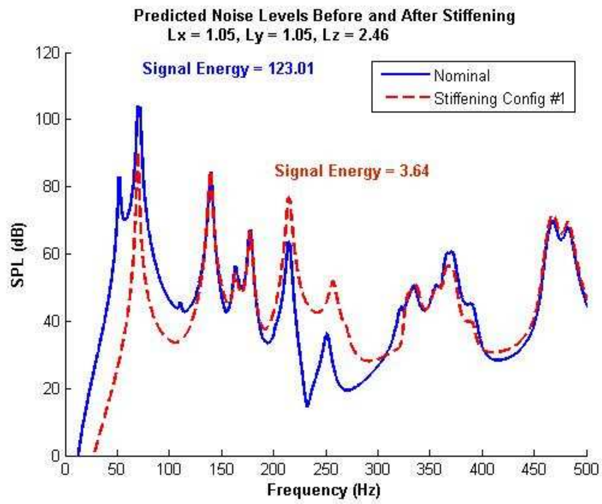

Figure 4.9 Stiffening Optimization for an Small Enclosure

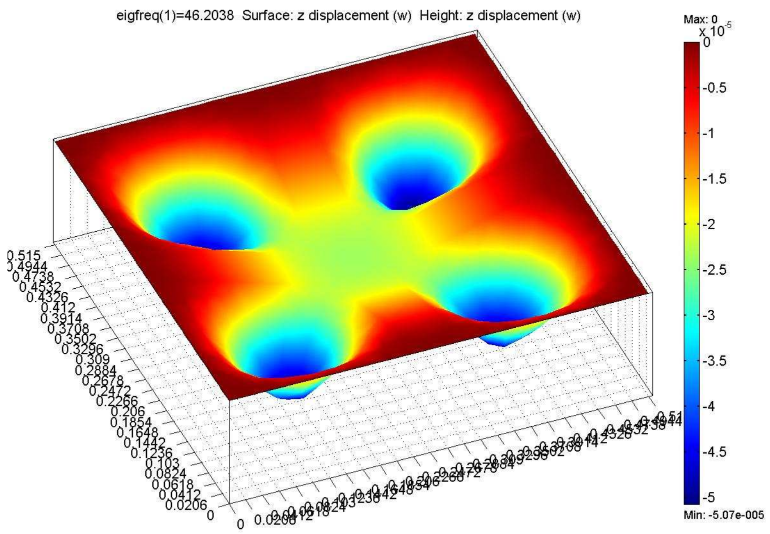

Figure 4.10 Redesigned Fundamental Mode After Stiffening

This presents an interesting question: since the design target has been the significant coupling terms of the modal interaction model, how effective will these redesigns be when the panel is placed in enclosures of different size? One would expect the reduction in the destination SPL would be drastically affected by using this design in different enclosure sizes, but would the result be worse? This question brings up an important point the coupling redesign is very dependent on the geometries and acoustic modeshapes of the two enclosures, and its effectiveness is dictated by how modally dense the enclosure models are (and consequently how accurate they are). This approach, in contrast to the volume velocity approach of Koopman [59], doesn't necessarily guarantee that the mode shape will have a lower volume velocity; only the minimization of the integrated product of the structural and acoustic modeshapes will be lower. It is entirely conceivable then that this approach could lead to modeshapes with greater volume velocity but lower coupling and hence lower transmitted noise. Similarly it is entirely possible that in an resonant enclosure the volume velocity approach may have little or even adverse effect on important coupling terms even though volume velocity is decreased. Furthermore, in the practical application of such a design, say in an appliance, only one of the enclosures will be explicitly specified. In the different case of room partitions, both rooms would have to be described explicitly for such a redesign to be highly effective.

To investigate this, the size of the source and destination enclosures was changed in the following ways. First the size of the enclosures was doubled and quadrupled successively for both the mass redesign and the stiffness redesign and the effect on the signal energy of the spatially averaged acoustic pressure was computed. Second the source enclosure was held constant at the nominal size while the destination enclosure doubled and quadrupled in size. The signal energies of the spatially averaged acoustic pressure measurements were then calculated and tabulated in table 4.2. Note that small indicates a 1.05 x 1.05 x 2.46 m^2 room, medium indicates a room whose dimensions are double these, and large indicates a room whose dimensions are quadruple these. Simulations of successively larger chambers displayed higher noise levels than the smaller chambers. This is due to the nature of the sound source considered, and the fact that the number of resonant acoustic modes is more dense with each successive increase in size. For example, in the 0 to 500 Hz range, the small room has only 26 modes, while the medium and large rooms have 125 and 512 modes, respectively. The number of modes to evaluate were selected on the basis of keeping the range of frequency of the acoustic model nearly the same for each different room size. For the largest room the response behavior could be accurately characterized with a statistical model.

The results of this investigation are encouraging. For the cases of both larger enclosures, both the mass redistribution and the stiffening design reduce the overall signal energy, albeit not as drastically as for smaller enclosures. Furthermore, the stiffness redesign seemed to be less sensitive to this change in the enclosure size than the mass redistribution. There are two plausible explanations to this. First, the stiffness redesign has a smaller effect on the rest of the response (the part not containing the primary radiating mode) than did the mass redistributions. Therefore it follows that when the

Table 4.2 Tabulated Signal Energies for Changing Enclosure Size

Case	**Design Tech.**	**Source Side**	**Dest. Side**	**% Energy Compared to Undesigned Plate**
1	Mass	Small	Small	3.3%
2	Mass	Medium	Medium	84.4%
3	Mass	Large	Large	84.8%
4	Mass	Small	Medium	43.2%
5	Mass	Small	Large	45.8%
6	Stiff	Small	Small	3.0%
7	Stiff.	Medium	Medium	56.6%
8	Stiff.	Large	Large	53.7%
9	Stiff.	Small	Medium	29.1%
10	Stiff.	Small	Large	25.9%

acoustic modes become more compacted this greater adverse effect of the mass redistribution technique becomes more of a liability and thus the reduction is less. Second, another plausible explanation lies in the nature of the technique. Mass redistribution decreases the mass normalized modeshape in some places, while increasing it in others (due to the subtraction of thickness and mass). The net effect is that the product of the acoustic and structural modeshapes when spatially integrated is lessened. For the acoustic mode at 70 Hz this implies that the spatial integration of the structural velocity is closer to zero (since the first acoustic modeshape is constant over the plate surface). In this case designing for decreased coupling is the same as designing for decreased volume velocity. However, for the stiffness design the net effect for the target modes is to decrease the magnitude of their modal velocity pattern not the value of its integration. This type of design is analogous decreasing the spatially averaged value of the squared normal modal velocity or the $\langle v_N^2 \rangle$ term in the representation of radiated sound power of a plate. A decrease in this value will always lead to a decrease in the sound power (for the same σ) regardless of the value of the wave number. The same claim cannot be made about the volume velocity source. It is possible that for the larger enclosures the radiation efficiency is higher at lower kd thus the better design is the one that minimizes $\langle v_N^2 \rangle$. For the situation at hand, it is likely that the true cause of this difference between the stiffness and mass redesigns is a combination of these two explanations. This demonstrates the true strength of this approach for modal resonant enclosures. By using an optimization objective that attacks the coupling coefficients the method can exhibits the properties of both a sound power based or a volume velocity based optimization.

For the cases similar to situations experienced by an appliance enclosure, where the source room stays small and the destination is allowed to grow, the results are extremely positive, as the desired decoupling still occurs between the source enclosure and the plate. Less than half of the original signal energy still remains in all these cases but more than in the case of two small chambers. This indicates that this method should still be highly effective in real world applications.

4.1.3 Continuing Modeling Efforts

One future direction of investigation that will be explored in continuing work outside of this dissertation will be in the simulation of several concepts for active stiffness control. A proof of concept system was designed and constructed using MR fluids, permanent magnets, and dummy masses (to simulate the masses of the magnets). This system will be discussed in greater detail below but the results were promising enough to explore further in simulation. Also to be developed in the near future is a better stiffness optimization approach that will allow better pattern designs for stiffening multiple modes not just one or two (which the current pattern is limited to) optimization. One envisioned approach will utilize a library of parametrically defined stiffening elements that can be linked together upto a certain number in any combination. Then using genetic algorithms to alter organization and parameter values of the various elements and evolution based environment various candidate patterns would be allowed to evolve under different selective pressures. A preliminary code to do this for a limited scale of parts has been developed and will be integrated into the simulation and optimization environment in the future.

4.2 Experimental Validations

This next section discusses the experimental validation of the passive redesign on a real plate and plate enclosure system matching as closely as possible the one modeled above. First is a discussion of the equipment used. Next the procedure followed is summarized. Finally the experimental results for mass redistribution are presented. Also presented are preliminary experimental results on a possible active stiffness control concept.

4.2.1 Mass Redistribution Plate Only Study

4.2.1.1 Equipment Used and Procedure

Two plates were used representing as closely as possible the starting nominal plate and then the optimized mass redesigned plate from above. These plates are shown in Fig. 4.11. Using a PCB ICP accelerometer (PCB Model 352A24) and a portable,

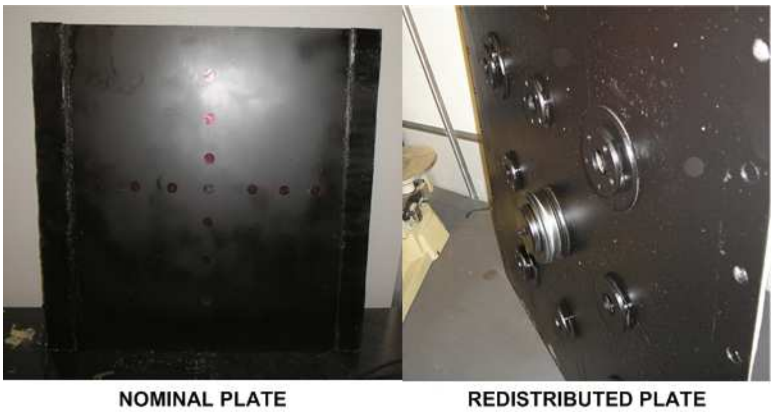

Figure 4.11 The nominal left and redesigned right plates utilized in the experimental testing

single channel, battery powered ICP conditioning unit (PCB model 480C02) the plate acceleration was measured under harmonic swept sine excitation at 49 discrete locations on the plate. To drive the plate an adhered Thunder PZT actuator (FACE Model TH-10R) was utilized in the upper right corner. To generate the input waveform and measure the signal a Stanford Research SRS785 two channel dynamic signal analyzer was utilized. The input waveform is then put through a piezo driver (Trek model PZD700-2) and then sent to the PZT actuator attached to the plate. The accelerometer signal from each plate location was put into the signal conditioner and into then into the SRS785. Magnitude and phase (measured relative to the applied signal phase) were measured at each plate location and saved before the accelerometer was moved to the next prescribed location. The resultant data was converted to matfile format and analyzed in MATLAB^{TM} to identify the resonant modes and extract acceleration modeshapes.

4.2.1.2 Experimental Results

Since both the actuator and the sensor have a flat response over the entire range of measurement, the plate should have the same intrinsic damping. Also, because the driving voltage is the same in both cases, the acceleration magnitude patterns may be compared directly. Furthermore, these patterns are directly proportional to the modeshape, thus by measuring and plotting the magnitude and sign of acceleration, it is possible to see differences in both the shape and magnitude of the modeshape due to redesign.

As you can see from these experimental plots, all of the modeshapes have been affected. These changes should translate well to reductions in low frequency acoustic response in the two chambers. This is because the resultant mode shape in nearly all cases has been significantly reduced and in some cases has been completely reshaped at the same time as in modes 1 and 4. Results for modes 2 and 3 are very similar to those that would be achieved by redesigning using $\langle v^2 \rangle$ as an objective. In contrast, the

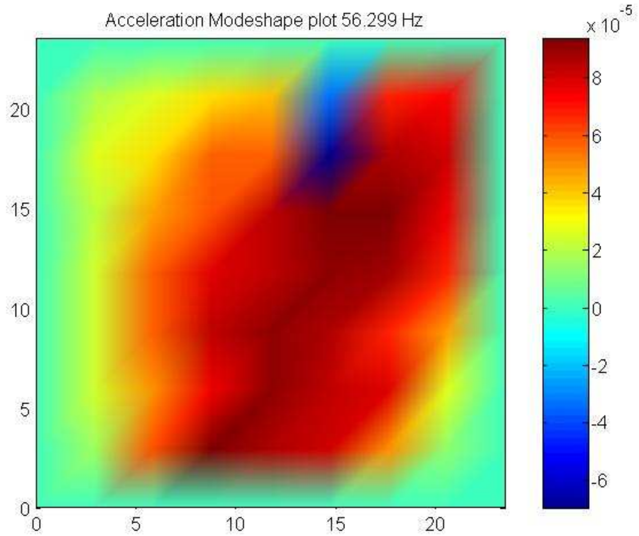

Figure 4.12 Nominal Modeshape 1

results from mode 1 show that mode shape not just reduced but is spread out, indicating a difference between the $\langle v^2 \rangle$ approach and coupling approaches. This is also seen in mode four where the $\langle v^2 \rangle$ is basically unchanged. In mode four the result is more like that achieved by a volume velocity objective. Moreover, the modeshape of mode 4 has been altered in addition to the lower integrated spatial velocity. This is possibly a result of the strong and unbalanced coupling of this plate mode to acoustic modes 10, 11, and 12 (at 241.2795Hz, 269.8083Hz, and 326.6667Hz respectively).

A quantitative comparison of quantities proportional to the redesigned volume velocity ($Q(t)$) and velocity squared ($\langle v^2 \rangle$) terms is given in table 4.3. The quantities $Q(t)$ and $\langle v^2 \rangle$ may be computed from the measured acceleration response by first developing relations for the steady state driven acceleration and velocity response. From the assumed modes approach to modeling the structure, the physical relation of real position at a modal frequency is determined by the separable solution to the plate PDE ($w(t, \vec{(x, y)}) = \Phi_p(x, y)q\vec{(t)}$).Assuming that the inherent cross-coupling of structural modes due to modal damping will not be a significant factor (which is a reasonable

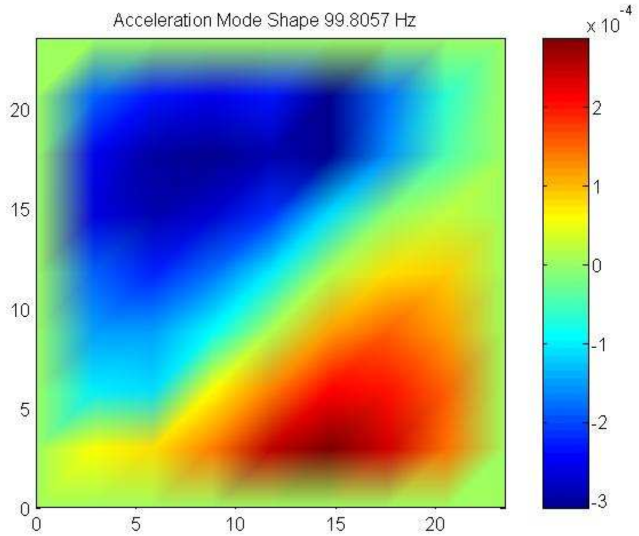

Figure 4.13 Nominal Modeshape 2

assumption if the plates are not otherwise damped in any way), the individual second order systems of equations at each modal frequency can be mapped to $w(t,(x,y))$ and the steady state driven response at this frequency can be represented as follows:

$$
\begin{aligned}
w_{ss}(t,(x,y)) &= \Phi_{p_n}(x,y)A|G(j\omega_n)|\sin(\omega_n t + \angle G(j\omega_n)) = \frac{\Phi_{p_n}(x,y)A}{\omega_n^2}\sin(\omega_n t + \angle G(j\omega_n)) \\
\dot{w}_{ss}(t,(x,y)) &= \frac{\Phi_{p_n}(x,y)A}{\omega_n}\sin(\omega_n t + \angle G(j\omega_n)) \\
\ddot{w}_{ss}(t,(x,y)) &= -\Phi_{p_n}(x,y)A\sin(\omega_n t + \angle G(j\omega_n)) \\
\dot{w_{ss}}(t,(x,y)) &= \frac{-\ddot{w_{ss}}(t,(x,y))}{\omega_n} \qquad (4.1)
\end{aligned}
$$

The term A is a constant of proportionality capturing the gain from the amplifier to the actual forcing of the structure and as great care was undertaken to ensure that this doesn't change from structure to structure meaningful comparisons of the velocity terms can now be made drawn from the signals measured on both structures even if the redesign has changed the natural frequency. Since this was an experimental measurement where there were gains in the signal and in the driven response these gains have been

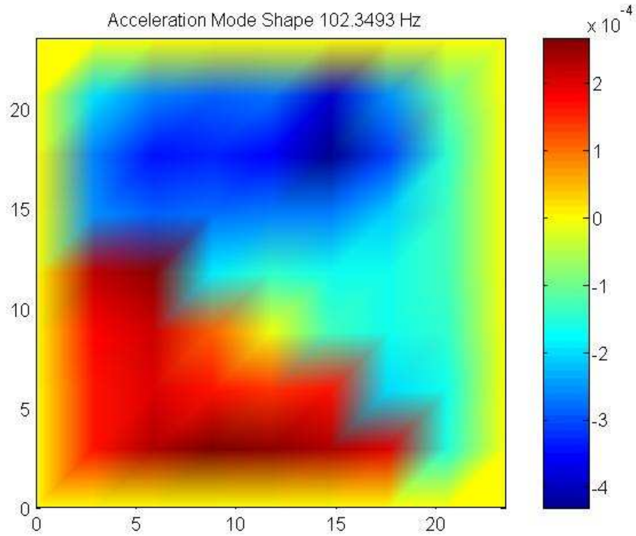

Figure 4.14 Nominal Modeshape 3

lumped together into a constant K that doesn't change from plate to plate or frequency to frequency. 4.4.

Table 4.3 Comparison of $Q(t)$ and $\langle v^2 \rangle$

Mode #	**Nominal** $KQ(t)$	**Redesigned** $KQ(t)$	**Nominal** $K < v(t)^2 >$	**Redesigned** $K < v(t)^2 >$
1	6.078E-05	5.333E-05	3.866E-09	2.041E-09
2	-2.806E-04	-1.333E-05	1.524E-08	1.563E-08
3	-4.985E-05	-1.642E-05	2.626E-08	1.810E-08
4	-8.820E-05	4.273E-05	6.697E-07	3.995E-07

4.2.2 Mass Redistribution in Acoustic Enclosure

In this experiment, both plates were mounted in between the two specially designed acoustic enclosures. These enclosures were of essentially the same dimensions and surface impedance as those in the computational model discussed earlier in this section. After initial tests, the plate redesign routine was refined to give larger weight to modes of greater importance to this experimental system.

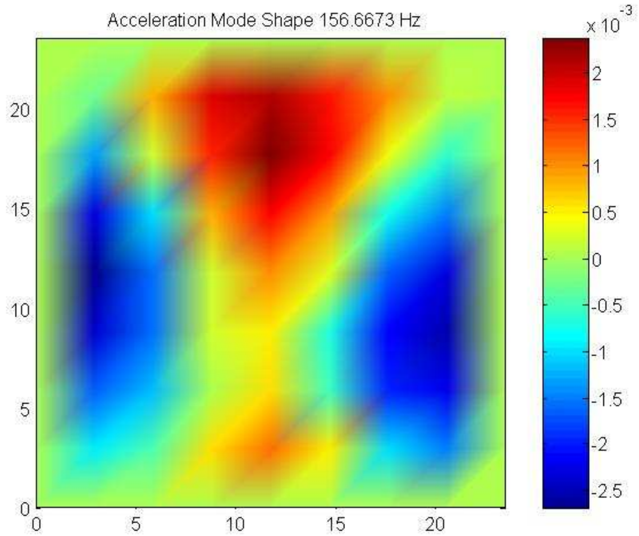

Figure 4.15 Nominal Modeshape 4

4.2.2.1 Equipment Used and Procedure

In this investigation the piezo was removed from the plates and in its place several loudspeakers were used, in conjunction audio amps to excite the acoustic modes of the source chamber. The noise responses were then measured using 16 microphones in 8 different locations and were averaged to get an accurate idea of the spatial sound environment in the enclosure for each plate. These measurements were run through an analog anti-aliasing filter/amplifier (f_b=5000Hz), and sampled using the d-Space system (1105 board). The signal was further filtered before being sent to the SRS analyzer, where the swept sine response at each location was calculated. Each location's FRF's were RMS averaged to get the average response at each microphone location. In turn these averaged locations were averaged over the entire enclosure to produce a single frequency dependent measure of noise over the entire enclosure. The sound level in the destination enclosure was estimated at around 100 dBA and was created by outputting bandlimited white noise 0-3.6kHz to five channels of speaker amp that then drove the speakers. The frequency response of the speakers was flat above 75Hz and rolled off

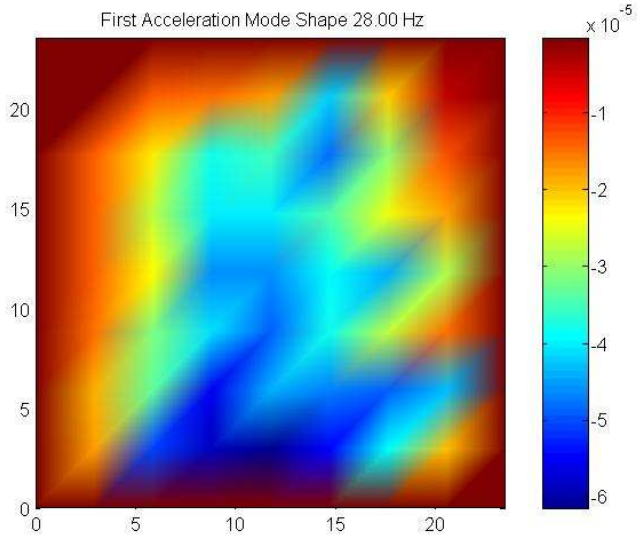

Figure 4.16 Redesigned Modeshape 1

below this value this later necessitated the use of a subwoofer in the active control experiments.

4.2.2.2 Experimental Results

The first pair of plots (in figures4.20, and 4.21) show the resultant spatially averaged microphone responses. The initial mass redesign is shown to have an effect of about 6dB at lower frequency and about $4-5$dB in the target coupling with acoustic modes at near 70 Hz as intended but less of an effect at high frequency. In simulation, this was not an issue because the speaker high pass effect was not modeled to be as high as 75 Hz. In the real system, however, the importance of the 70 Hz acoustic mode is greatly reduced as it is more difficult to excite using the speakers availiable, with better drivers this may still be the case. Instead of this being the dominant coupled acoustic enclosure mode the most dominant low frequency acoustic-enclosure modes are now on the range from 230 to 350 Hz. These correspond strongly to acoustic modes 10-15 and the plate modes that couple most strongly to these acoustic modes are plate modes 4, 1, 6, and

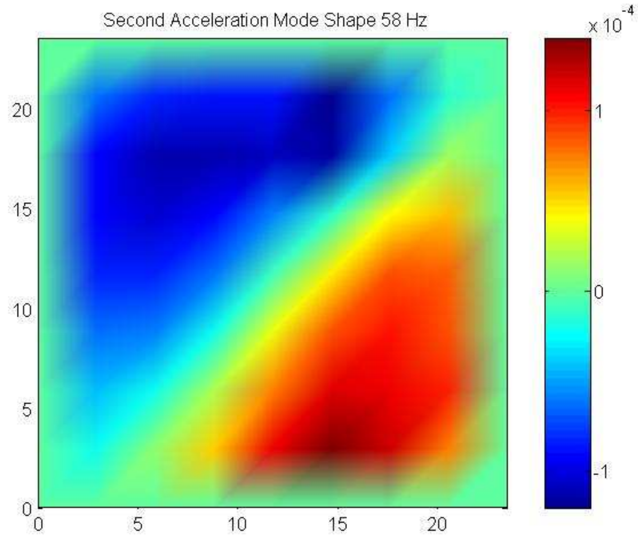

Figure 4.17 Redesigned Modeshape 2

7, in that order. To improve upon this design for the realities of the actual system the optimization routine for the mass was again run. This time, additional weight was given in optimization to the coupling terms relating mode 4 with the structure (subject to the same rules as above). The values chosen by the optimizer for the masses to be used are shown in table 4.4. After this second redesign the coupling of these higher modes were reduced by 3-5 dB. Future efforts should take into account the effect this different importance has on the optimal locations for mass placement to make sure the redesign is better suited to tackle this difference.

4.2.2.3 MR Fluid Proof of Concept

I aim here to determine the feasibility of active stiffness control to tailor acoustic modeshapes. To do this, I designed and built panels which had the potential for active stiffness change. The proof-of-concept apparatus is comprised of two parallel sheets of Plexiglass with magnetorehological (MR) fluid inserted between them. This sample was clamped in place at the edges and a small Thunder PZT was utilized to vibrate

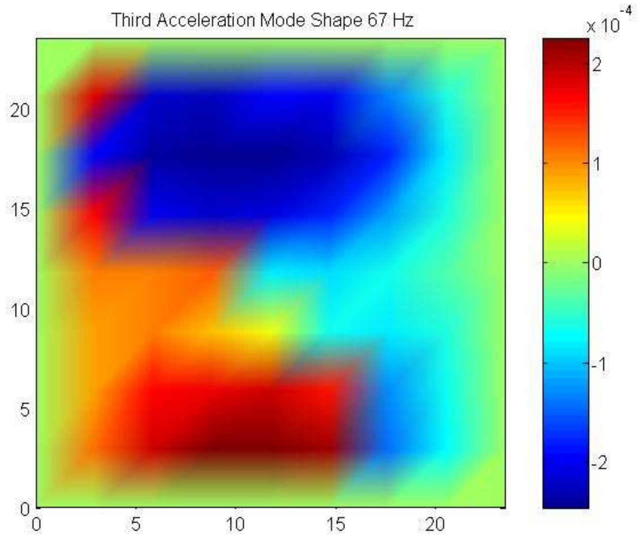

Figure 4.18 Redesigned Modeshape 3

the sample panel, as was the case in the plate investigations above. Here, the panel could be activated by using several permanent rare earth magnets spaced close enough to cause a continually solidified expanse of MR fluid across the plate. This is done to cause noticeable changes in the stiffness properties. A baseline case was tested utlizing dummy weights with the same general mass and shape as the magnets and running the same frequency response. This is shown in figure 4.24.

4.2.3 Experimental Results

Figure 4.25 shows that when the magnets were utilized in place of the dummy masses there was a major change in the response of the plate proving that this MR fluid concept has the potential to drastically change the response of the plate. The results of these changes would need to be studied more and simulations should be developed to aid in the design and layout of a electromagnet version of the plate that will utilize this change to greatest effect. Future investigations will refine this prototype and examine control

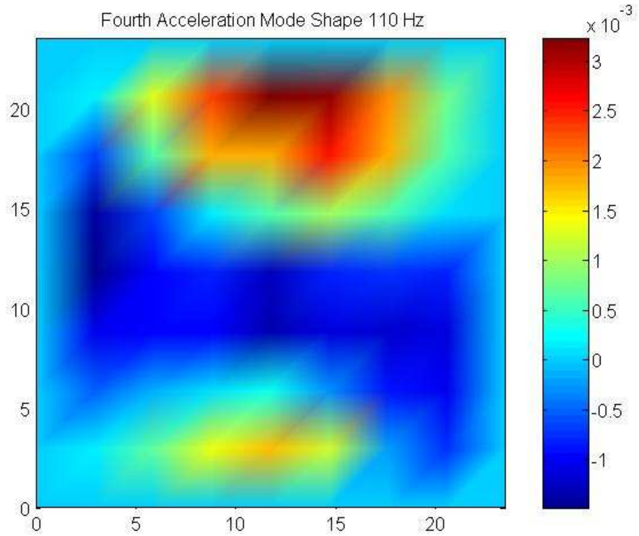

Figure 4.19 Redesigned Modeshape 4

approaches that will best utilize such a panel, as well as examining the bandwidth and nonlinearities associated with this method of stiffness change.

4.3 Concluding Remarks

The computational model developed in the previous section were adapted and expanded for redesign the plate structure for reduced coupling by both stiffening and by mass redistribution. The mass redistribution design was then evaluated in experiment and refined using the realities of the actual system.

As stated earlier there were several reasons for this effort. First and foremost was to develop relatively quick and systematic approaches to passively tailoring the structure as the first half of the combined active passive control design problem. This approach can now be readily integrated into the model generation routines allowing future studies of combined active and passive control synergy and optimization. Second, although this was not the objective of the above redesign, the above methodology provides an approach for modeshape reshaping in order to "concentrate" vibrational energy (both

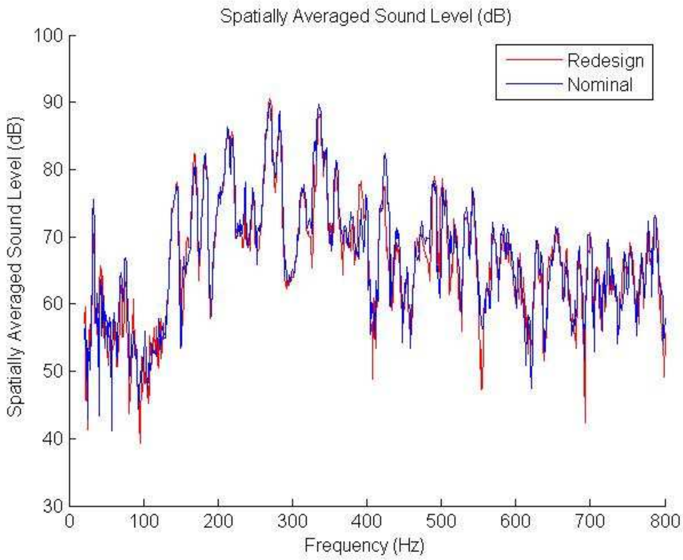

Figure 4.20 Redesigned Structure One Acoustic Enclosure Results

in space and in frequency). This will then make the job of active controller much easier in practice with fewer sensors and actuators required (which is always desirable from an implementation standpoint). Third, is that this redesign effort provides insights into how active control may be applied judiciously both spatially and in frequency to affect certain modeshapes. Finally, there are some corollaries between the active passive design problems. Mass redesign for a particular modeshape can be mimicked with accelerometer feedback (with the added flexibility of doing things no passive mass could ever do like "disappearing" at different modeshapes). These correlations and insights will now be explored in the second half of the active passive control problem, how to design and implement robust and performing MIMO active noise controllers.

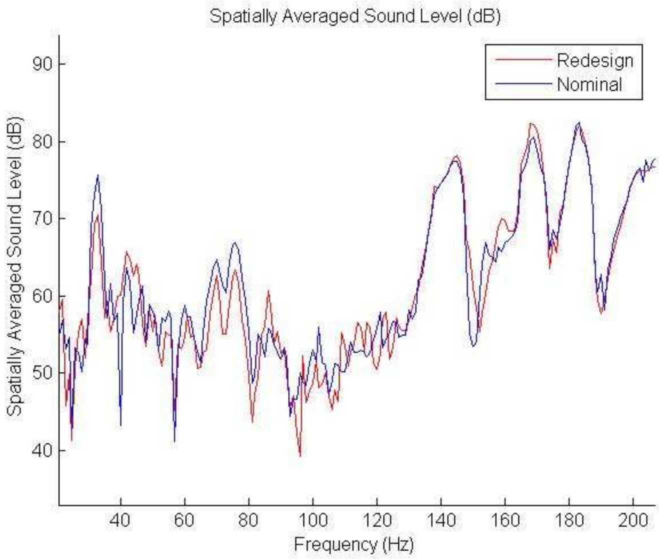

Figure 4.21 Redesigned Structure One Acoustic Enclosure Results Closeup

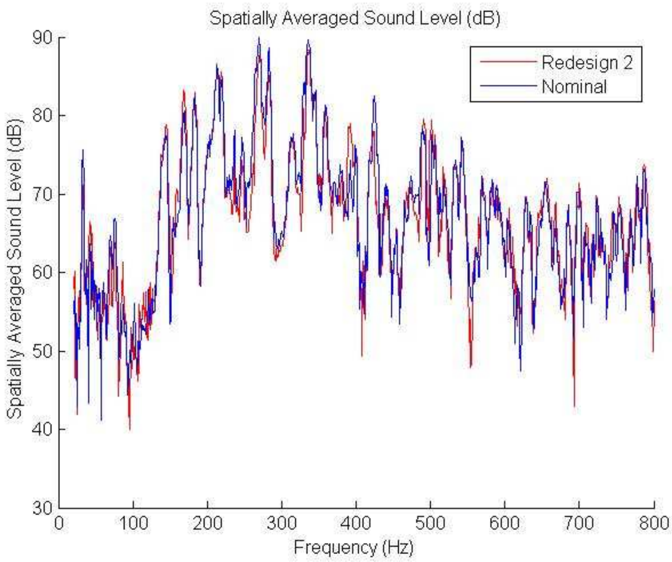

Figure 4.22 Redesigned Structure Two Acoustic Enclosure Results

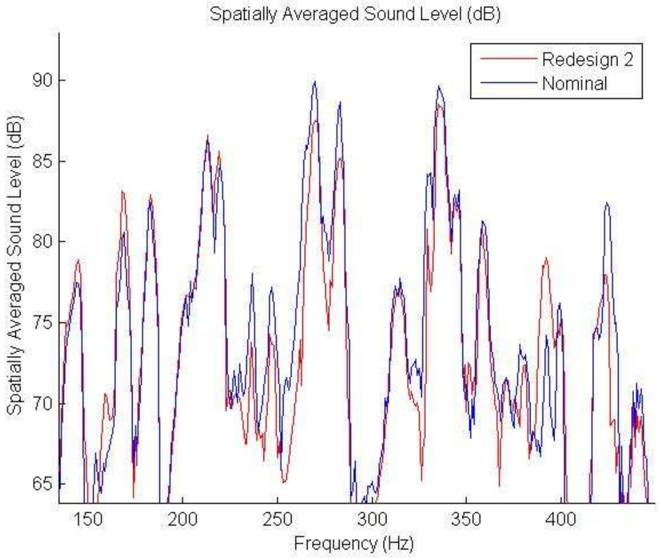

Figure 4.23 Redesigned Structure Two Acoustic Enclosure Results Closeup

Table 4.4 Redistributed Subdomain Masses Design # 2

Subdomain	**Thickness (m)**	**Mass (kg)**
1	0.00124	2.472
2	0.0087	0.081
3	0.0133	0.123
4	0.0111	0.103
5	0.0131	0.120
6	0.0624	0.579
7	0.0134	0.124
8	0.0087	0.081
9	0.0133	0.123
10	0.0087	0.081

Figure 4.24 Concept Prototype for Stiffness Control

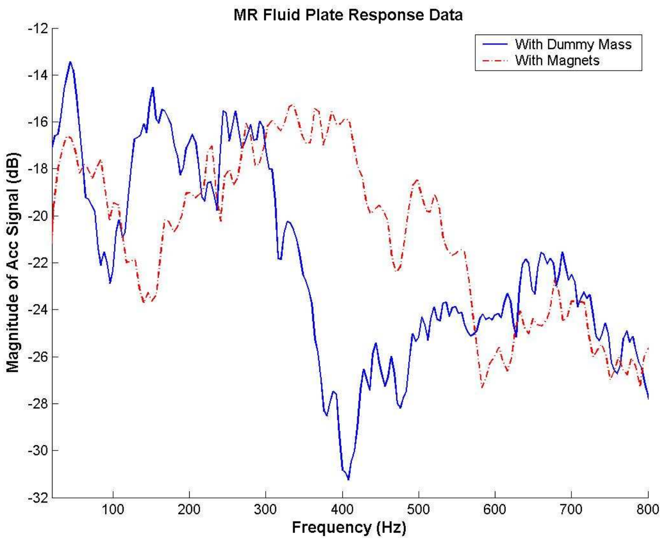

Figure 4.25 Concept Prototype Response Data

5 Simulation of Active Control Approaches in Flexible Panels

The representation of the fully coupled control design model was developed in section 3. The particular sensor actuator pairings utilized in this paper are those of a point force actuator and a point acceleration sensor on the plate and a spherical acoustic source (on the source side) and a randomly placed array of 200 microphones (on the destination side).

First investigated are two LQG designs first utilizing only the plate states (accelerometers only) for weighting and then utilizing all the system states (accelerometers and microphones) for weighting the system. Next several traditional structural control approaches were investigated using differing forms of centralized and decentralized velocity and acceleration feedback with and without the consideration of actuator dynamics. Finally based on these results several passivity based approaches were investigated utilizing sensor blending, actuator clustering, actuator blending, series passification, and resonant mode control. All throughout this effort there is a general theme and that can be summarized as follows:

1. There are significant uncertainties in the models due to neglected dynamics, approximations, and non-idealities of sensor and actuator.

2. These uncertainties demand a robust control approach in design; however, most small gain based approaches and other robust synthesis and analysis techniques prove difficult to nearly impossible to implement with such high order systems and MIMO configurations.

3. An attractive alternative is to use passivity based approaches whereby the controller order can be kept manageable and the design approach is slightly more straight forward.

4. Efforts are made to optimally locate and collocate sensors and actuators.

5. The actuators and sensors are designed and utilized such that the collocated pairing at each location give a passive combination.

6. Decentralized approaches are utilized when possible.

7. When it is not possible to get a passive collocated channels, blending, clustering, passification, and high Q passive filters are used in various combinations to passify the system and yield a robust and performing controller.

5.1 LQG

In this section, the simulation results are presented for two LQG approaches to ANC. The results of these two approaches in terms of the performance objectives are listed in table 5.1.

Table 5.1 Results for Two LQG Controllers

Controller Target	**Acoustic Peak Reduction**	**Structural Peak Reduction**
Panel States	7 dB	13 dB
All States	13.5 dB	8 dB

First the plant was transformed into modal canonical form so that the modes were decoupled and the modal states could be weighted separately. For the LQG design targeting the plate states, 3 separate structural modes were equally weighted with values of 150 in the diagonal Q matrix. The remaining states were all weighted with values of

0.1. The weight on control effort R was set to identity, and in the absence of spectral noise data Q_e and R_e were chosen to yield reasonable convergence of the state estimates. This design essentially seeks to regulate the "structurally affiliated" modes in an effort to increase the structural damping and hence the transmission loss and dissipation of the plate. Looking at the controller gain matrix it was observed that the "non-structural" states had very small gains associated with them as was intended. This design was shown effective in reducing the peak response of the structure from the acoustic disturbance by the greatest amount of any attempted design. The open and closed loop frequency responses of this design are given in Fig.(5.1). For the LQG design targeting several

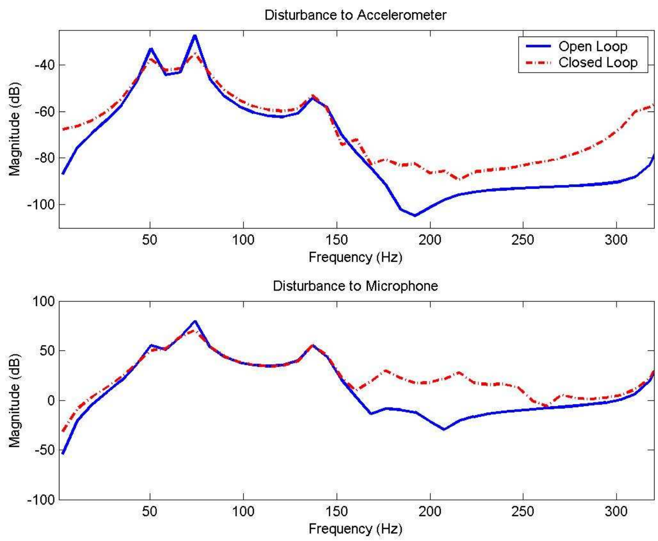

Figure 5.1 LQG controller targeting panel states

"acoustic and structural modes", 5 separate modes were equally weighted in the diagonal Q matrix with values of 50 for the generalized position terms and 500 for the generalized modal velocity terms. The remaining states are all weighted with values of 1. The weight on control effort R was set to identity, and in the absence of spectral noise data Q_e and R_e were again chosen to ensure reasonable convergence of the state estimates. This design essentially seeks to regulate a combination of the "plate and acoustically affiliated" states in an effort to decrease the noise sensed by the microphone in the destination enclosure. Looking at the controller gain matrix it was observed that it was fully populated as expected. This design was shown effective in reducing the peak response of the destination enclosure acoustics from the disturbance by the greatest amount of any attempted design. The open and closed loop frequency responses of this design are given in Fig.(5.2). These two designs illustrate some of the problems

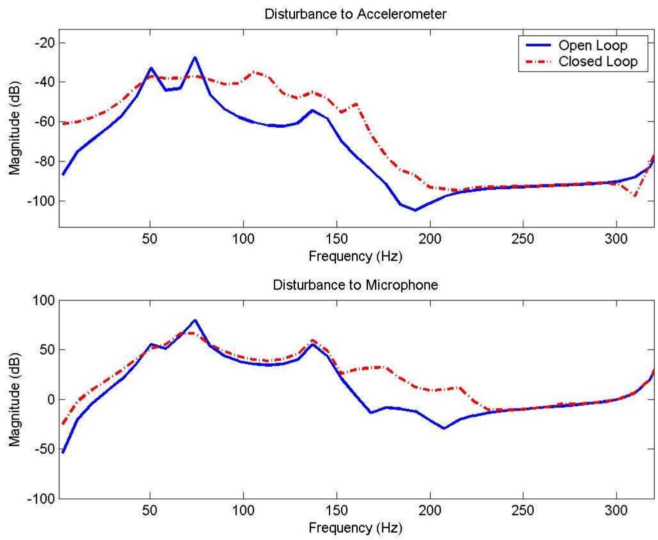

Figure 5.2 LQG controller targeting all states

that are common with ANC in resonant enclosures. First, is that it is very difficult to achieve broadband reductions in acoustic energy. In these examples only one or two peaks could be targeted at one time, and it was not possible to reduce the frequency response over the entire region of interest. This is partially due to what is known as the waterbed effect. However, it was only desired to have this reduction over the 0 to 300 Hz region so this effect should not be insurmountable. The biggest detractor from broadband reductions in acoustic enclosures (in this work) appears to be the coupling between acoustic and structural modes. When targeting the plate modes you can be very effective at increasing the damping of some structural modes however it is very difficult to predict exactly how this will actually affect the excitation of the acoustic modes and thus simply suppressing the most dominant plate mode doesn't always work. Similarly when the coupled plant is in a modal canonical form it is sometimes hard to identify what transformed states contribute most to the frequency response (since the analytical intuition is gone and the B and C matrices are altered). This means that a modal state can be singled out but it may not contribute significantly to the frequency response. In some situations a balanced realization could prove useful, but under this transformation the modal structure and weighting intuition is completely lost. A final related problem is that both of these controllers were only designed to achieve reductions in the frequency responses at a point and thus the results of this design may not and often do not hold at another location. One solution to this is the synthesis of passivity based controllers, that only dissipate energy along a given trajectory. Another possible solution is to add more sensors to ensure that synthesized controllers are suppressing noise and vibration spatially.

5.2 Summed SISO Velocity Feedback

Now consider a more tried and true method of controlling structures, constant velocity feedback. Specifically in this case, summed velocity feedback, where the 9 integrated accelerometer inputs (velocities are summed by a weighted sum and the actuator drive voltage is similarly summed by the same weighted sum. First considered is a case where actuator dynamics are not considered and the inertial actuators are able to provide a constant level of force at any frequency. In this case because of the choice of velocity, and forces as the input output pair, and the symmetry of the input and output weighted sum the resulting SISO system between the sensors and actuators is passive, and as a result a simple constant gain controller will work well at stabilizing the system. As is shown in figure 5.3 furthermore this feedback gain can be any physically realizable value (limited only by the voltage limits on the actuator). This particular value is $K_v = 1000$ which corresponds to an actuator voltage of about 100mV (at least 50% under the maximum allowable voltage). At the onset this would indeed appear to be an ideal controller

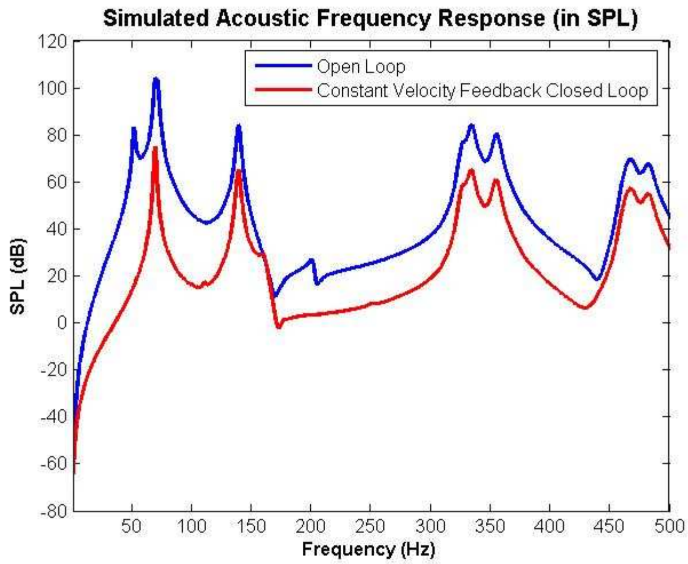

Figure 5.3 Summed constant velocity feedback controller no actuator dynamics

for controlling this type of passive system it is simple, it works well in either SISO or MIMO (as is shown in the next section), and it is easy to implement. However all it takes is the addition of some more realism to our simulation for this approach to have some difficulties. Consider now the same system as before, but with the addition of actuator dynamics describing the inertial actuator producing the forces. As stated earlier this actuator has poor low frequency response and its acceleration (force) response has the characteristics of a second order low pass filter until the device's resonant frequency. Now with this description the simple velocity feedback controller can no longer be utilized with any gain. This is because the new system description from control sensors to control actuators contains new dynamics and no longer meets the definition of a passive system (although it has passive properties at high frequencies). This means that even though the constant gain controller is passive it will destabilize the lower frequency plant dynamics at higher feedback gains. The maximum feedback gain possible with this new configuration is now a $K_v = 5$. Open and closed loop response, plate velocity, and microphone SPL simulation s are shown in figures 5.4, 5.5, and 5.6.

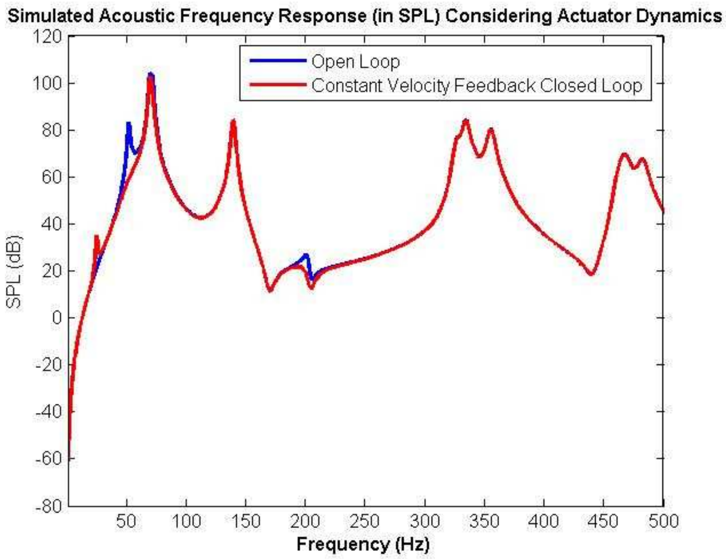

Figure 5.4 Summed constant velocity feedback controller with actuator dynamics

This unfortunate result motivates the design of a slightly more complicated passivity based controller. There are three approaches to this problem that have been considered in this work.

First is resonant mode control. Since this is a resonant system most of the time very high control action is needed only at the resonances of the plant and this action can roll off rapidly away from this point. A resonant mode controller meets these specifications. In a resonant controller the control action allows very high gain but is bandlimited to the width of the designed resonance. If the system is passive these simple controllers are passive so they can be used without fear of destabilizing the system. If the system is only bandlimited passive most of the time these controllers can still be used without problem. Even if the system is not passive often times it is possible to use these controllers because

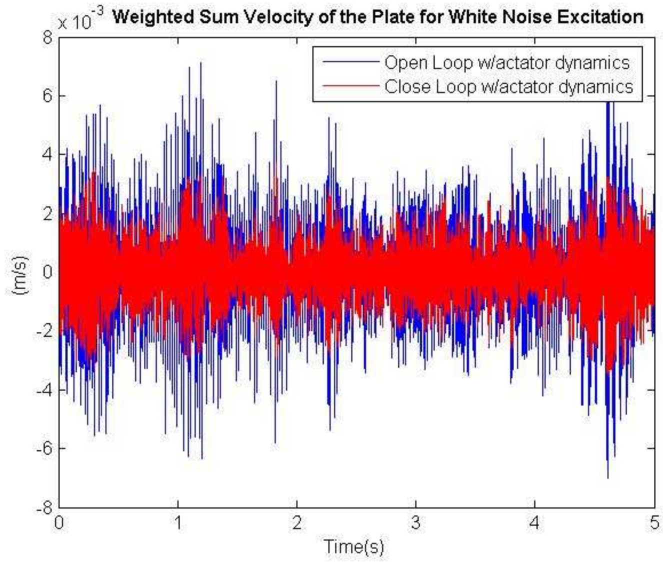

Figure 5.5 Plate velocity for summed velocity feedback controller with actuator dynamics

their bandlimited action limits the chances that the nyquist plot will be made to encircle -1 even if the phase is not constrained between -90 and 90.

The second approach to passivity based control is to passify the system with sensor blending. If the system is rectangular and has a greater number of sensors than actuators a combination of these sensors may be blended to yield a system that is passive. In this work this approach was utilized in combination with actuator clustering to enhance the ability to control the resonant modes/modeshapes of the plate.

The third approach toward passivity based control was to develop passifying compensators (feedforward, series, or feedback) that first passify the plant, and then to develop passive controllers that add performance to this system. These approaches will be utilized in the sections that follow.

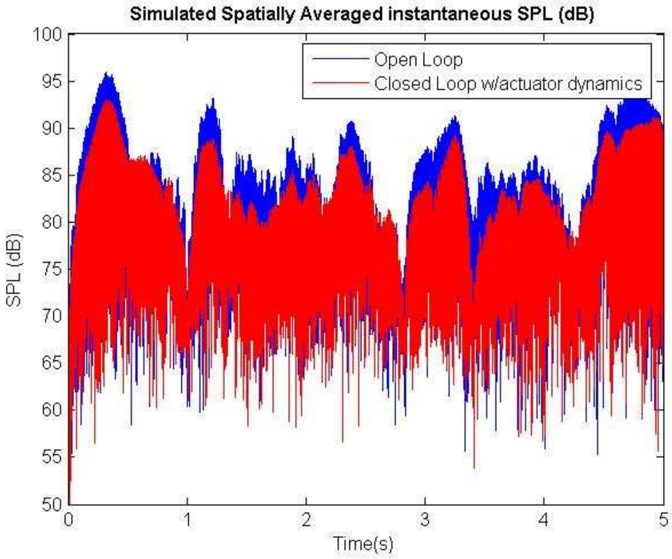

Figure 5.6 Instantaneous sound level for summed velocity feedback controller with actuator dynamics.

5.3 Decentralized Constant Gain Velocity Feedback

Rather than simply reducing the MIMO control design problem to a SISO problem by summing the actuators and sensors together. Another approach is to decentralize each of these collocated passive systems and apply local control only. This allows greater control action in regions of the plate of greater importance to the acoustic structure interaction. Because the transfer matrix for a decentralized control approach is diagonal and the diagonal transfer functions are all passive it can be shown that like the SISO example the decentralized system is unconditionally stable for any amount of velocity feedback. When actuator dynamics are not considered the only limiting factor on how high the control gain can be set is the saturation level of the actuator. However just as in the summed velocity case the addition of actuator dynamics makes the system not passive. This limits the feedback gains that can be applied to each of the channels; the maximum feedback gain on any channel is $K_v = 35$ and the minimum is $K_v = 5$. Again this eliminates all but a few dB of reduction and consequently the signal energy relative the open loop is reduced only 22%.

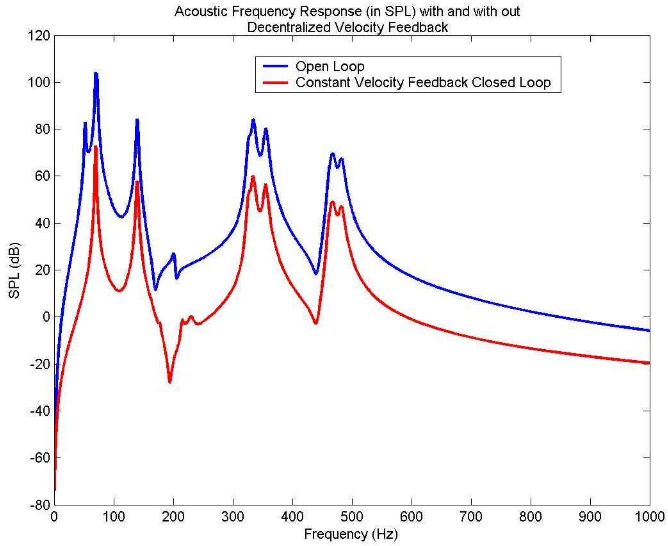

Figure 5.7 Decentralized velocity feedback controller (no actuator dynamics)

5.4 Decentralized Constant Gain Accelerometer Feedback

One of the major difficulties with active structural control is the effects are often localized. That is to say the control action is often less effective at reducing vibration globally than it is at the location of the sensor or actuator. One way to avoid this is by judiciously placing the sensors and actuators on the structure so that the SISO system is able to achieve a noticeable global result. Another way is to use distributed sensors and actuators on the structure [29]. Still another method is to use multiple sensors and actuators in unison or independently to achieve a global control of a structure. In this last case, the control design can either be centralized (having one multi-input multi-output controller that is designed to use all of the sensors and control all of the actuators), or decentralized where a number of independent controllers control individual or small

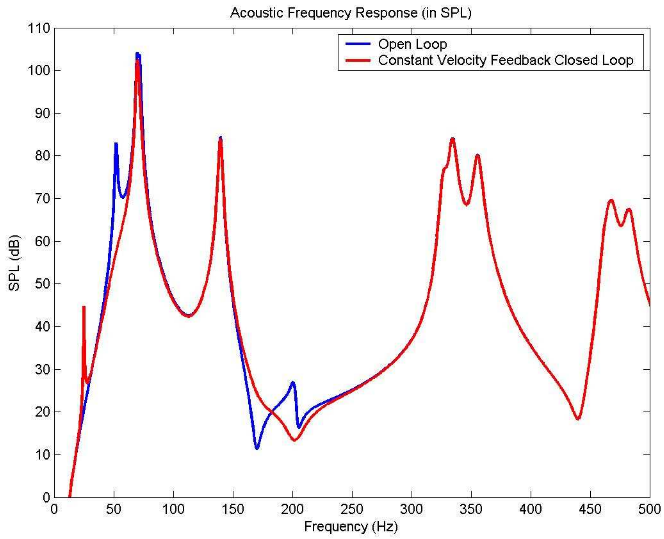

Figure 5.8 Decentralized velocity feedback controller with actuator dynamics

groups of sensor actuator pairs. Centralized controllers for MIMO are plagued by the difficulty of their design and their complexity (large numbers of states). However decentralized controllers while often simple in form and implementation can suffer from undesired stability problems. Some of these problems can be avoided by spatial collocation of the actuator and sensor pair, since this results in a passive system response between the input and output when they are force and velocity respectively. In these cases passivity based designs can be used to avoid instability in the collocated channels of the closed loop system. However there are still instabilities that could arise from the cross channels of the MIMO closed loop system. Only through MIMO loop shaping techniques, MIMO passification and passivity designs, or small gain theorem based techniques can this problem be dealt with systematically.

One popular design approach for decentralized systems is constant gain velocity feedback with collocated sensor and actuator pairs. The advantage of this method is that the closed loop collocated channels are assured stability due to the passivity of these channels in the open loop. However, in general the decentralized MIMO system is not assured passivity as these collocated sensor and actuator locations are rarely physically decoupled from each other and thus the cross channels may be non-passive. In these situations the plant must be passified (either by a passifying compensation [53], or a blending of extra sensors and actuators) then a controller can be designed to yield closed loop stability. However in this paper another controller approach was explored with the goal of developing simple, effective, and stable decentralized MIMO controllers for multiple collocated sensor and actuators.

The reasoning behind this control design is that if a structure may be passively redesigned with stiffeners and discrete masses to reduce the vibration, coupling, and radiated noise, then a control scheme that mimics these passive redesigns should be able to do the same. Furthermore, since a realizable mass redistribution design doesn't destabilize the structure (although it can make the noise or vibration worse), if a controller were to exactly mimic such a passive design then it should benefit from similar stability properties. To accomplish this active control a simple constant gain accelerometer feedback between collocated pairs was utilized. A finite dimensional LTI representation of a vibrating plate may be written as in Eqn. 2.28. In this equation η_n corresponds to generalized coordinates, and for this model these generalized coordinates include Θ_x, Θ_y, and z displacements. Looking at the equation of motion for a single generalized coordinate the contributions from several of the adjacent nodal locations and possibly (depending on whether it is a rotation or translation coordinate) coordinates that are farther away are noticeable. However the lumped mass contribution from $\ddot{\eta}_n$ term usually has the largest effect on the inertial forces. An increase in this term will correspond to an increase in the translational or rotational inertia at this point. This can be accomplished passively by physically changing the structure (and thus $\mathcal{M}$), or actively by letting the force input equal the desired change in the inertial portion of the equation ($f(t) = -\Delta\mathcal{M}\ddot{\eta}_n$). The case where η was z displacement at a point was investigated in this work by using constant gain accelerometer feedback. In this paper a controller of this form consisted of a 9×9 diagonal matrix of constants that multiplied into the 9 accelerometer outputs and then fed back into the 9 point force actuators. However it should be noted that this addition of a virtual mass is not exactly the same as passive mass redistribution. This is because it is not considering the fact that the rotational inertia terms will also change when a real mass is added, so these controllers will only approximate a realistic mass distribution when the $\Delta\mathcal{M}$ is small. Future control investigations should take into account the changes in these terms as well.

5.4.1 Simulation Decentralized Constant Acceleration Feedback

The metrics of interest are the stability and the spatially averaged reduction in sound pressure level (SPL). This spatially averaged value was evaluated from 200 randomly placed microphone locations in the destination enclosure. The simulation of the constant acceleration feedback control shown in Fig. 5.10 demonstrates that this control almost exactly mimics the effect of redesigning the mass distribution of the plate. The weighting matrix considered was meant to imitate the passive mass redistribution discussed earlier. A reduction in spatially averaged microphone signal power of nearly 75%, and reduction in the peak SPL of nearly 15 dB were achieved. Like in the passive redesign the feedback controller attenuates the first two resonances in the acoustics and worsens the third (at 140 Hz). For this design the closed loop MIMO system is stable and the controller gain may be increased significantly without destabilization. The Nyquist plot of this system showed that the mass mimicking weights targeting the key modeshapes yield a loop transfer function completely in the RHP. Simulations suggest that acceleration feedback that closely imitates a realizable mass distribution will yield a stable closed loop. In fact only when the feedback gains were set extremely high did the closed loop lack stability. There are two potential reasons for this: 1) the numerical solution of the closed loop eigenvalues wasn't accurate enough (scaling issues) to identify system eigenvalues close to the imaginary axis, and 2) the large gain on the acceleration began to represent a mass redistribution that was no longer physically realizable.

5.5 Decentralized Resonant Mode Filters

Another type of decentralized controller that was investigated was the passive resonant mode filter. This design utilized a number of passive resonant mode filters that targeted the peaks of the acoustic frequency response. Additionally since mimicking the addition of discrete masses to the structure with constant gain acceleration feedback should be very stable even for large gains these constant gain weights on the accelerometer outputs were applied in the hopes that the MIMO closed loop system would be stabilized over a wide range of gains. The steps to design this controller are now described.

First, several constant gain weighting matrices are designed to mimic different passive mass redistributions. These different weighting matrices are each optimized to reduce the coupling of the structure to a specific acoustic mode. Next since these weights essentially are meant to be optimal only for specific acoustic modes (which are a narrow band phenomenon) a series of filters were designed to band limit these weights. This allows the weighting to only be effective in a desired frequency range and thus different weights can be applied simultaneously to target different modes. Because these acoustic modes are densely packed a very "sharp"(in terms of roll on and off) filter was needed. One form that fits this description very well is a lightly damped second order system (or a resonant mode). Hi Q resonant mode controllers were designed that draw their structure from series implemented RLC networks. The mathematical representation of these controllers is given in Eqn. 5.1,5.2.

$$\mathbf{A(s)} = \sum_{n=1}^{N} A_n(s) \tag{5.1}$$

$$A_n(s) = k_n \frac{C_n s(R_n + L_n s)}{L_n C_n s^2 + R_n C_n s + 1} \tag{5.2}$$

The resonant frequency of each $A_n(s)$ is given by $\omega_n^2 = \frac{1}{L_n C_n}$ and ω_n is selected to attenuate a desired tone (such as a machinery related tone) present in the noise environment. Now since the sensors and actuators are collocated, it would be nice to exploit passivity-like properties of the collocated channels. The channels corresponding to the

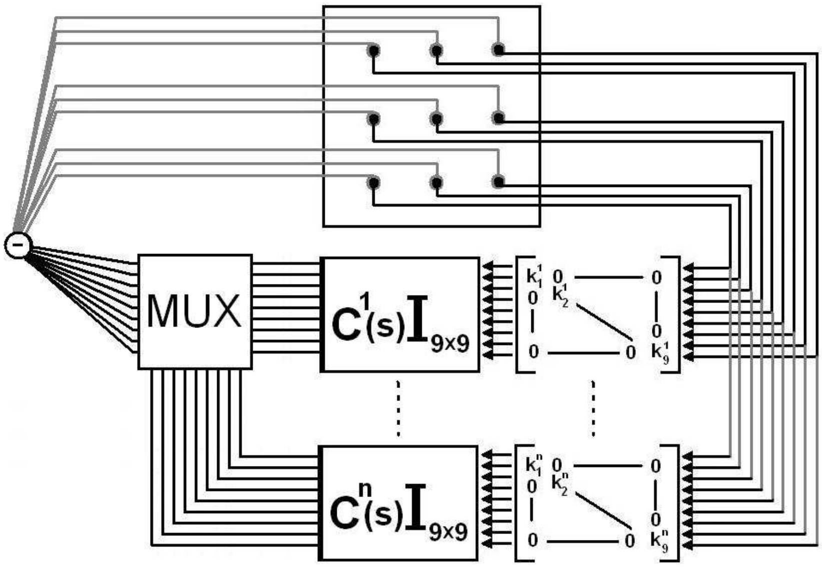

Figure 5.9 Structure of Decentralized Resonant Mode Feedback Controller

collocated pairs are not passive since the output is acceleration and the input is force. However if these outputs were integrated (to yield velocity) then the collocated channels of the plant would be passive. This means that a diagonal controller where each of the diagonal entries is a passive system would result in a stable response in these collocated channels. Therefore, if a series of decentralized passive resonant mode filters is designed and then multiplied by an integrator as in Fig. 5.9 the resulting collocated channels are stable. Furthermore the hope is that the non-collocated channels should also be stable because the outputs are being weighted in a way that mimics adding mass. The only thing that must be accounted for is the additional gain on each resonant mode to account for the roll off of the integrator and place the peak of the resonant mode near 0dB. The form of these decentralized controller are shown in Fig. 5.9 and Eqn. 5.3.

$$\mathbf{C(s)}_{9\times 9} = \sum_{n=1}^{N} C(s)^n_{1\times 1} I_{9\times 9} \begin{bmatrix} k_1^n & 0 & \cdots & 0 \\ 0 & k_2^n & & 0 \\ \vdots & & \ddots & \vdots \\ 0 & \cdots & 0 & k_9^n \end{bmatrix} \tag{5.3}$$

As Fig. 5.10 shows the resonant filter design was not only stable but also has excellent performance. The reduction in spatially averaged microphone signal power was nearly 96%, and reduction in the peak SPL of nearly 18 dB was achieved. Additionally reductions in lesser peaks of 6-10dB were attained. When utilizing the set of mass mimicking weights the plant/weight loop transfer function (the loop transfer function in the absence of the resonant mode filters) is constrained to the RHP and this is an indication of the passivity properties of their combination. Since the resonant mode controllers were designed to be marginally strictly positive real and bandlimiting it is not surprising that the closed loop is both stable and avoids significant control spillover effects often present in other MIMO control designs. However the addition of actuator dynamics again complicates things. When this is considered the feedback gain must be significantly reduced to avoid instability and as a result the SPL reductions are only about half a dB. This motivates a different approach to passifying and controlling the system.

5.6 Passivity based Control

A first step toward passivity was to collocate the sensors and actuator channels but sometimes even with 'force' as the system input and velocity as the system output it is still not possible to achieve passivity due to sensor, actuator, and filter dynamics. In

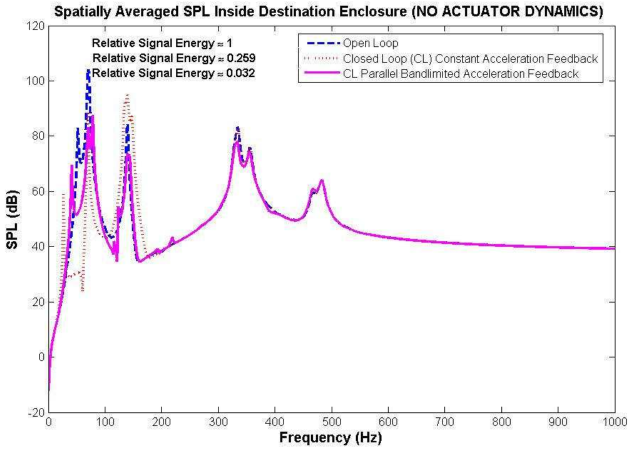

Figure 5.10 Open and Closed Loop Responses for Acceleration Feedback and Resonant Filter Control

these cases system passification is necessary before a passive compensator (constant or otherwise) may be used and stability will be assured. The general approach to passivity based control in this work is shown in figure 5.11.

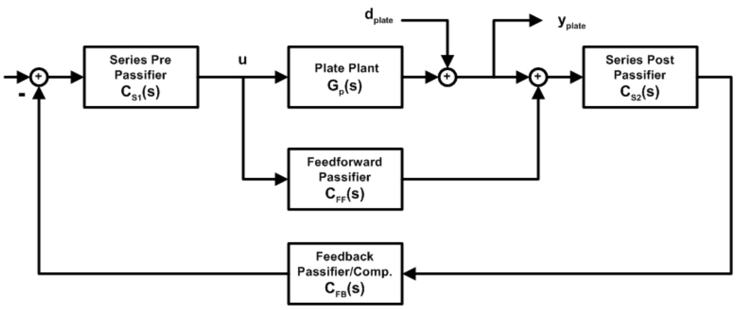

Figure 5.11 Control Structure for Passification and Control of Plate

In general, although not shown explicitly in the figure, the plate plant G_p may contain modeling errors, parametric uncertainties and certain actuator and compensator and sensor nonlinearities (deadband, hysteresis, and saturation). A passivity based approach may be used with all of these uncertainties, nonlinearities to robustly passify and thus robustly control the system. This approach may in fact lead to better results than a robust technique based on the small gain theorem (say H_∞) as the restriction placed on the system is not one of magnitude but instead of phase.

5.6.1 Modal Clustering

When controlling particular plate modes naturally some of the actuator locations are better suited than others. For example consider the first plate mode. This domeshaped mode is most affected by those actuators lying close to the center of the plate. For the second mode, actuators lying in the center of the plate and along a diagonal line of symmetry have little or no effect on the second mode. For other modes different actuators are most important. This motivates a concept called actuator clustering. In actuator clustering different subsets of the full complement of actuators are utilized in order to control a particular mode. The various cluster groups are illustrated for the first six modes in figure 5.12. The advantages to clustering or spatial filtering are:

1. It decreases the total number of individual channels to consider simplifying control design effort.

2. It decreases the control effort, as a large voltage is no longer necessary to get some result out of an actuator with marginal effectiveness for a mode.

3. It helps prevent some of the spillover that occurs with unmodeled dynamics, by effectively bandlimiting the actuation at some spatial locations.

4. It helps keep unwanted noise out of the system from unused channels.

In all cases this clustering is used in conjunction with other methods like sensor and actuator blending to insure a passive system for velocity feedback or resonant mode control. Reducing the set of actuators to 5 from 9 greatly aids in the convergence of the LMI solver for sensor and actuator blending as well. This will now be discussed.

5.6.2 Sensor Actuator Blending

Consider the cluster targeting mode one. For this cluster of 5 actuators and using the 9 available sensors it is desired to find a blending of these 9 sensors and a blending of these 5 actuators that yields a passive system. Furthermore the simplification of the compensator design to a SISO greatly speeds the design process and simplifies the hardware implementation. Therefore it was desired to blend these 9 sensors and 5 actuators with blending matrices $M \in \Re_{1\times 9}$ and $N \in \Re_{5\times 1}$. This was done using the procedure discussed in sections 2.5.2.2 and 2.5.2.3. The plant dynamics before the passive blend are shown in figure 5.13. The passified SISO plant (for cluster 1) is shown in 5.14. The resultant SISO plant has been largely passified (even in the presence of the problematic actuator dynamics from above) except at frequencies below 1 Hz. This should again allow much more control action without fear of destabilizing the plant.

This improvement is for the case of constant velocity feedback in Fig. 5.15. The feedback gain can now be set considerably higher ($K_v \approx 500$) before the low frequency (non-passive) region is destabilized. The primary reason that this blending approach doesn't perfectly stabilize the system is that in order to get the LMI system to converge on the solution a very small D matrix term was added to the state space system. This additional feedforward term was not enough to completely passify the system (just to aid the numerics) but when neglected from the system as in the control implementation of figures 5.15 and 5.16 the result is that the low frequency $<$ 1Hz is not constrained between 90 and -90 of phase. To rectify this the D term can be added back in (this represents a form of feedforward passification). However this term was not added back in as it was not necessary to achieve excellent reductions. At this point it should be noted that while targeting the plate with control the response of interest is the sound source to microphone. Therefore it is important to target plate modes that couple most strongly to the acoustic enclosures. The highest acoustic mode of the coupled system is at 70 Hz and this couples most strongly to plate mode 1. This is evident in the results of the controller which show that targeting plate mode 1 greatly reduces the 70 Hz acoustic mode but has less effect on acoustic modes that do not strongly couple with the first plate mode (as expected). This can be remedied by targeting another mode using a different cluster like (5 or 6) for the same procedure. The results of this are shown in figure 5.16. As expected the 70Hz mode is not strongly reduced but the modes in the 300Hz range (that couple more strongly with modes 5 and 6) are reduced significantly. This a nice, simple, and effective technique for controlling but is limited in that it only allows for using a single cluster at one time. This limitation is addressed in the frame work of passivity through the use of passive resonant mode filters/controllers. These controllers have a form given in Eqn. 5.3 and are passive. Their high gain at the designed resonance and high roll off elsewhere ensure that any control action is extremely bandlimited. By using several of these resonant mode filters, each centered on a particular target acoustic mode, different clusters and blending may be implemented together in parallel. The resultant controller will also still retain its passive properties as is shown in figure 5.17. When simulated this controller works extremely well and performs as expected. However to get even better reductions in the 70Hz mode a larger gain is needed for the plate mode one cluster/blending/RMC filter and this still eventually destabilizes these low frequency dynamics.

5.6.3 Series Passification

To fix this problem the system either needs to roll off more a low frequency naturally (perhaps by a passive redesign) or the system could be passified. One approach that works extremely well at passification is feedforward control action. Unfortunately this also has the undesired effect of reducing the performance of the control. To avoid this a different approach was utilized to passify the system using a post applied series compensator. This compensator to was designed to be a high pass filter to eliminate the adverse effects of the actuator dynamics on the passivity properties of the system. The plant dynamics before and after compensation appear in figure 5.19. This compensator was utilized in addition to the controller designed in the prior section and can be implemented either as a diagonal transfer matrix just before the blending (if every collocated channel has its own unique dynamics this would be best) or just after the blending matrices (to limit the total size of the controller in implementation). In the following plots the first approach was taken. This new control approach is now able to target any desired resonance in the acoustic response and do so with any control gain on each of the parallel filters. The effectiveness of this approach is evident. Now the ultimate performance is limited by the saturation of the actuator and not by the stability of the controller.

5.7 Summary of Simulation Results

Below are the summarized results for each of the controllers considered above. The relative or normalized signal energy is defined as the signal energy of the closed loop response divided by the signal energy of the nominal open loop response (Eqn. 5.4).

$$E_{rel} = \frac{E_{CL}}{E_{OL}} = \frac{\sum_{i=0}^{\infty}(|p_{CLi}(j\omega_i)|^2)}{\sum_{i=0}^{\infty}(|p_{OLi}(j\omega_i)|^2)} \tag{5.4}$$

Also indicated is what the limiting factor for performance was. In most cases this translated to a stability issue. However in the cases where the system was appropriately passified this was an actuator saturation issue. At this point it should be noted that the saturation defined was an artificial one that was determined would protect the actuators (used later in experiment) from damage although they could potentially be driven harder. This was set at a level of 4 Volts supplied to the actuators which are 8 ohms. Furthermore the saturation nonlinearity of the actuator may be characterized as a passive operator and as such it can be shown that control approach will still be robustly stable in the presence of this nonlinearity. Certainly some types of model uncertainty will not affect the passivity properties of the plant. If the uncertainty description of a passive plant is itself passive this will certainly be the case. However if the nominal plant and its uncertainty are not passive or their combination makes the plant not passive then passification problem both for the blending, feedforward, or series passification may still be utilized. However, in the passification synthesis one must make sure that the compensator or blending matrix passify all plants in the uncertainty class.

Table 5.2 Summarized Results for Considered Controllers

Controller Type	**Relative Mic. Signal Energy Reduction**	**Limiting Factor**
LQG (Panel)	0.2042	Stability
LQG (All)	0.0417	Stability
Summed Vel. (No Act. Dyn.)	0.0016	Act. Saturation
Summed Vel. (With Act. Dyn.)	0.8175	Stability
Decentralized Vel. (No Act. Dyn.)	0.0008	Act. Saturation
Decentralized Vel. (With Act. Dyn.)	0.7791	Stability
Decentralized Acc. (No Act. Dyn.)	0.2599	Stability
MIMO RMC Acc. (No Act. Dyn.)	0.0321	Stability
MIMO Blended Vel. (With Act. Dyn. Mode 1)	0.0933	Stability
MIMO Blended Vel. (With Act. Dyn. Mode 2)	0.1585	Stability
MIMO Blended Vel. (With Act. Dyn. RMC)	0.1318	Stability
MIMO Blended Vel. (RMC series Passifier)	0.0071	Act. Saturation

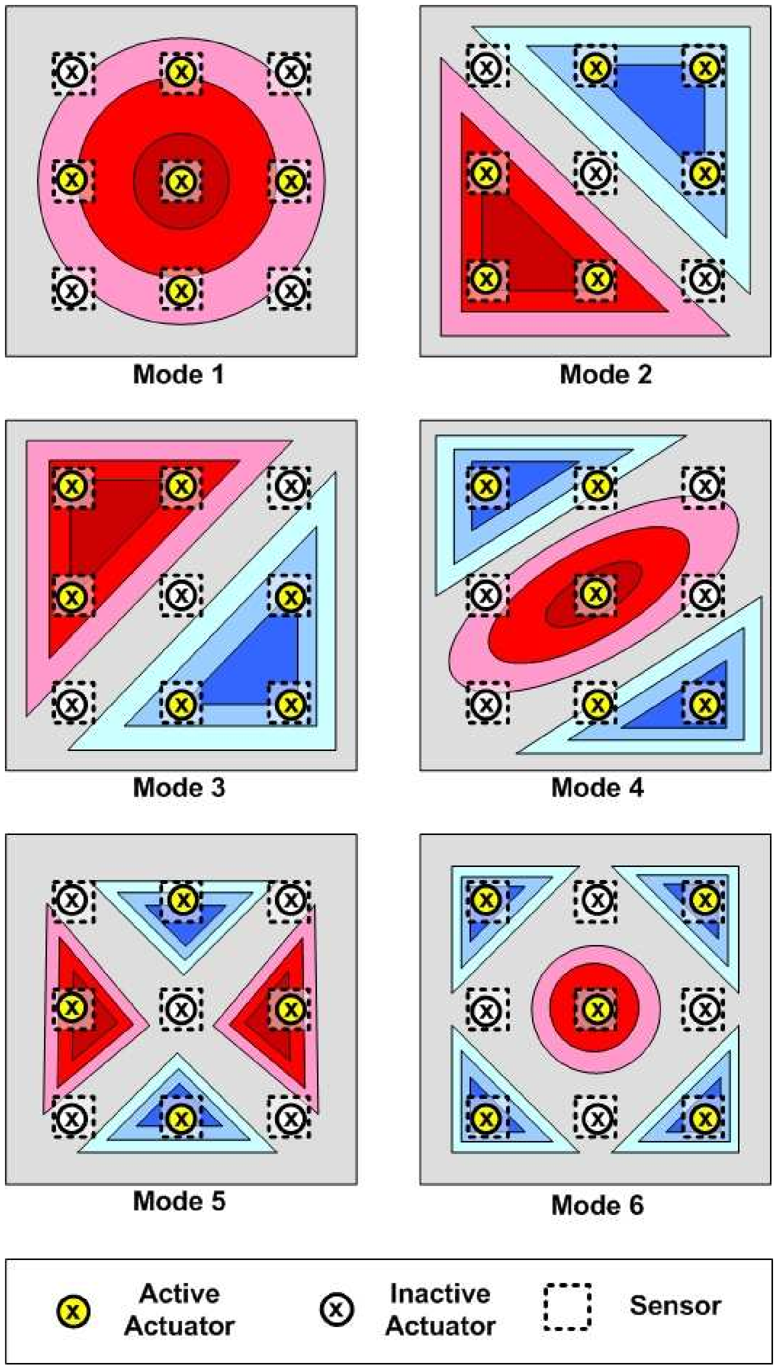

Figure 5.12 Actuator Clustering Subsets for each Mode

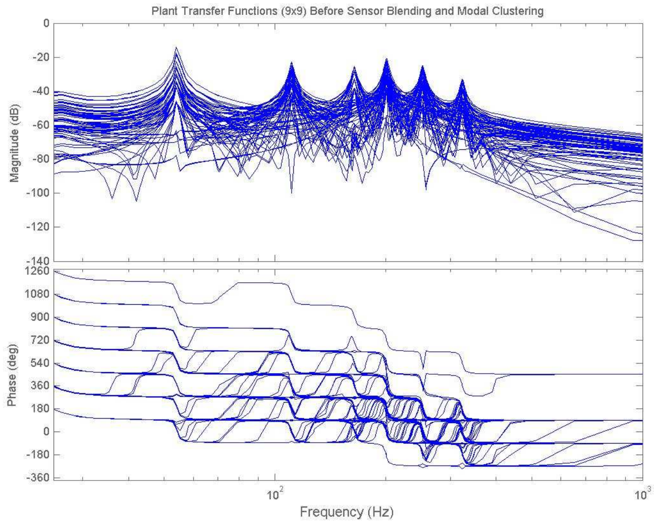

Figure 5.13 Plant before sensor actuator blending

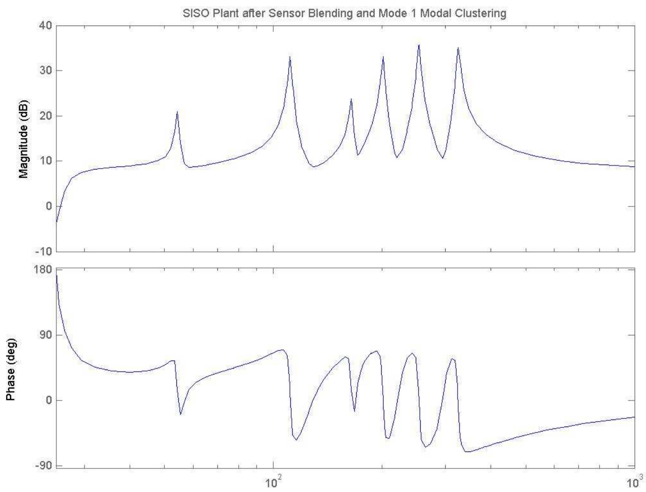

Figure 5.14 Plant after sensor actuator blending

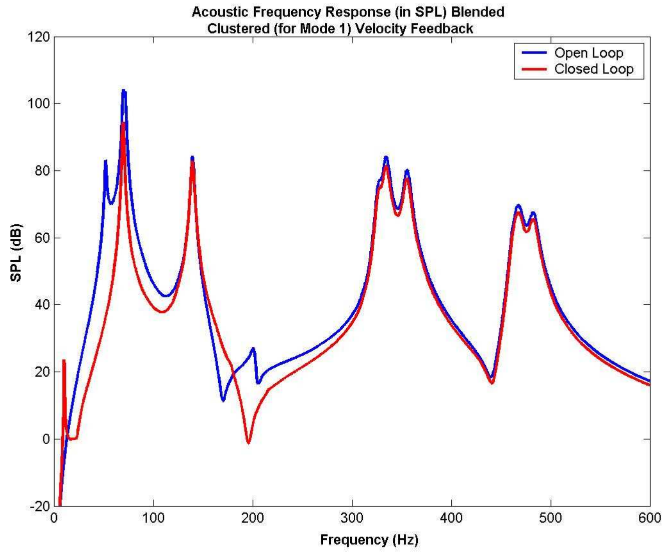

Figure 5.15 Control of plate with sensor/actuator blending targeting mode 1

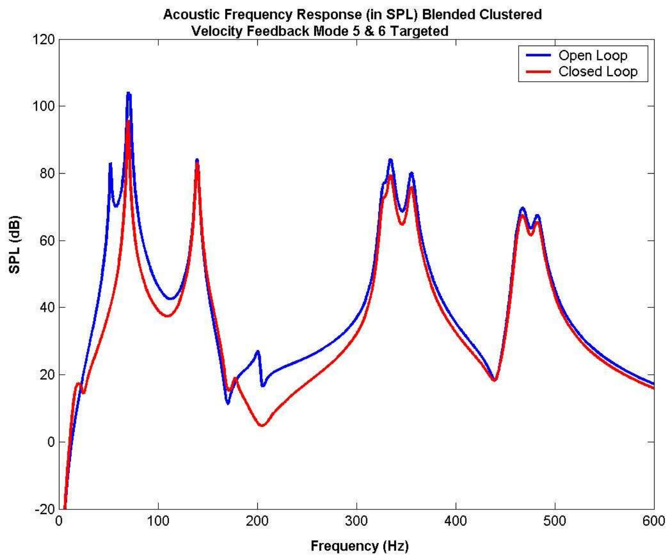

Figure 5.16 Control of plate with sensor/actuator blending targeting mode 2

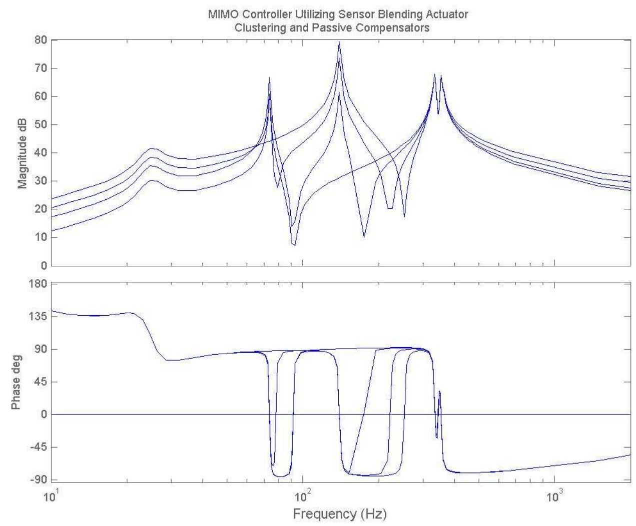

Figure 5.17 C_{FB} transfer function

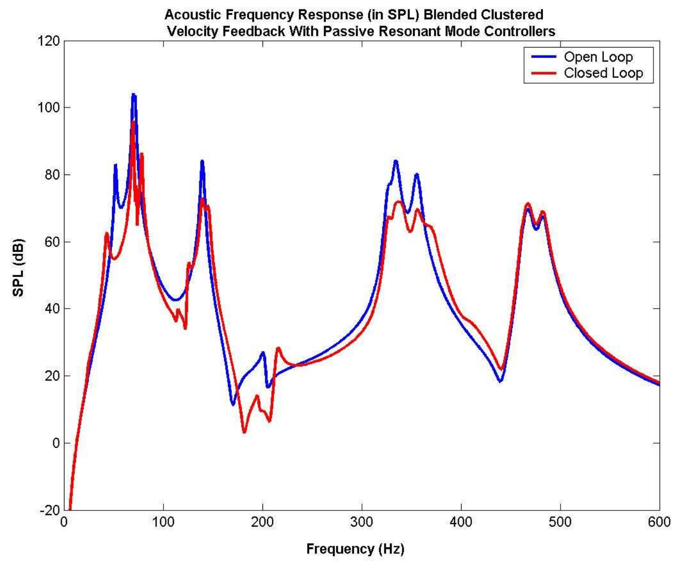

Figure 5.18 Control of plate with sensor/actuator blending and resonant mode controllers mode 2

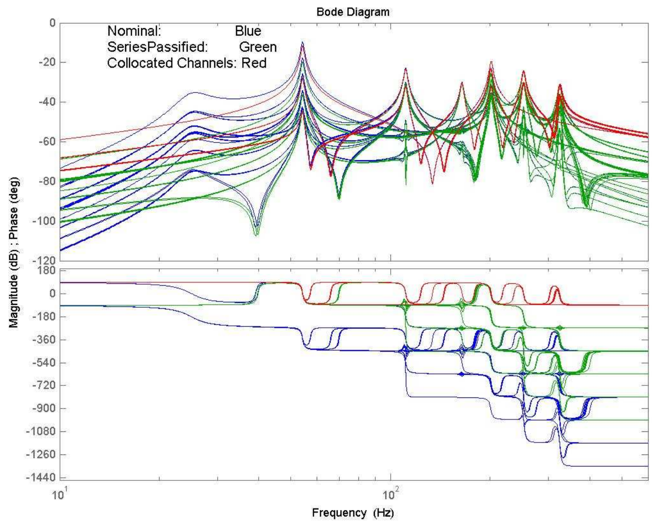

Figure 5.19 Plant Dynamics Before and After Series Passification

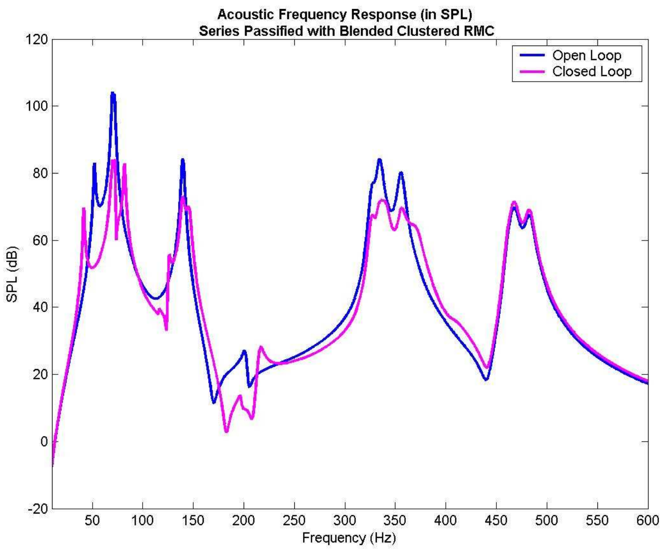

Figure 5.20 Open and closed loop comparison for series passification and RM filters

6 Construction of Actuators, Sensors and Electronics

The analytical–computational modeling of a coupled acoustic enclosure and structural barrier (and subsequent control simulations) indicated several promising approaches, both to redesign and active noise control for the system. Before meaningful experiential tests of these results could be achieved, the experimental hardware and setups needed to be constructed. This hardware falls in to several groups including: 1) power amplifiers for speakers and inertial actuators, 2) piezo amplifiers for driving piezo actuators, 3) signal amplfiers/filters for sensor signals, 3) Piezo actuators and sensors, 4) Inertial actuators, 5) and microphones and accelerometers for use in these setups. The considerations and details of each of these items will now be discussed. The setups that these systems were applied to are depicted in section 7.

6.1 Power Amplifiers

In order to drive disturbance speaker(s) and voice coil actuators requires the use of power amplifiers. Amplifiers of this type are commercially available at any number of home audio stores. Typically the metrics of importance for these devices are that they have nice flat frequency responses over a wide range of audio frequencies and that they are capable of supplying a certain amount of power per channel (ie 25 Watts). However, for control applications there are some further requirements that are typically lacking in most modern commercially available audio power amplifiers.

First, the amplifier should not introduce unnecessary delays into the system. Most modern amplifiers utilize digital FIR filters that produce an excellent quality audio reproduction when playing music but at the same time introduce a pure time delay. In traditional audio applications this is not an issue. However, when using this amplifier to power an actuator for doing realtime active control, the introduction of this pure time delay is a real problem. The pure delay is difficult to model as a linear system over a wide range of frequencies and furthermore when fitting a numerical model (for example with SOCIT) the presence of the pure delay causes the ERA fitting algorithm to introduce many RHP zeros. These RHP zeros consequently will severely limit the performance of the active noise controller, which is undesirable. It is important to note that these zeros could be avoided in this case by not using an amplifier with a FIR filter. Second, the amplifier for a control application needs to have many (in this case 10) independent channels with considerable power. Typically, most available audio amps do not have this feature, and those that do only have two independent amplifier channels. This could be remedied by purchasing multiple amps but this quickly becomes costly.

After an exhaustive search of commercially available amplifiers from both home audio and high-end audio measurement companies (like Larson Davis or B&K) no suitable solutions for less than $10,000 were found. Therefore an analog power amplifier was designed and constructed, then replicated to supply the necessary number of channels for the MIMO control application. This power amplifier utilized an LM3875 high-performance 56W audio power amplifier and a layout architecture based loosely on the "gain clone" design. A picture of one of the finished amplifier boxes (there are 5 total with 10 channels) appears in Fig. 6.1. When each of these were completed they were tested and found to have excellent response characteristics over the entire audio range, low ripple, and extremely low signal noise (in fact better than the commercially purchased single channel system that we had been using in prior control work in the lab). Most importantly this system didn't introduce any pure delay terms into the system, a must as per the above discussion. These amplifiers cost about $60 per channel to produce making them very reasonable. When finished, this design was capable of supplying 56W at up to 12V for each channel. The voltage gain of this design is approximately 33 times.

Figure 6.1 The constructed custom audio power amplifier

6.2 Piezo Amplifier

To drive the piezo actuators also requires a power amplifier; however, these power amplifiers must be able to deliver high voltage (upto 400Vpp). There are several commercially available choices for such amplifiers, for example there is a Trek 2 channel piezo driver in the vibrations lab. However, this amplifier is even more expensive than a power audio amplifier $3500 and is limited to two channels. There few other options when it comes to affordable piezo drivers and virtually none that have the required number of channels. Therefore several (16 total channels) piezo amps were designed and built to meet this need at a reasonable price. This design utilized the HA13118, 18W audio power amplifier from Hitachi in conjunction with a 1:25 audio step-up transformer. Together, these produced an affordable piezo driver with an output approximately up to 450Vpp at 16W of power. The voltage gain of this driver amp design is approximately 50 times.

This is more than suitable for driving the PVdF and PZT samples we investigated here. Figure 6.2 shows the final assembled design.

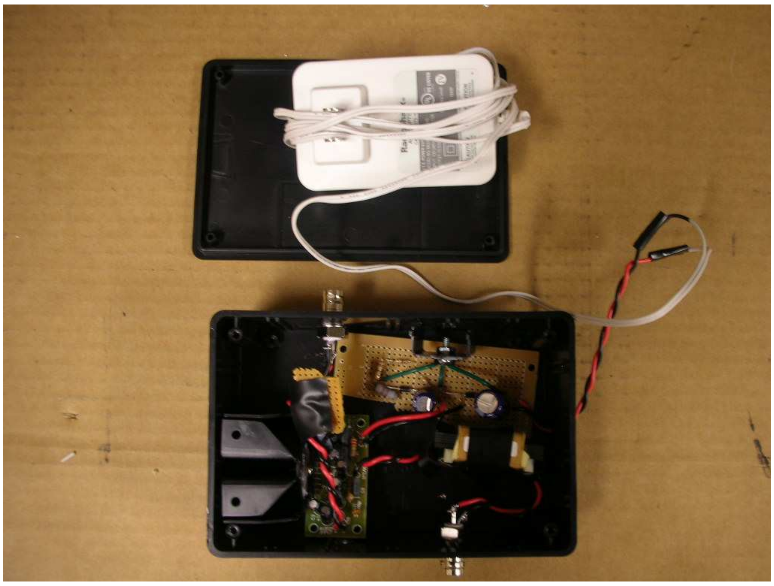

Figure 6.2 The constructed piezo driver amp

6.3 Signal Amplifiers

In the MIMO control investigations of this work there were at times as many as 30 sensors of differing types measuring simultaneously and being used either as control feedback or as performance sensors. All of these signals required scaling (amplification or division) to take full advantage of the 10 Volt range of the data acquisition hardware. Similarly, all of these signals needed signal filtering in the form of High Pass filters to remove undesired low frequency components and DC bias from the sensors, and Low Pass filters to serve as anti-aliasing filters when sampling and also to reduce the spill-over effects of the controller on the unmodeled system dynamics. Unlike the power amplifiers above there are many commercially available multichannel signal amplifier/filters. However, they suffer from one or more of the following fatal drawbacks: 1) many (but not all) of these signal amplifiers are not intended for use in real time control applications, and hence they are implemented using FIR digital filters instead of IIR or analog filters (and this is unacceptable for the same reasons mentioned in Section 6.1; 2) they are very expensive ($4k-$5k) and would not be suitable for use with all sensors like the electret button microphones which require bias power to function. Again, the best solution for these problems was to construct several custom multichannel amplifiers and filters. Specifically, a 16 channel amplifier/filter/power supply was designed and constructed for use with the electret microphones, and another 25 channels of signal amplifiers and filters without DC bias power capability were designed and constructed for use with piezo sensors, accelerometers, and PCB microphones.

The LP filter designed for both systems was an analog 2 stage Salen-Key design using the LM386N-1 op-amp and having a break frequency at 5kHz. The HP filter used was a 1 stage Salen-Key Design cutting in at 10 Hz. The general amplifier/filter utilize both a preamp and post amp. The non-inverting pre-amp had user selectable gains of 1, 2, 4, and 10. The non-inverting post-amp had gains of 1, 2, 4, 10, or 100. Figures 6.3 and 6.4 show these two designs in the process of being constructed.

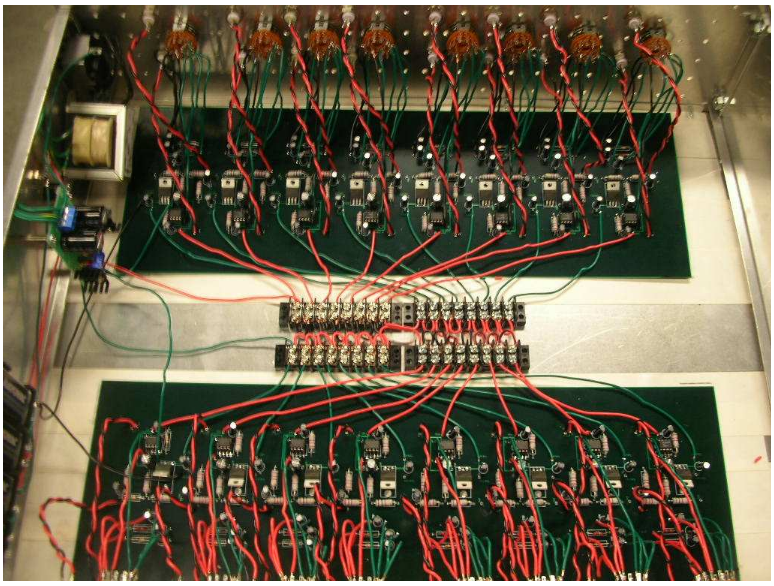

Figure 6.3 The signal amp/filter/power electronics for button mics

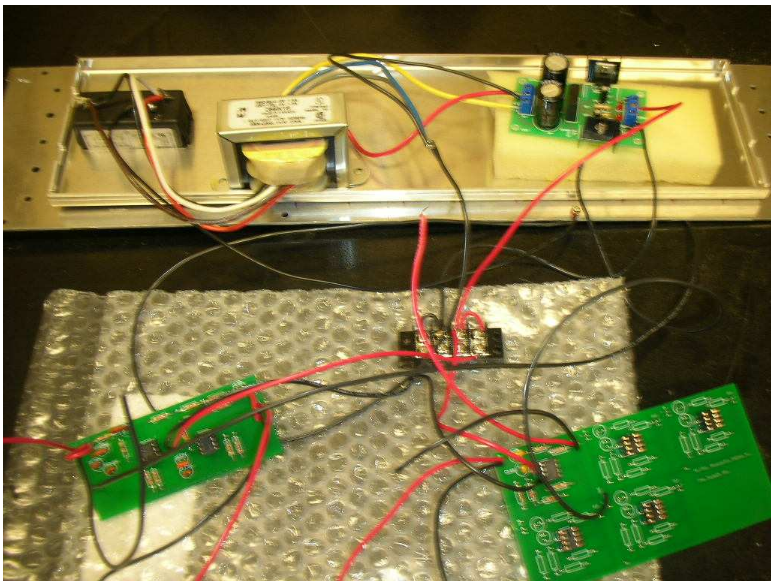

Figure 6.4 The general signal amp/filter electronics for sensors

6.4 Piezo Sensor and Actuator Construction

When investigating acoustic structural noise control problems like this one, a popular choice of actuator is a piezoelectric material. Materials that exhibit the piezoelectric effect will experience strain under the application of an electric field, and, consequently, will experience an electric field under strain. This makes them popular materials for both actuation and measurement. A number of materials experience the piezo electric effect: quartz, cane sugar, some salts, PVdF (polyvinylidene fluoride), PZT (lead zirconate titanate), even things like tendon and bone. Depending on the configuration and the crystal structure of the material this effect may be large or small and is indicated by the anisotropic piezoelectric coefficients for the material. Piezoelectric materials with large mechanical to electric coefficients make excellent sensors, those with large electrical to mechanical coefficients make excellent actuators, and many with both can be used in either fashion. The two types of material used in this work are PVdF, a flexible polymer, and PZT, a rigid ceramic. There are pros and cons of each of these. PVdF is commercially available as a prepoled polymer sheet of varying thicknesses ready to be fashioned into any number of shapes with a little bit of effort. While not extremely strong, PVdF functions respectably well as both an actuator and a sensor (in fact it is often used in small piezo tweeters). However, there are some drawbacks to the material due to the lower mechanical coefficient than other materials (like PZT), and higher voltages are necessary to exhibit equivalent strains. But perhaps more important is that PVdF is a flexible polymer whose elastic modulus is low (compared with rigid ceramics, metals, and polymers). This means that much of the strain that is developed in the material is lost in the interface of the material and the substrate it is attached to if the elastic properties of the actuator and substrate are not of approximately the same order. This makes the material a poor fit when working with metallic structures. However, the material makes an excellent sensor for measuring the vibration in a structural material, and, as mentioned earlier, exhibits a voltage output that scales with velocity. Particularly interesting is the use of this sensor in conjunction with a like-shaped and placed actuator as a sensor actuator pair. In this configuration these two devices form a collocated strain actuator and velocity sensor and comprise a mathematically passive sensor and actuator pair. This has excellent properties when later designing controllers as it can lead to simple controllers with excellent robustness properties.

PZT makes up for many of the short comings of PVdF and introduces some new ones. PZT is much more stiff meaning that the strain it develops has greater transference to the metallic plate. Furthermore, it is an even stronger piezoelectric material than PVdF, meaning that it is capable of developing larger strains (forces) under lower voltages. However, two major drawbacks of this material are that it is expensive (small 2 by 2 inch squares cost well over \$100, and unless you have specialized material fabrication facilities or pay someone who does, one can not make it into any desired shape easily.

The PVdF sensor/actuators used in the work of this dissertation are 4 by 4 inch squares. To construct theses devices 52 μm prepoled sheets were oriented into the poling direction and then cut to the appropriate size. Next, the contact of the devices were created by using XYZ axis conductive adhesive from 3M. These two pieces of adhesive were cut so as to leave $1/8^th$ of an inch around the edge of the PVdF (to avoid accidental or undesired arcing across the two parallel contacts on either side of the PVdF). Along one edge of the contact a piece of conductive copper tape adhered to each contact, and multi-stranded 28 gauge copper wire was soldered to the copper tape. Last, the device was finished by sealing it in an encapsulating layer of 2 mil polypropylene packing tape. When finished the translucent sensors/actuators look like those in Fig. 6.5. Several variations on this design were constructed and the responses of these samples measured. Two types of PZT actuators were initially investigated for use in this project. The

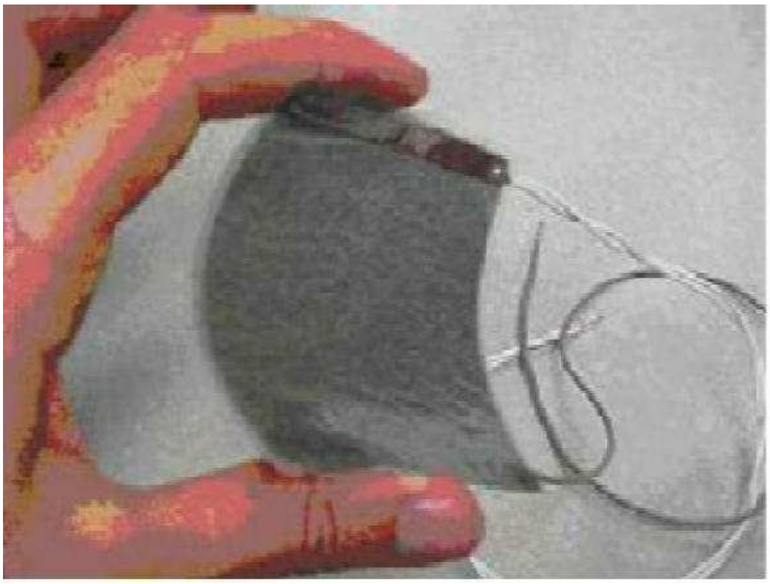

Figure 6.5 A finished PVdF actuator

first was a flat rectangular PZT actuator from PCB piezotronics. This piezo, although strong, also added significant rigidity to the region to which it was applied and was not removable once adhered (with epoxy), and this is not ideal. A second choice was a prestressed THUNDER^{TM} actuator, where the PZT was deposited and sintered to a curved metal carrier, which greatly amplified the forces generated by the device. Since these were approximately the same cost, and the THUNDER actuators were more easily removed from the substrate and reused, these devices were chosen. A picture of the THUNDER actuator appears in Fig. 6.6.

THUNDER TH-6R PHYSICAL PROPERTIES					
Mass	Footprint (domed)	Footprint (flat)	Piezo-layer Thickness	Total Thickness	Dome Height
0.0358 lbs	2.985" x 2.040"	3.00" x 2.040"	0.015"	0.028"	0.167"
16.3 g	75.82mm x 51.82 mm	76.20mm x 51.82 mm	0.38 mm	0.71 mm	4.24 mm

Figure 6.6 The selected THUNDER PZT Actuator

6.5 Inertial Actuators

One problem with using PZT actuators is that it is not easy to exactly collocate a sensor due to the layout of the actuator. This means that although the actuator will be more powerful there will likely be RHP zeros associated with the combination of sensor and actuator, and this will lead to limitations on the control. Furthermore, the form of actuation experienced when using the THUNDER actuator is more like the application of two line shearing loads along the attached edges of the actuator leading to a bending moment on that region of the plate. Although not necessarily a problem, depending on the size of the actuator it may lead to difficulties attacking some of the structural modes of the plates. One more problem is that these piezo actuators have poor low frequency response and may not be able to effectively act on some of the lower frequency modes. To resolve these issues and increase the direct force applied to the plate at a location, a direct forcing actuator was designed. This actuator (often called an inertial driver, proof mass actuator, voice coil actuator, reaction mass driver, etc.) essentially consists of a voice coil like in an audio speaker, a permanent magnet, a spring mechanism, and a certain amount of desired proof mass. Just like in an audio speaker the actuator is driven by an amplifier and the electromagnetic action of the coil on the permanent magnet/mass-spring combination sets the mass into motion, thus transmitting a reaction force through its base and into the plate at the attachment point. The advantages of this type of an actuator include: 1) you are directly forcing the plate at a point of your choosing (easily modeled), 2) this actuator requires no specialized amplifier to drive just a power amp, 3) by properly selecting the mass and spring stiffness values, the maximum strength and cut out frequency of the actuator can be designed, and 4) the material to construct this type of an actuator is not expensive or exotic.

There are some commercially available proof mass actuators but these existing products either lack the power, frequency range, or are far too massive to be mounted on a plate surface. In addition to the expense of the actuator, there was also added expense from specialized driver amps. In order to get exactly the characteristics desired from the voice coil actuator, a specialized actuator was designed, constructed, and tested for use in later control investigations. The following is a brief description of these efforts.

6.5.1 Design of Actuators

First, the overall mass of the actuator was designed to be approximately 112 g for the large one and 101 g for the low profile actuator, with the majority of this concentrated in the reciprocating part to maximize the reaction force at the base. After several design iterations, the configuration utilized a central post, a linear sleave bearing, an annular permanent rare-earth magnet, a low carbon steel field concentrator/inertial mass, magnet wire, two compression springs, and an aluminum base. The first part of this effort sought to enhance the field strength of the gap where the voice coil would lie. At the same time, the uniformity of the field experienced by the voice coil at all points on the stroke of the device was optimized to yield the most linear forcing behavior possible. This investigation of the EM properties of the gap was accomplished by finite element solution.

6.5.1.1 FEM Simulation

The freeware package used for the EM finite element simulation is called FEMM4.0. This package is specialized for solving 2-D and 3-D axisymmetric electromagnetic problems, and solves the relevant Maxwell's equations using triangular elements. All investigations here considered axisymmetric formulations of these equations on a semicircular domain.The EM properties of the various materials were entered into the program and then different designs and orientations of the magnets, field concentrators, and voice coils were explored. The following assumptions about materials and boundary conditions were made in this modeling process. First, the solution was assumed to be for low frequency (¡1000Hz), and it was assumed that the EM properties of the materials in the model were essentially constant over this range. Second, there was a symmetric boundary condition along the y axis, and an asymptotic boundary condition (approximating the impedance of unbounded space) along the semicircular edge of the meshed region. Third, the permanent magnet was modeled using the equivalent sheet current method. Given the energy product E of the material (from manufacturer) in MGOe, the coercivity (H_c in A/m) of the material was determined using Eqn. 6.1 and this value of the linear current density was applied to the domain properties of the magnetic material.

$$H_c = \frac{(5E5)sqrtE}{\pi} \tag{6.1}$$

With these assumptions several configurations were investigated. Figures 6.7 and 6.8 show the solutions for the field string in low profile lower mass and high profile higher mass designs respectively. The area of interest is in the gap between the two poles of the concentrator.

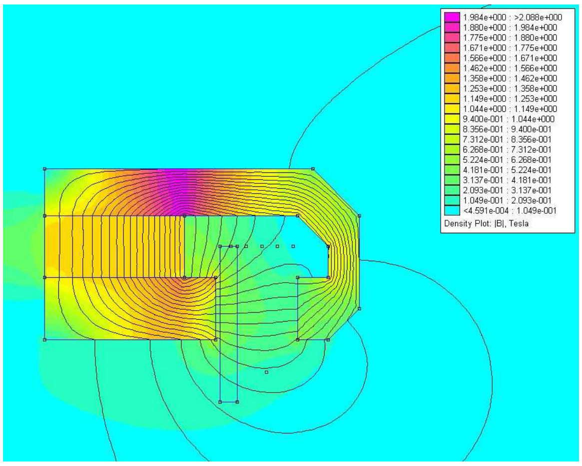

Figure 6.7 The low profile solution for field strength

6.5.1.2 Construction and Testing

After numerous configurations were simulated using the above described method, annular 1/4 inch thick neodymium magnets with 48MGOe energy density were purchased along with small springs (7/8 in compression 8.33 lbs/in). The concentrator was composed of two pieces of machined 1018 steel: 1) an exterior core piece (measuring 1.50 in OD 1.25 in ID and .562 in height) and an interior core piece (measuring 0.843 in OD and 0.25 in height). A support bar for seating the springs and the sleeve bearing was designed and fabricated from aluminum, as was the base for seating the voice coil, and the cylindrical voice coil holder. Lastly, a polished 1/8 inch linear motion shaft and nylon sleeve bearings were purchased for supporting and guiding the reciprocating parts. The springs were chosen such that in conjunction with the reciprocating mass the fundamental resonant frequency would be at approximately 30 Hz, and would have a strong and uniform reaction force response from 40Hz to 500Hz, as well as reasonable strength (although not smooth response) over the range of 20 to 1000 Hz. To assemble the voice coil, a length of enamelized magnet wire equivalent to 8 Ohms of resistance was wound around the cylinder, soldered to lead wires, and then coated with epoxy to hold it tightly wound. This coil assembly was seated on the base and then

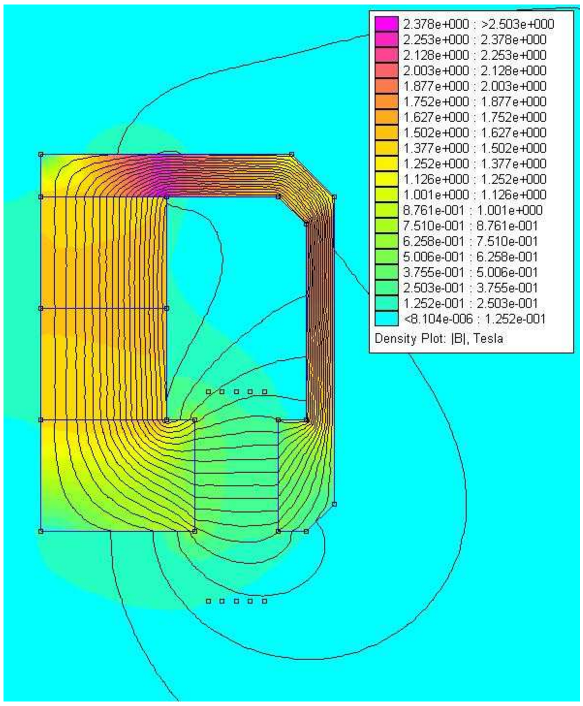

Figure 6.8 The big version solution for field strength

epoxied into place. Next, the concentrator/magnet/support bar assembly was epoxied together, and the nylon bearings were press fit into the assembly. Next, a finely polished high tolerance shaft was threaded on one end and bolted into place on the base. The magnet/concetrator assembly was then put onto the bearing shaft, and the compression springs were epoxied into place, completing the assembly. Figure 6.9 shows a finished low profile prototype and Fig. 6.10 shows the acceleration response data for this actuator design. To drive these actuators the power amplifiers developed and constructed (Section 6.1) were used. For the linearity study the actuator had been affixed to a flexible beam structure cantilevered at one end.

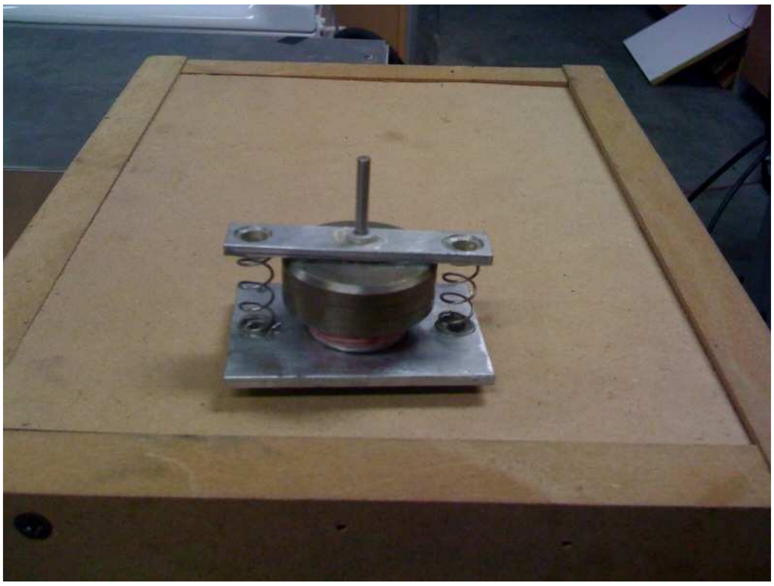

Figure 6.9 A finished low profile inertial actuator prototype

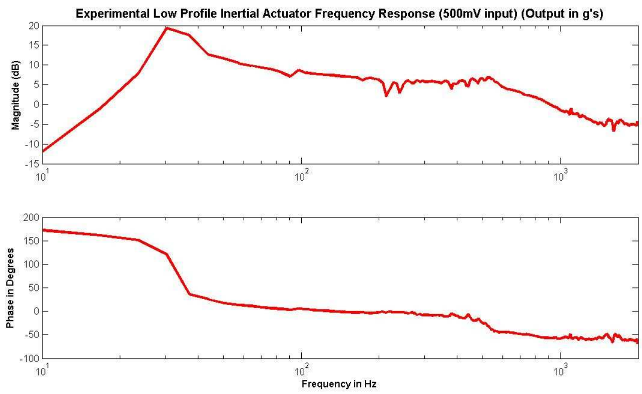

Figure 6.10 The experimental frequency response of designed inertial actuator

7 Experimental Validation of MIMO Active Control Approaches in Acoustic Stucture System

There are many approaches and controller strategies found in the literature for the control of vibrating structures. Many of these approaches lead to elegant solutions in theory and simulation, but are very difficult to put into practice on physical hardware. Ultimately from an engineering standpoint, if the control design can not be implemented, or the hardware implementation lacks the benefits of the theoretical controller, then the design is not an acceptable one. In this thesis, the guiding principle is use control strategies that will increase the likelihood of success not just in simulation but in actual hardware implementation. The most important factor is not whether these controllers reduce enclosure noise in simulation (which they do) it is whether or not these control design methods were actually effective in hardware on the real system.

In this section the details of the control implementation study are presented. The blanket description of "control implementation", refers collectively to four intertwined problems (each with many substeps). These four problems are:

1. Experimental system identification (system ID ,or just ID) to gather the complex frf's of the physical plant.

2. Control design modeling to produce an accurate mathematical model from this experimental derived frf.

3. Design of a control law for this mathematical model and subsequent simulation of this law.

4. Implementation of this control law in discretely in hardware (in this case on a digital signal processor).

The effectiveness of these designed controllers is then measured by the amount of reduction in the peak acoustic response of the destination enclosure that can be attained with and without control.

7.1 Experimental Hardware Setups

7.1.1 1-D Tube with Barrier

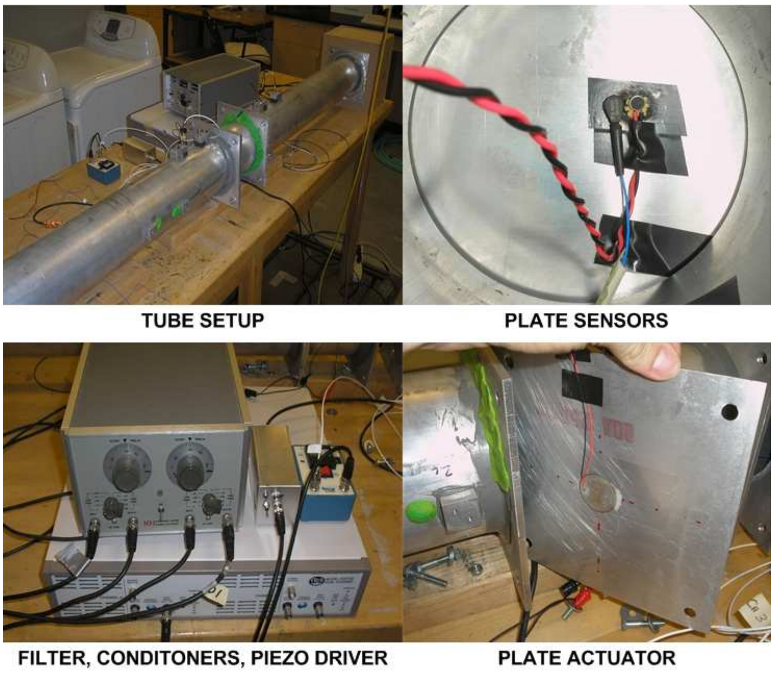

Figure 7.1 The experimental apparatus of the 1-D Tube investigation

The first setup that was considered was a 1-D tube setup with a barrier plate halfway down its 6 ft length. At one end of this tube is a driving speaker, and at the other is an anechoic termination (achieved with a foot and a half of acoustic foam). Epoxied to the center of the separating plate was a Thunder^{TM} (Model TH5-C) piezo actuator. Adhered directly on the opposite side by temporary adhesive was a PCB accelerometer (Model 352A24). This accelerometer signal was then sent to a battery powered ICP conditioning unit (PCB model 480C02). The conditioned signal was then routed through a Kronhite (KH) two channel analog LP filter with the filter bandwidth set to 3000Hz. This filter was primarily used as an anti-aliasing filter. After the AA filter, the acceleration signal was sampled using a D-Space 1103 board at 10,000Hz and carefully designed digital LP filters at 900 Hz were applied to limit control action above 800 Hz without adversely affecting the response below this point. Finally, this signal converted back to a continuous domain and routed directly to the SRS075 two channel analyzer. To drive the plate the SRS075 analyzer was used with swept sine excitation. The source signal was used internal to the analyzer to compute the input-output response, and was also routed through the d-SPACE. In the d-SPACE the signal was sampled at 20000 Hz then outputted directly to Trek model PZD700-2 2 channel piezo driver. The output of this high voltage amp was then connected to the piezo actuator on the barrier plate thus completing the loop. A diagram of this setup appears in figure 7.2 and pictures of the tube, the plate, and the filtering/conditioning equipment appear in figure 7.1. For this investigation the microphone response was measured using a electret button microphone placed in the tube approximately 4 inches from the sample surface on the destination side.

7.1.2 Two Chamber Acoustic Enclosure

The second setup was that of the two chamber 3-D acoustic enclosure system (modeled and simulated in previous sections). This system is comprised of two identical 4x4x8ft chambers constructed of MDF so as to be highly reflective, and closely approximating a rigid acoustic boundary condition. In one chamber were 5 acoustic drivers (4 speakers and 1 woofer) each driven by independent custom made analog power ampli-

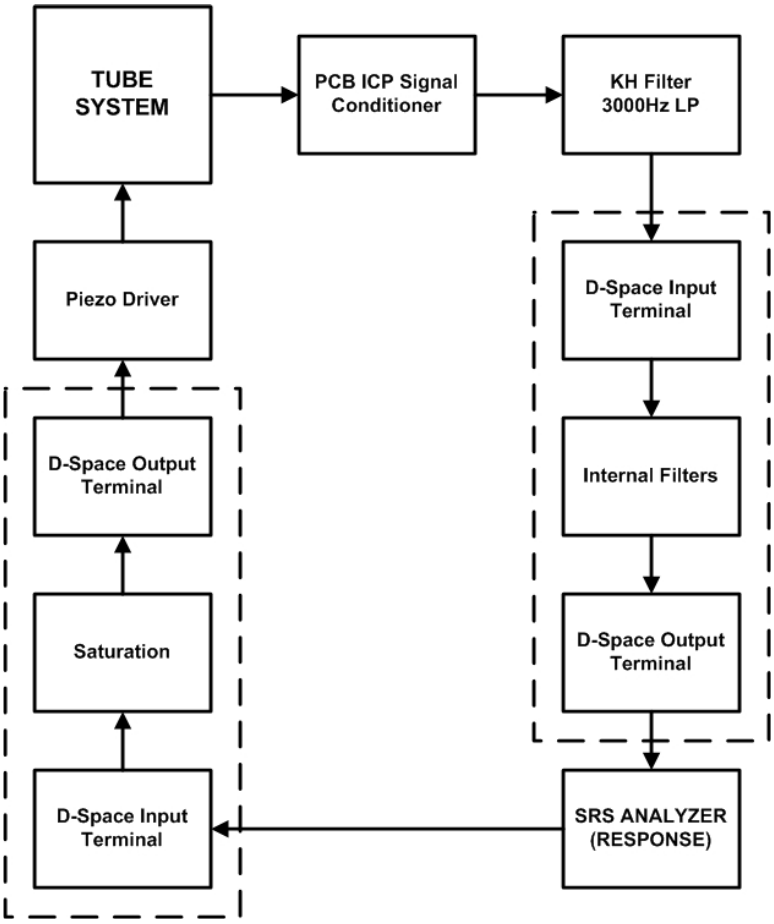

Figure 7.2 Hardware Interconnection Diagram for 1-D Tube System

fiers. In the other chamber were several microphones (8) arranged in spatially diverse and irregularly spaced x,y, and z locations. These 8 locations were kept the same from test to test so as to allow meaning full comparison. Separating the two chambers was a clamped-clamped steel plate with 5 attached proof mass actuators on one side. On the opposite side of the actuators were a 3x3 grid of accelerometers (PCB 352C65). Five of the accelerometers were located directly opposite the point of attachment for the proof mass actuator so as to form a collocated pair. The accelerometer and microphone signals were then sent to ICP conditioning units with 12 channels and 16 channels respectively. The 12 channel unit also had a built in analog integration capability for use when desired signal of interest was plate velocity. The signals from both of these types of

Figure 7.3 The actuators and sensors for the 3-D enclosure system

sensors (microphones and accelerometers) were then routed through the custom made signal amplifiers and filters described in section 6. These were necessary to properly scale and AA filter the signals for sampling by the D-space. The D-space utilized in this investigation was the 1105 module capable of sampling 32 separate inputs and driving 32 separate outputs simultaneously in real time. After sampling at 20,000Hz a digital Low Pass Filter with a high roll off was implemented at 1500Hz. When identifying the plant this signal was then converted back to continuous time domain by a D2A converter. Then this signal was supplied directly to the sensor input channel of the SRS analyzer. In this same mode the analyzer source signal was sampled by the D-space then outputted and directed to the custom made audio power amplifiers. These amplifiers where then used to power the custom made proof mass actuators thus completing the loop. A diagram of this setup appears in 7.5. Again, when taking the closed loop

Figure 7.4 The analyzer, control hardware, signal electronics, and power amplifiers for the 3-D enclosure system

speaker to microphone responses the d-Space is bypassed and the signals out of the signal amplifiers are routed directly to the analyzer. Similarly the analyzer directly drives the custom power amplifiers when exciting the acoustic enclosures.

7.2 System Identification 1-D Tube

7.2.1 Data Collection Procedure

The tube apparatus was experimentally identified using a blackbox ID technique. This begins by driving the piezoelectric actuator with swept sine input from 0-800Hz using the SRS analyzer. Then the accelerometer signal is measured, conditioned, filtered and sent to the SRS analyzer as per the description above. Then the analyzer compares

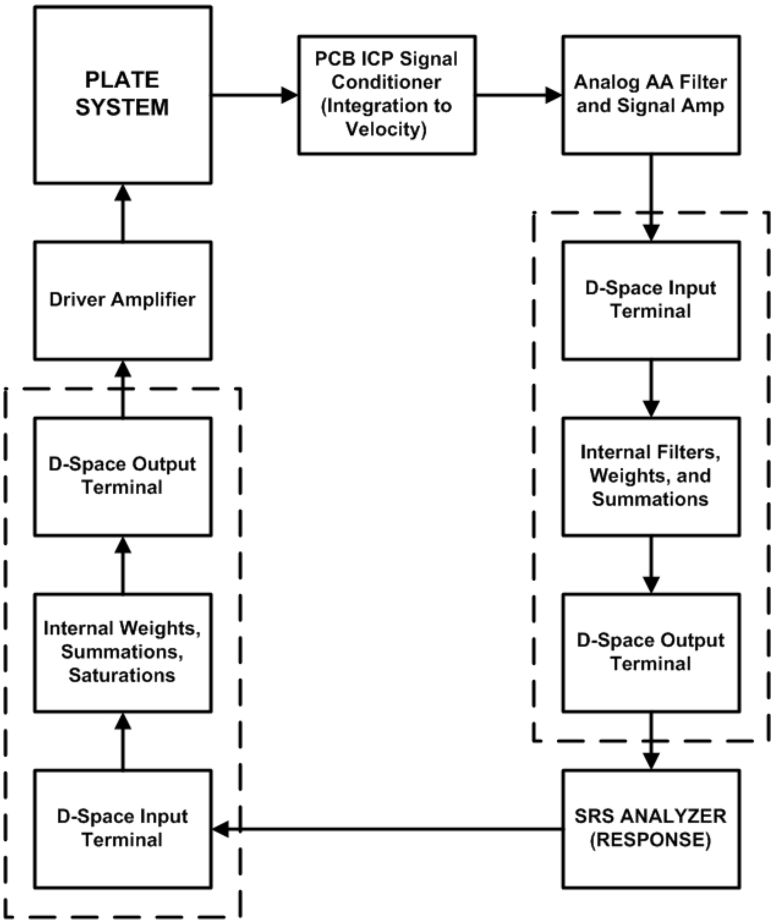

Figure 7.5 Hardware Interconnection Diagram for Plate Enclosure System

the magnitude and phase of the original sinusoid with the magnitude and phase of the final measured and filtered signal to determine the experimental complex frf. This data is then stored to disk for later use. When it comes time to implement controllers on the d-Space the only change is that the analyzer which drives and the system and measures the response is replaced with the control design inside d-Space.

To measure the closed loop microphone and accelerometer response the only change to this procedure, is to instead drive the source speaker with an one of the custom gain clone audio amplifiers. Then the conditioned microphone or accelerometer signal is sent directly to the SRS analyzer bypassing the D-space (since these are not used in control design or implementation).

7.2.2 Control Design Modeling

After the collected data was imported into Matlab, it was noticed that the velocity measurement was corrupted (very noisy and low in magnitude). Further debugging was able to track down the source of this noise to a problem with the integrator function on the ICP signal conditioner. However the only problem was when the velocity signal. The standard non-integrated signal was still fine, so it was decided to instead use the acceleration signal for subsequent investigations. This has the consequence of changing the system from one that was a passive collocations to one that was not, but it also presents the opportunity to test out approaches for "passifying" the system and implementing this in hardware.

In Matlab$^T M$, this signal was imported in to the SOCIT toolbox where the (Eigensystem Realization Algorithm) ERA and a custom response optimizing m-file was used to fit the best possible (and lowest order) control design model to this data. The resultant fit had 38 states, and was reduced using the previously discussed balanced residualization approach to a more manageable 28 state. This reduced model experienced minimal degradation in the fit of the magnitude or phase. Figure 7.6 shows the data and the reduced order fit (for the reduced order 28 state fit). This illustrates one of the problems with control id and implementation for active noise control. Even on this simple 1-D system a relatively high order model (28 states after model reduction) was necessary to achieve a decent fit.

7.2.3 Passification of Control Design Model

Next, for some of the control approaches, it was necessary to have a plant that was passive. In situations where this was not already the case, this was accomplished by passification of the fitted plant dynamics. Specifically a set of plant passifying compensators were designed. Although several approaches would probably work merely adding

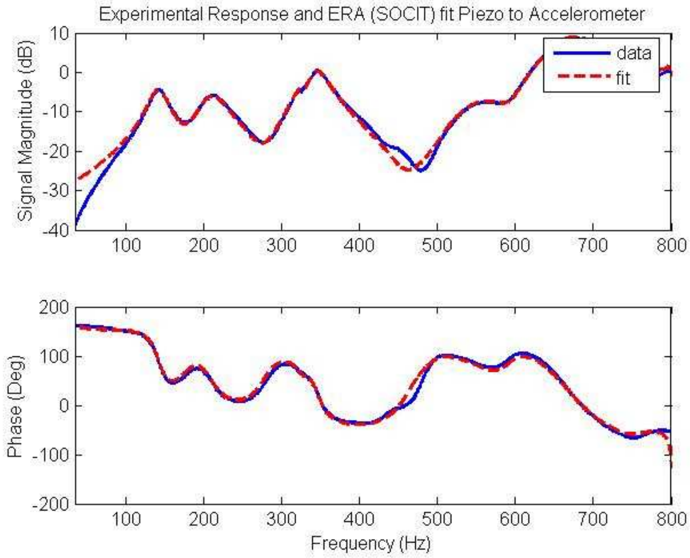

Figure 7.6 Impedance tube Response and Fitted Control Design Model

a series integrator would not. Instead, two passifying controllers were utilized. One was a simple series lag compensator with a pole at 20Hz and a zero at 200Hz. The other was a constant gain feedforward compensator (with a high frequency pole at 4000Hz to avoid an algebraic loop in implementation). As you can see in figure 7.7 the plant is passified with by these designs and the resultant C_{s2} and C_{ff} then become part of the eventual controller implementation.

7.3 Control Design Simulation

7.3.1 LQG

The first type of controller designed was a standard LQG design with $R_c = R_e = 1$, $Q_e = I * 1E6$, and $(Q_c = diag(0, 0, 0, 0, 5000, 5000, 4000, 4000, 2500, 2500, 0, 0 \cdots) + I * 1000$. Note that this controller was designed before the system was passified. A bode plot of the resultant controller appears in 7.8. The closed loop actuator to acceleration simulation shows that the controller should be very effective at suppressing the vibration

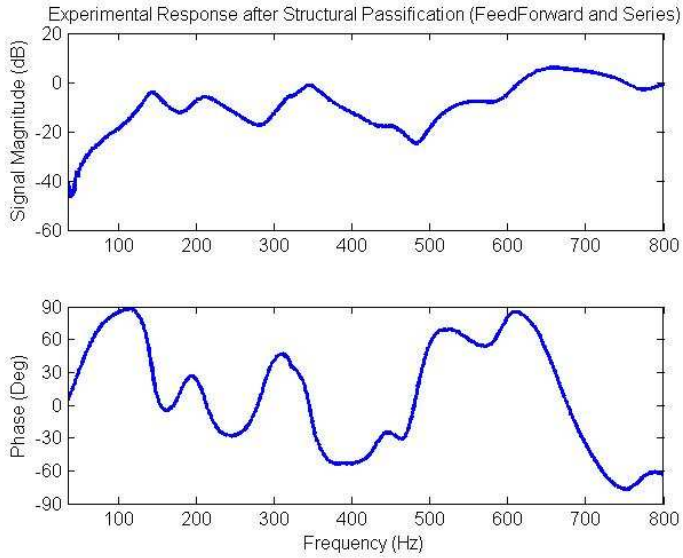

Figure 7.7 The plant (tube) control design model after passification

of circular plate in a broadband way. This should translate to similarly large suppressions of the acoustic frequency response. At this time it should be noted that all of the control simulations focused strictly on the plate plant and did not consider anything except regulation of these plant dynamics. This means that although it was possible to fit a transfer matrix with speaker and actuator as inputs and microphones and accelerometer as output only the SISO plant dynamics were utilized. This is because it was nearly impossible to get the ERA routine in SOCIT to reconcile these different frf types of data sets (even for a simple 2x2 case). Essentially the resultant fit from SOCIT created 4 lightly coupled (or uncoupled in some cases) transfer functions who did not share many common states (which is no different than just fitting 4 distinct transfer functions). Furthermore when compared to experimental results these lightly coupled MIMO fits never accurately predicted the impact of control on the plate. So it was decided that it would be acceptable to neglect the acoustics states in the control design plant model, and focus modeling attention strictly on the plate (a strategy which worked in analytical simulation and in this investigation). Figure 7.9 shows the simulated improvement

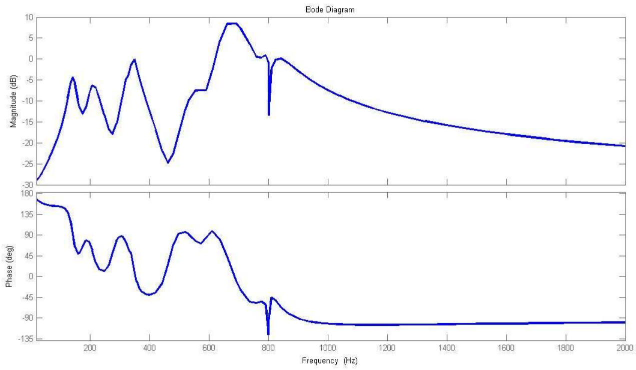

Figure 7.8 LQG controller targeting panel states

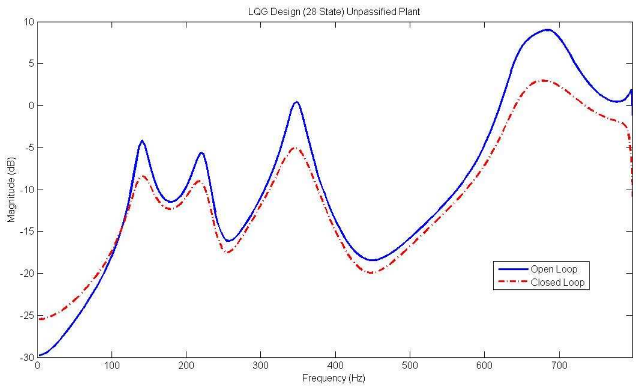

Figure 7.9 Control Design Simulation of LQG controller on Experimentally fitted Nominal Model

in plate acceleration response. This particular design was predicted to be very stable in simulation. Consequently its gain could be increased by an additional large margin before the closed loop system was destabilized. However it was desired to maintain a certain restricted level on the control output to avoid actuator saturation in implementation. To do this the gain was dialed back to an appropriate level. Even with this restriction closed loop reductions of 5-7 dB were predicted which would be an excellent result if achieved in hardware.

Next consider an LQG designed by the approach of section 2.5.2.4 and for the passified plant from above. Again the same weighting matrices for the LQG design problem were utilized as for the non-passive case with the new states from the series passifier (at the end of the state vector) receiving near zero weighting. Next the LMI LQG design problem was formulated for the passified system using Matlab's LMI toolbox and the feasibility problem solved after the inclusion of small fictitious D matrix terms to help convergence. Then the resultant controller is not necessarily an optimal controller anymore but the suboptimal solution is still stable, allows the user freedom in weighting the states designing the observer and most importantly is passive (as is seen in figure 7.10. When simulated the closed loop system shows nearly the same level of reductions

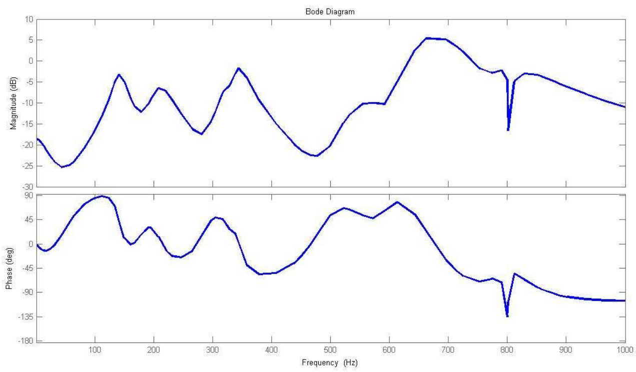

Figure 7.10 Passivity based LQG controller

as in the non-passified case with between 5-6dB of reduction in the response do mainly to addition of the small feedforward compensator. This systems simulated close loop response is shown in figure 7.11.

7.3.2 Passive Resonant Mode Control

After passification several passive resonant mode controllers were designed to be implemented. The individual RMC controllers were designed to attenuate plant dynamics at 131, 156, 199, and 383 Hz respectively which also correspond strongly to resonances in the acoustic response. These controllers were designed have a peak gain between $5 - 8dB$ which was well short of saturation leaving plenty of room to adjust the gain

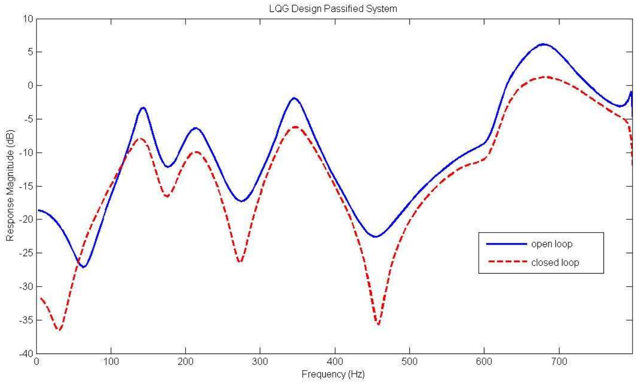

Figure 7.11 Closed Loop Simulation of Passivity Based LQG Controller

in implementation. For brevity only the simulation results at 131, and for the parallel combination of controllers at 156 ,199 ,and 383 are presented. As you can see from figure 7.12, the designed controller has a very simple structure and is clearly passive. When

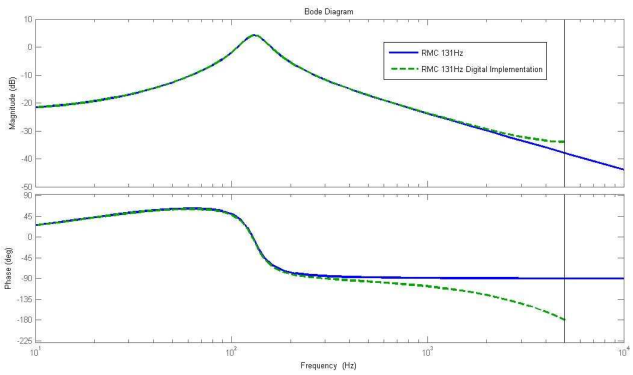

Figure 7.12 Passive RMC at 131 Hz

implemented in simulation the closed loop dynamics are stable and a reduction in the closed loop response of around 6dB is predicted (Fig. 7.13) in the structural response around the target frequency. The simplicity of designing and implementing these controllers along with the bandlimited nature of the control action are very attractive features. When used with a passive plant a controller such as this has a very large amount of robustness in implementation. With most problems occurring not because

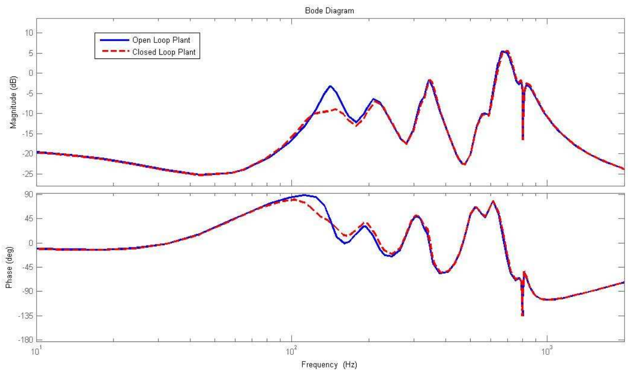

Figure 7.13 Closed loop response of passive RMC controller targeting 131 Hz

of the control design but because of nonlinear saturation effects. One limitation of this approach is that it only targets a very narrow frequency band. However this is easily remedied by utilizing several of these RMC's together in a parallel configuration. This controller is still passive because the parallel combination of passive systems is still passive. The following is a controller formed from the parallel combination of RMC's at 156, 199, and 383Hz (Fig. 7.14). When simulated, the parallel controller shows a

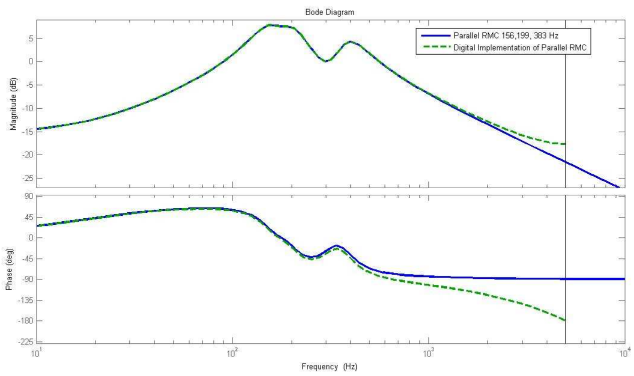

Figure 7.14 Parallel RMC controller targeting 156 ,199 ,and 383 Hz

reduction of about 5-6 dB in the targeted frequencies (Fig. 7.15). It should be noted that the large peak in the response around 780-800Hz was not targeted because the data from which the fit was constructed only went up to 800Hz. Thus the fit may not be accurate in this region and the plant system may not be perfectly passive. This is because the passification of the system did not completely passify the fit in this region (thus it is avoided).

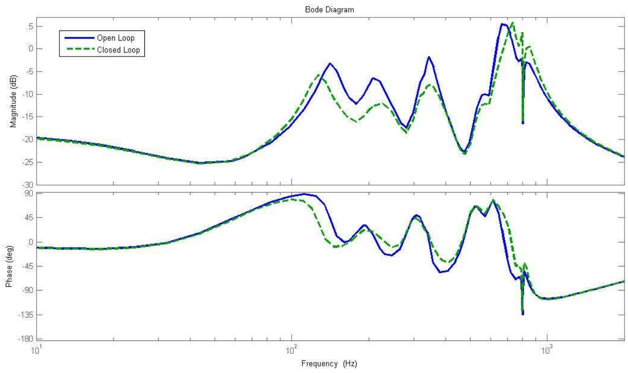

Figure 7.15 Closed loop simulated response of passive parallel RMC controller

7.4 Control Design Implementation

Next the controllers that were designed and simulated above were implemented on the DSP hardware described above. Then the speaker to microphone and speaker to accelerometer responses captured with the Stanford research systems two channel analyzer. These results were then imported back into Matlab for plotting. The same analog and digital filters described above for system ID data collection were utilized in the control implementations as well. In addition to the designed controllers the results were compared to a more standard constant feedback controller.

7.4.1 Constant Accelerometer Feedback

Typically one of the best ASAC approaches is also one of the simplest and that is to use collocated constant velocity feedback and actuator that whose action is proportional to force. In this case there is an actuator whose action is proportional to force and whose internal dynamics are predominantly high frequency, however the sensor in this case is neither perfectly collocated free from filter dynamics or proportional to velocity. Instead it is a filtered accelerometer and the resultant plant is not passive. However, if one first

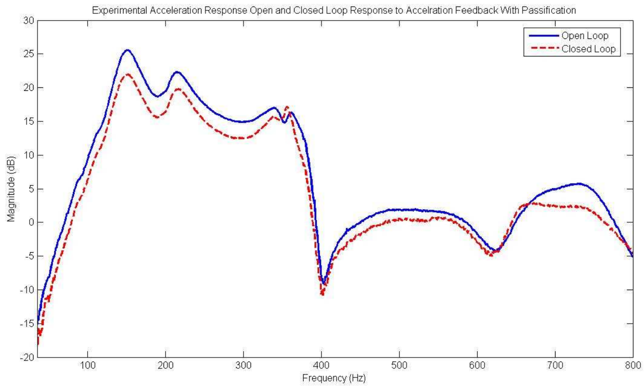

Figure 7.16 Closed loop experimental accelerometer response of passified constant feedback control

passified the plant with the aforementioned series lag compensator (which can be thought of as a bandlimited integration) then the passified plant can use direct accelerometer feedback for control. Furthermore, the gain can theoretically be set arbitrarily high. In practice this controller gain is limited by actuator saturation, unmodeled dynamics, and the effectiveness of the passifying compensator. Therefore this type of controller is really a test of how well the Passification works. As shown in figure 7.16 the closed loop acceleration response experiences between 3-5 dB of reduction with the constant gain set to $K_a = 10.25$. This is the limit before the resultant control action destabilizes plant dynamics above 1000Hz. If a more aggressive high pass filter is utilized on the accelerometer signal the performance of the passified compensator is further affected. The only way to improve this is either to use a more complicated control law, or to model and passify a larger frequency range. The microphone response also shows a slightly smaller but respectable reduction of around 2-3dB. The large notch and nearby

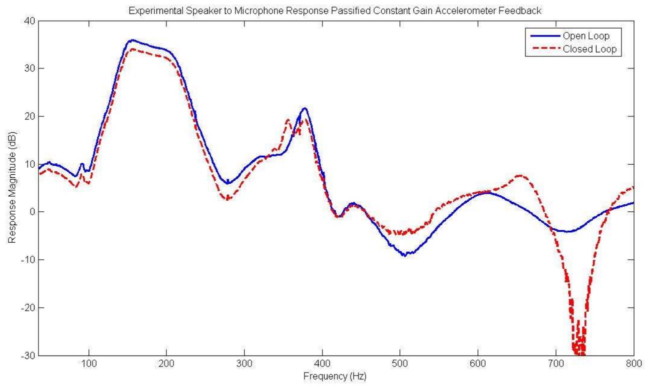

Figure 7.17 Closed loop experimental microphone response of passive constant feedback control

ripple in the response of the closed loop microphone signal is not from control action but instead from a very high order digital bandstop filter to take out unexplained sensor line noise before the signal was sent to the SRS analyzer.

7.4.2 LQG, and Resonant Mode Control Implementations

First implemented is the LQG design for the unpassified plant this controller was implemented originally as a 28 state controller at a sampling rate of 10,000 Hz (because the higher order controller would not implement on the older D-space control hardware at 20,000 Hz(with the filters, and gains all in the loop). Despite using the discrete algorithms for the formulation of the control law the controller would only stabilize a very small gain. This is most likely due to the control design destabilizing higher frequency dynamics that were not modeled in the control design process. Also attempted was a reduced order design (14 states) sampled at 20,000 Hz but this suffered from the same problems. The very low control gain required for stability of this closed loop system meant that the resultant performance of the controller was negligible (a half of a dB at best). What is even worse is that the microphone response was even adversely affected by about the same margin likely due to the added noise of these nearly unstable dynamics at high frequency (see figure 7.18). What was needed was a robust control approach to this problem. With the passivity based LQG approach a greater degree of stability should be imparted to the system. As seen in 7.19 this was indeed the case. As the gain could now be set as high as .75 before beginning to destabilize the closed loop. The best measured reduction was with a gain of .3 was about 0.5 to 1.5dB. Furthermore this reduction was largely broadband over the frequencies measured above 30Hz at least(at least until saturation). Clearly this is a better result from a stability stand point but the performance is still negligible. Needed is a control approach

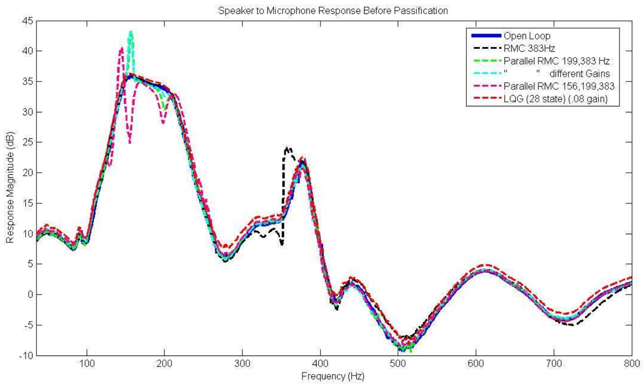

Figure 7.18 Closed loop experimental microphone response of control on unpassified system

to leverage the stability improvement imparted by this bandlimited passification of the system while not destabilizing the unmodeled and unpassified portions of the system. Hi Q passive resonant mode filters are an excellent approach that fit this description. Since these filters are passive they may be used with very high gain in the passified portion of the plant response and due to their bandlimited control action the filters are less likely to destabilize the unpassified portion of the response (at high frequency). As seen in figure 7.19 these control designs have excellent stability and perform remarkably well. All the filters have gains of between 20 and 40 and yield reductions between 5-7 dB in their target frequencies. In fact the gains may be set even higher without destabilizing but the performance is adversely affected by both the waterbed effect, and by actuator saturation at frequencies farther from the resonant filter.

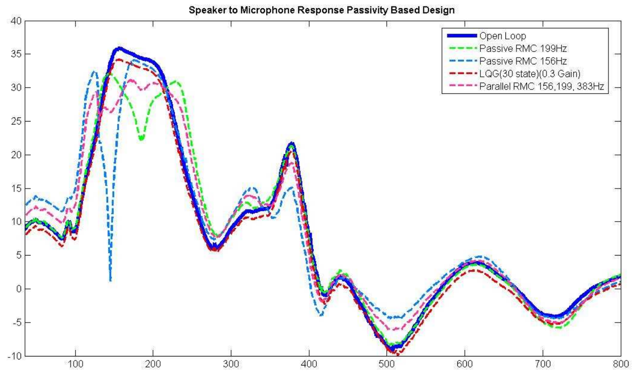

Figure 7.19 Closed loop experimental microphone response of passivity based control

7.5 Results Summary for 1-D Tube Experiments

The results of the designed controllers are given in table 7.1. Several controllers investigated did a reasonable job attenuating noise in the system. It is likely that these performance results could be improved or fine tuned with the design of better passifying compensators and the development of better control design models. Definitely the results as a whole demonstrate the need for robust control approach to structural acoustics problem. Spillover from the controller action adversely affects and eventually destabilizes the unmodeled dynamics. The bandlimited passification of the plant 0-750 Hz helps with many of these problems by ensuring a measure of robustness (when utilized with passive controllers) in the lower frequencies but without a perfect passification or more roll off in the controller, higher control gains still eventually destabilize the unpassified-unmodeled portion of the plant. Only one class of controllers studied (the RMC based filters) were able to avoid these pitfalls do to their bandlimited nature (and high roll off away from the resonance). As a result these were the best performing controllers.

One of the key limitations in the control of acoustic and structural problems (or in most control design problems for that matter) is the accuracy of the identified control design model. In this system it is be possible to fit an accurate model for a larger frequency range (up to 1500 Hz) using the ERA. However, the number of states in the resultant control design model, the complexity of the required passifying compensator, and number of states in the model based controllers quickly make this improved model a liability in implementation. Keep in mind that this system is a relatively well behaved 1-D SISO system and it is still experiences issues related to control design modeling.

This exercise has demonstrated that a by using a passivity approach to controller design, smaller, but effective compensators may be designed that will maintain stability. This investigation motivated the control design approaches utilized in the more complicated MIMO plate system.

Table 7.1 Summarized Results for Implemented Controllers

Controller Type	**≈ Speaker to Mic Peak dB Reduction**	**Limiting Factor**
LQG NOM	NONE (-0.5)	Stability
LQG PASS	1.5	Stability
RMC PASS 156	2.0	Act. Saturation
RMC PASS 199	3.5	Act. Saturation
RMC PASS PARA	5.0	Act. Saturation
CONST K_a PASS	2.0	Stability

7.6 System Identification 3-D Enclosures/Plate System

7.6.1 Control Design Modeling

While accurate control design models do not guarantee a control design will have good performance, the converse is most certainly true. When using any controller architecture other than simple constant gain feedback it is important to have a reasonably accurate model of plant to be controlled. Without an accurate model the control implementation will be plagued by problems (such as control spillover) and will have a very low gain margin (if it is stable at all). This is especially true when designing passifying controllers as the dynamic behavior (especially the phase) needs to be accurately captured so that any passifying compensator that is design will still passify when implemented on the real system. The only alternative to this modeling procedure is to passify the system with a human in the loop creating passifying compensators implementing them digitally and then tuning them to passify the response. This is a time consuming process for all but the simplest of passifications on a single channel.

The control design modeling efforts are now presented for a full MIMO system, a decentralized MIMO system, and summed velocity SISO system. The guiding principle to allow for success in the modeling and control implementation, was to impart as much passivity as possible to the system to start with. This was done by selecting actuator sensor pairs that would exhibit desirable passivity properties (i.e. point force and point velocity measurement). Then by collocating these pairs and using all analog electronics the resultant system if not passive was more easily ”passifiable”.

7.6.1.1 MIMO system

By far the most difficult (and least accurate) control modeling procedure was the identification and construction of a 5x5 (25 channel) MIMO transfer function of the plate plant. Here the limitations of the ERA algorithm to fit models to resonant responses are fully exposed. It should be noted that the ERA routine does permit a user to upload multiple channels of frf for a MIMO fitting procedure but the resultant fits for a MIMO model of this size and with so many resonant modes are so bad they rarely even approximate the collocated channels let alone the then entire MIMO system. As a substitute an ad hoc approach to modeling the system was undertaken. This procedure is summarized as follows:

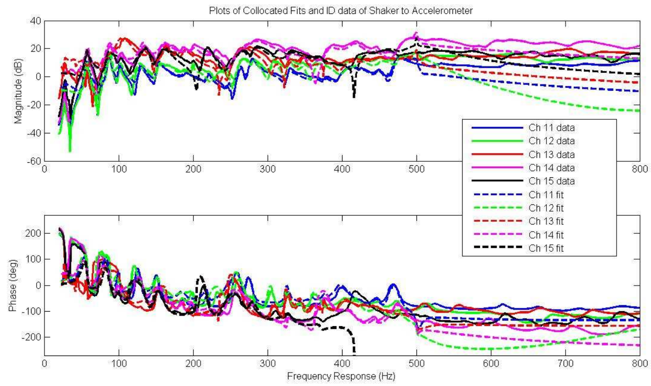

Figure 7.20 Plots of the Experimental and Fitted Diagonal(collocated) actuator to accelerometer responses

1. First, using swept sine (It leads to more accurate frf's with less noise to confuse the ERA) identify all 25 channels of the MIMO response.

2. Second, import each of the 25 channels in to the SOCIT based identification routine and fit a very accurate response over as wide a frequency range possible using as many states as are needed. At this point the MIMO model is 1468 states and is by far to large to be of any use even in simulation. However from this point on the reductions in model order will have a large effect on the phase response (less so the magnitude response). This meaning that passivity based control designs are out window as the designed passifying compensators will not have the same effect on the actual plant in all but the simplest of cases.

3. Third, perform a balanced residualization on each of the channels. The collocated channels were typically allowed to retain half their states. The cross channel typically were allowed to retain a quarter of their states. More effort was taken to maintain the accuracy of the collocated channel fits and less effort with the cross channels. This was because the cross channels were of lesser importance to the maximum singular values of the system.

4. Fourth, construct the transfer matrix from these reduced order fits. At this point the system has 263 states and shows very minor magnitude response difference from the extremely large system. This is slightly more manageable but still a bit large for control design.

5. Fifth, perform a minimum realization on this system with a moderate numerical tolerance to force several pole zero cancelations in this model (198 states), then perform another balanced residualization on the resultant system to reduce the total system size to a much more manageable 90 states.

Figure 7.20 shows the experimental ID data and resultant models for the collocated channels after first and second steps of this procedure. Shown in figure 7.21 are the collocated channels before and after step three of the above procedure.

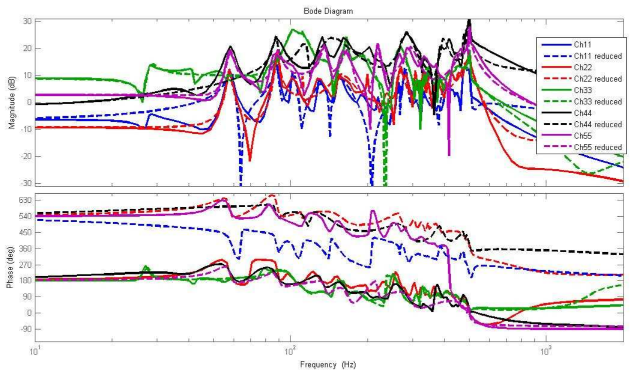

Figure 7.21 Plots of individual Full and Reduced Order (round 1) Fitted Diagonal(collocated) Actuator to Accelerometer Responses

Lastly in figure 7.22 the singular values of the control design model are shown before and after step five of the above procedure. This resultant model is 90 states and approximates the magnitude response well and the phase response to a lesser degree. As such passivity based approaches will not work well. For other approaches to be applicable a better modeling procedure that fits lower order models to MIMO systems needs to be

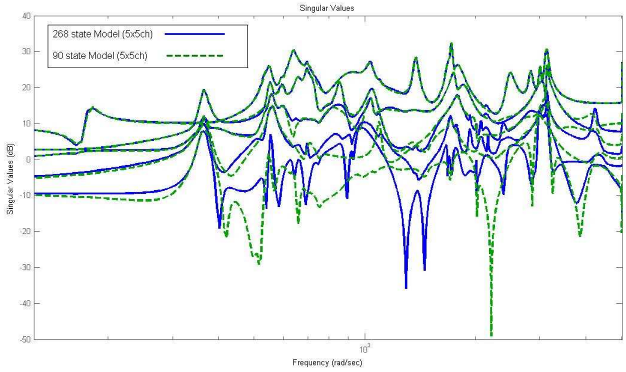

Figure 7.22 The singular values of the constructed MIMO system and reduced order (round 2) MIMO system

developed. This fully MIMO modeling and control investigation, points to the need for simpler (and thus more implementable) approaches to the MIMO control modeling and design problem.

7.6.1.2 Decentralized Feedback

One possible approach to simplifying the control modeling and design problem while improving model accuracy is to use decentralized feedback. In this approach each collocated location (5 total) is modeled as an independent SISO system. With these models control approaches based on the modal clustering and passive controller design (explored in section 7) could be implemented on each channel and as long as decentralized channel is passive or passified. To generate the fits of the experimental frequency response (shown in figure 7.23) a procedure mirroring that in section 7.2.2 was utilized with one small difference. In this case the accelerometer signals were integrated (analog) inside the 12 channel ICP signal conditioner. Without the additional notch filters, low pass filters, amplifier dynamics, and actuator dynamics these collocated channels should constitute a passive pair. However in the presence of these non-idealities each channel still requires passification despite being a passive collocated pair. The resulting fits range

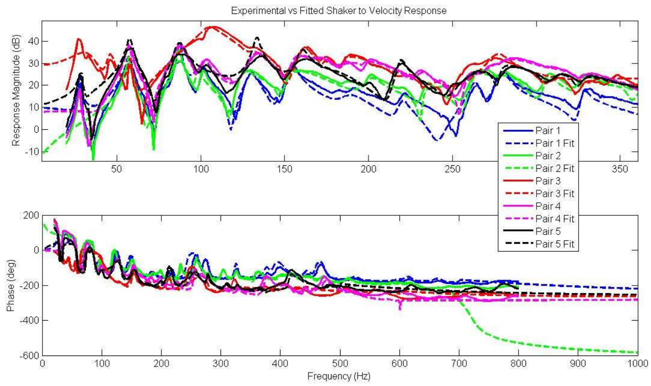

Figure 7.23 Decentralized Channel FRF's and Fitted Control Design Models

from 58 states to 104 states in size. Figure 7.24 shows an example passification for

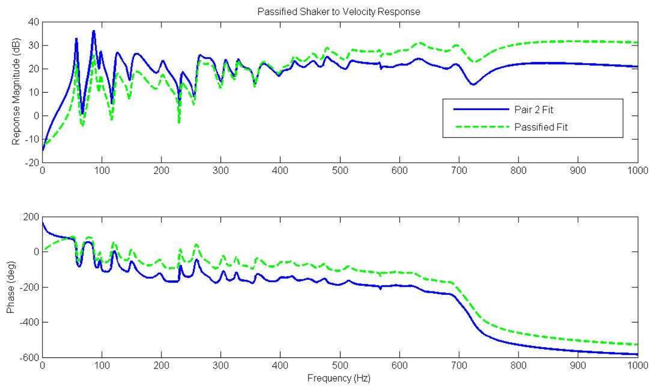

Figure 7.24 Passified Decentralized Channel Control Design Model for channel 2

collocated channel two of the decentralized model. Bandlimited passification was again accomplished with a series implementation of a several of lag and lead-lag compensators and constant feedforward compensators (with a high order pole at 5000Hz to avoid algebraic loop in implementation). The poles and zeros of these passifying compensators and the required value of the feedforward constant are listed in table 7.2.

Table 7.2 Decentralized Passifying Compensators

Channel	**Poles**	**Zeros**	C_{FF}
1	-10,-800,-800	-40,-70,-140	1.1
2	-60,-800,-800	-100,-120,-150	1
3	-800,-800,-3000	-70,-100,-180	2
4	-700,-700,-1000	-80,-30±197.7i	1
5	-20.5±409.5i,-27±549.3	-130,-46.3±179.1i	1

7.6.1.3 Summed Velocity (SISO)

The simplest approach to MIMO control is to sum the various feedback channels and demux the control outputs (inverting the same summation procedure) to effectively reduce the MIMO problem to a single SISO design problem. While the sensing and control are still distributed in nature and consequently better than simply controlling a single plate location, there is less freedom from a control perspective as the same scaled combination of sensors and actuators has be used at all frequencies. One approach to relax some of this rigidity is to passify the system and then cluster the collocated channels with different weighted sums (targeting different modeshapes (**see figure 5.12**). Then these different weighted sums (SISO) can be implemented in parallel with a passive bandlimited controller. To generate the fits of the experimental frequency response shown the sensor signals were again captured with the same setup and procedure as with the MIMO and decentralized approaches but with one small but important change. In the d-Space the driver signal is demuxed according to the chosen clustering summing procedure before going to the amplifier to drive all channels. On the sensors side the velocity signals are routed through the d-SPACE as usual but are then summed before being sent to the SRS analyzer. There were three distinct clusterings used, and these corresponded to the clustering for modes 1, 5, and 6. The clustered terms were all given equal weight of 1 and all other terms were weighted with zero then the various summed combinations were experimentally ID'd. After this wrinkle the procedure for

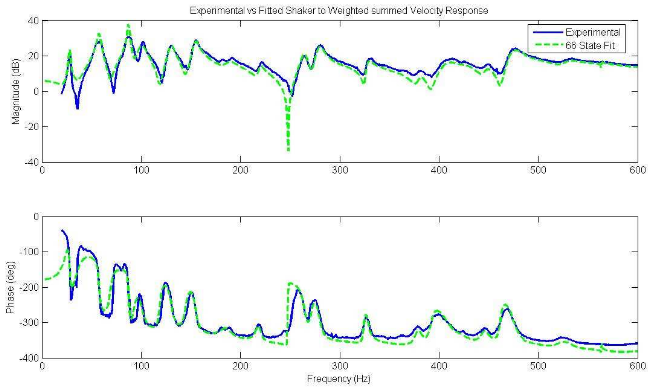

Figure 7.25 Weighted Summation of Collocated Channel FRF's (CLUSTER 1) and Fitted Control Design Models

fitting these three models was essentially the same as before. Figure 7.25 shows an example of the frf data and fit for one of these summations corresponding to the mode one clustering (a straight sum). This response was passified (from 0 up to 500 Hz) with a series compensator (poles at -600, -600, -800, -1000 and zeros at -10, -40, -80, -100). The size of the state space model before passification ranged from 54 states for mode 5 clustering, 66 states for the mode one clustering, and 88 states for the mode six clustering. In the next sections different controllers are designed and simulated using the MIMO, Decentralized and SISO models before being implemented in hardware.

7.7 Control Design 3-D Enclosures/Plate System and Simulation

This next section discusses the control design effort for each of the varieties of system model (MIMO,Decentralized,SISO Summed). For brevity only a single controller design's plots are presented although all approaches are discussed.

7.7.1 MIMO System

For the MIMO System the approach utilized in modeling the system reasonably approximates the singular values of the MIMO system, but less accurately approximates the phase response. This inconvenient fact means that using a passivity based approach is ill-advised because the passification effects of the compensator will not transfer to an actual implementation. For this reason, the only MIMO control designs investigated were both Quadratic controllers. The first was a simple LQR output feedback controller with state weighting matrix $Q_c = C^T C$ and Control weighting matrix $R_c = 1E - 1$ this controller was able to show moderate reductions of the peaks approximately 2 dB in all of the singular values in simulation over the frequency range from 35 to 700 Hz. A slightly better performing LQG controller was then designed. First, the 90 state

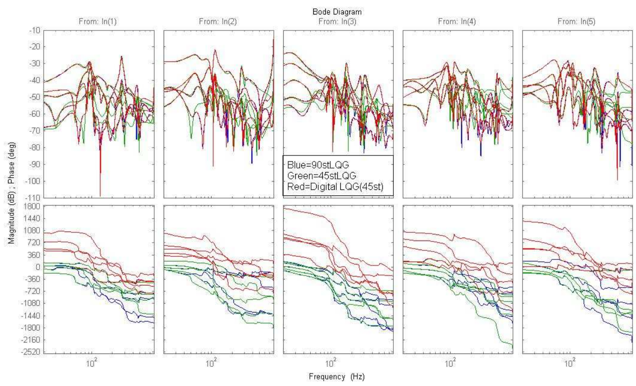

Figure 7.26 The designed 25 channel MIMO LQG controller

control design model was transformed to a Modal canonical form using state similarity transformation. Then under this new state description, the states whose entries most closely corresponded to frequencies of the resonances in the singular value plot were weighted with stronger weighting according to $Q_C = I * 10 + \mathcal{N} * 3000$. Where in this relation $\mathcal{N}$ indicates a diagonal square matrix the same size as A with the diagonal of $\mathcal{N}$ composed of ones and zeros with ones for the subset of states described above and all the rest zero. In this design the R_c, and R_e matrices were set to identity (size 5x5), and the Q_e matrix was set to $Q_e = I * 1E4$. The response of the resultant controller for this LQG design is shown in figure 7.26. The simulated closed loop response of this

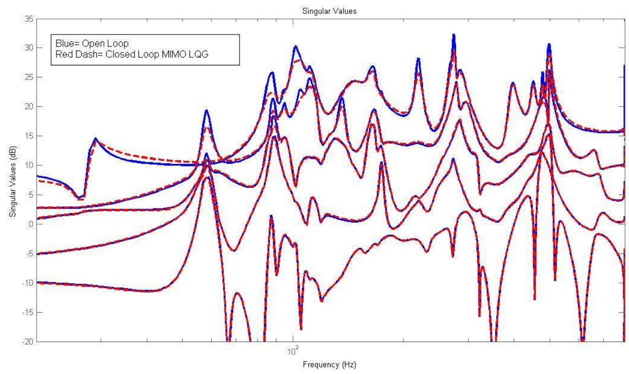

Figure 7.27 The simulated open and closed loop singular values of the MIMO system with LQG control

controller is shown in figure 7.27. Simulation predicts that the closed loop response for this controller should show peak reductions of between 3-4 dB in the maximum singular value plots from open to closed loop over the entire range if interest. As stated before this can be interpreted a reduction in the maximum gain of the system in any direction and is an excellent way to determine the effectiveness of a fully MIMO control design on a fully MIMO system.

7.7.2 Decentralized System

For the decentralized system, the problem is still really a MIMO one. However to simplify both modeling and control design the non-collocated cross channels are ignored. It should be noted that in general this is a really bad idea for approaching the MIMO control design problem unless each of these channels is decoupled from the other (which is not the case here as the various locations couple through the modeshape of the plate). In general such a design would be subject to the unintended and potentially unstable feedback loops created in the cross channels a disaster for implementation. However if the designer is careful about sensor and actuator selection and placement on each channel and then takes great care to passify each of the responses as was done in section 7.6.1.2 the overall MIMO system can be shown to be stabilized by a passive controller that acts locally only. So at least in the worst case the system dynamics will not be destablilized. However such a control design will definitely suffer from a lack of optimality as information from other actuators and sensors can not be used to help decrease the effort of the controller and increase its performance. As a result, this approach will require a larger control effort than in the optimal case. In practice this problem was mitigated in two ways. First, a series of passive resonant mode controllers were designed to ensure that each channels closed loop dynamics were stable and performing. It also means that the control action away from the targeted area is minimized lessening the chance of spill over. Second, a clustering approach that utilized only the collocated pairs which should have an effect on the targeted mode of the plate. This means that at any one particular modal frequency the less effective sensor actuator pairs are "turned off" and thus are not trying to suppress "noise" generated by the other channels' control actions. Together these two approaches should help reduce the control action.

Besides RMC's another option for control might be a passive LQG. In simulation such an implementation was attempted and yielded a respectable 3-4 dB in the peak sound level of the enclosure. The size of the controller to be implemented (even with controller reduction) was far too large to work. If each individual channel had its own LQG controller which after reduction was between 30 and 50 states. With the passifier, this translates to a total controller size well over 150 states for the whole system. This is far to large for hardware implementation at 20,000 Hz.

The various RMC controllers were designed to suppress different modal responses of the plate. However, the ultimate goal of these designs was a reduction in the overall level of sound in destination enclosure. This means that the goals of suppressing the maximum response of the plate and the maximum response of the enclosure may not (and in fact do not exactly correspond). So the effort that followed for determining what plate modes to target was largely a trial and error approach guided by insights from the analytical modeling effort. The specifics of this effort are discussed in the experimental results section.   All of the controllers designed for these models showed excellent reductions

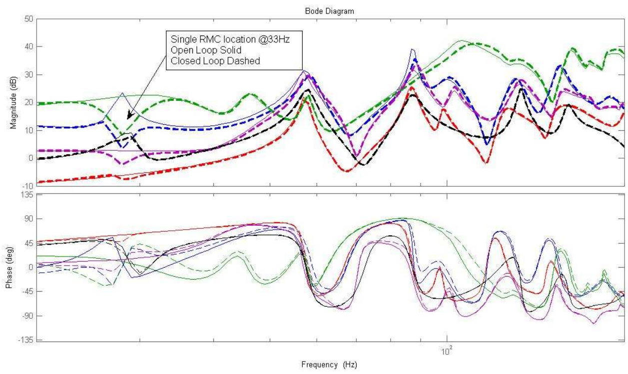

Figure 7.28 The simulated open and closed loop singular values of the decentralized system with 33 Hz passive RMC control

of 7-8 dB in the response at the target frequency and the parallel implementations (combining these individual RMC's) similarly showed a reduction of between 4-6 dB in the included targeted modes. There is still the potential for improvement of these controllers by tuning the damping and exact location of the resonant peak. However since the exact location the plate resonance (in frequency) varies slightly on each experimental response it was decided to use a resonant filter with a wider sigma value. Figure 7.28 depicts the simulated closed loop results of one of these controllers targeting the 33Hz frequency (plate mode 1).

7.7.3 Summed Velocity System

The last and simplest model develop was as a essentially a SISO reduction of the MIMO problem. This was accomplished by mirrored weighted summations of the sensors and demuxes of the control signal. As stated in section , three such combinations (SISO models) were considered. The first of these corresponded to a mode 1 clustering (a straight summation), and the other two to a mode 5, and mode 6 clustering. Each of these clusterings was fitted and passified and then treated as a SISO control design problem. Several types of controller were designed which included: 1) a non-passive LQG controller designed for the original unpassified model, 2) a passive LQG controller for use with the passified system, and 3) several passive resonant mode filter both individual and parallel. Of these designs, only the the resonant mode controllers could be practically implemented while using the clustering approach of the simulation section. However in simulation the best controller predicted was a "band limited passive" LQG design. Unlike the SISO problem in the 1-D tube the LMI approach to designing the LQG controller for this system was not effective because the control design model could only partially be passified from 0-450Hz. Before abandoning this approach entirely an alternate method for designing passive LQG controllers utilizing specific restrictions on the weighting matrices was attempted (as set forth in [75]). While again the bandlimited nature of the passification meant that even this approach might not work it was worth a try. Q_c was designed to for a balanced realization to penalize the states having contributing most to the response The first 20 states modes were penalized with a weight of 3500, and the remaining states a penalty of 10. Then the state weighting matrix was modified by the addition with a $BR^{-1}B^T$ term before use. The matrices R_c and R_e were chosen such that $R_c = R_e$, and the Q_e matrix was selected such that $Q_e = -(A^T + A) + BR^{-1}B^T$. Although there is no guarantee that this would happen the this more restrictive approach did lead to a bandlimited passive controller design as shown figure 7.29. The respectable reductions of 3-4 dB in the peak response achieved by this compensator in simulation are shown figure 7.29. However this controller exhibited poor performance when implemented.

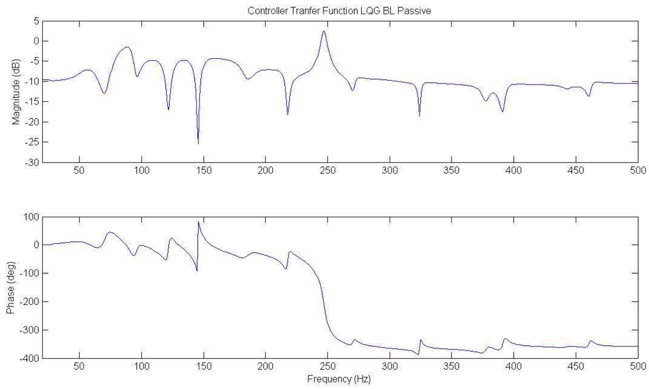

Figure 7.29 The mode 1 clustered controller response for the bandlimited passive LQG

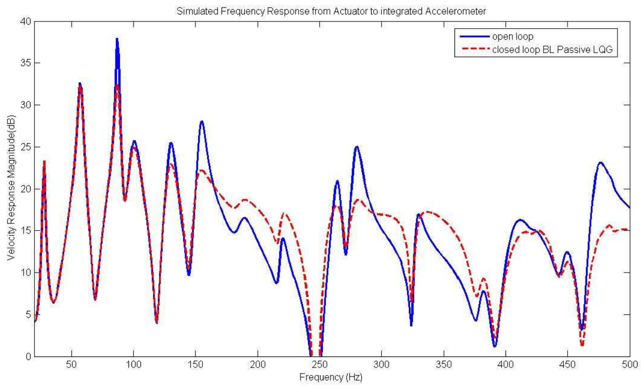

Figure 7.30 The simulated open and closed loop SISO response for the bandlimited passive LQG controller

7.8 Control Implementation 3-D Enclosures/Plate System

In this section the results of controller implementation on the MIMO plate system are presented for each of the control strategies (Full MIMO, Decentralized, and Summed Velocity). In all cases only the best performing control's sound source to microphone response is shown. The rest of the controllers results are discussed as well as quantitatively summarized in table of section 7.9.

All controller implementations in the following sections also had a two pole digital low pass filter at 850 Hz on each measured input channel (before the controller), and had a saturation after the controller with a value set to 150mV. This saturation was implemented to protect the custom actuators from being driven too hard and damaged (either by overheating or by being shaken apart). The need for this feature and the necessary level was unfortunately learned the hard way through the destruction for several of the proof mass actuators. Digital implementations of the controllers and filters used were developed for a 20,000Hz sampling rate. In addition to the controllers and filters several scopes were built into the simulink/control desktop setup to allow the various signals into and out of the system to be monitored. This allows the control experiment to be terminated if the closed loop was unstable or experiencing saturation.

To produce the summed microphone responses shown below, the 8 microphone locations were measured independently on the SRS analyzer. Using a swept sign 150 mV was applied to all the audio amplifiers (5 channels total) which were then used to drive the 5 acoustic sources in the source chamber. The level of this source excitation was set to achieve a peak level around 85 to 90 dBA in the destination chamber as measured with a handheld dB meter (this ended up being at least 3-4 dB higher when both chambers were sealed). A frequency response was measured for each of this independent sensor locations that was comprised of 3 swept sign averages. This was more than sufficient with the swept sine approach and auto scaling because there was virtually no variation from measurement to measurement above 20 Hz (at most 1-2 dB at the lowest response levels and less than half a dB at higher response levels). When these three responses were calibrated (using manufacturer supplied data),RMS averaged, and averaged over each of the 8 locations, the result was an excellent and repeatable measure of the spatially averaged sound field. This data was then collected for the open loop (no control action), and the closed loop responses for each of the control designs considered.

7.8.1 MIMO System

By far this control design approach performed the worst in implementation. Several iteration attempts were made to improve this performance, but little improvement was made. The best resultant control design from this process was a 42 state reduced order LQG. For this design the overall gain on the controller needed to be reduced by 44% to avoid instability (as found through trial and error). Even though the closed loop is stable it is clearly plagued by spillover effects due to inaccuracies in the modeling process. As seen in figure 7.31 there is a large increase (resonance) created in the closed loop system at 500Hz. Furthermore the peak reduction of the closed loop system is minimal on the order of only a 1 dB. It is felt that this does not represent a failing

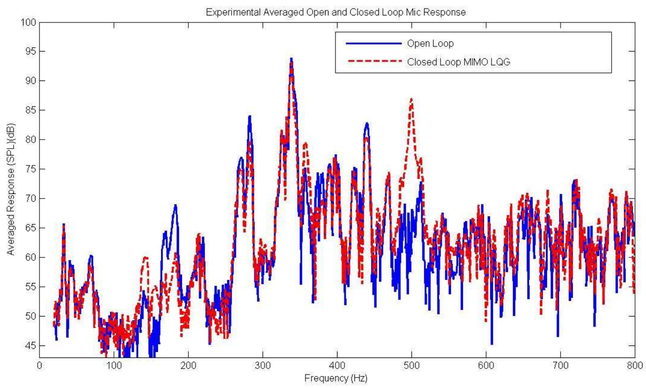

Figure 7.31 The open and closed loop speakers to microphones experimental response of the MIMO system with LQG control

of this control design method so much as it represents a failing of the control modeling method. Unfortunately this modeling method was the only approach by which a small enough model for practical control design could be achieved. This improved MIMO control design modeling effort represents one area that should receive additional future study.

7.8.2 Decentralized System

In the experimental response of the sound source to the microphones the peak resonance in the range of interest occurs at approximately 333 Hz. There are several possible explanations for this peak in the response that were considered. First was that the modal interaction model for this system was flawed and this resonance corresponded largely to direct plate radiation at this frequency (there are two predicted plate modes, 9 and 10, close to this region). Under this assumption it would be necessary to suppress the 333Hz vibration of the plate despite the fact that there are no indicated couplings from modes 9-10 in the analytical investigation. To do this a resonant model controller was designed to suppress plate velocity at 333Hz and then implemented on the decentralized system. This particular design was stable for a very large gain but did not reduce the response at 333Hz by more than about 1 dB by itself and made it worse at higher frequencies 600-700 Hz range. Several interations of the approach were tried to no avail. While this is by no means an conclusive or exhaustive study the actuator and sensor pair had plenty of authority and observability at this frequency and plate vibrations at this modes were significantly reduced. So if the resonance was indeed due primarily to direct radiation of the plate at 333Hz the lack of effect of this designed controller on the resonance was an unexpected result. Perhaps instead, this resonance could be better explained by the modal interaction model of the plate enclosure system. In analytical simulations, the peak resonance was always found to be due to the first 70Hz acoustic mode. However when one considers the roll off due to the speaker dynamics at low frequency (not considered in analytical model) this may not be the case. The closest acoustic mode in the analytical model corresponding to the 333Hz mode seen in the experimental response were acoustic modes 14 and 15. Looking at the analytical coupling terms for these modes indicates that plate mode 1 is the dominant factor followed closely by plate modes 5 and 6 again modes 9 and 10 were not indicated. In a trial an error procedure it was indeed found that mode 1, 5, and 6 of the plate could be suppressed independently with clustered RMC controllers. The controllers had an effect on the microphone response not only at their target frequencies but also in the peak response of the acoustic system (333Hz) and this was a reduction of approximately 1-2dB (without tuning the gains) for each one. While this is also is not conclusive it did provide something to work with. Again, harkening back to the analytical model, it would be expected that the level of relative coupling of acoustic modes 14 and 15 with plate mode 1 was should have by far had the greatest effect on the response. However this also fails to consider that the frequency spectrum was not being excited equally in frequency as in the analytical simulation due to the response of the acoustic sources. Consequently even though this mode may have the strongest coupling the sound levels may not be high enough to truly excite it to the levels experienced by other modes (at other frequencies). This implies that perhaps a RMC controller targeting mode 1, mode 5, and mode 6 with the effort of mode 5 and mode 6 much larger than their relative coupling importance would suggest may do better. After some tinkering with the gains in experiment this was indeed

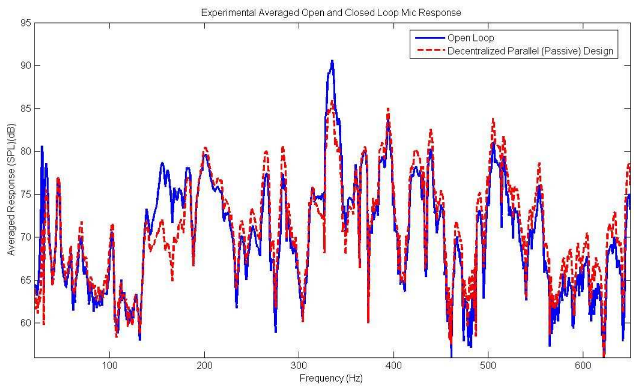

Figure 7.32 The open and closed loop speakers to microphones experimental response of the Decentralized system with clustered RMC (31,161,170)

found to be the case. This is the best performing controller from a peak response reduction perspective as well. To design this controller the passive resonant filters designed in the simulation section were normalized to a peak response of roughly 0 dB then each filter (33Hz,161Hz, and 170Hz) were weighted independently in a trial an error method and tested in experiment. The best relative weighting of each of these filters was found to be 1:1 for the 33Hz filter, 16:1 for the 161 Hz filter, and 28:1 for the 170 Hz filter. In these ratios an with an outer gain factor applied to their parallel combination for each collocated channel of about 4.5 (limited by saturation imposed inside the d-Space of 150 mV) the resultant closed loop peak reduction was shown to be between 4.5 to 5 dB. Figure 7.32 shows this best experimental result for the decentralized approach. Note again that there are spillover, or perhaps waterbed effects elsewhere in the experimental response. Also note that the regions around the plate modes themselves have also been reduced. In addition to the resonant mode controllers several constant feedback controllers for the passive system were tested. However, due to the bandlimited nature of the passification the gain could never be set high enough (without destabilization of the system) to achieve sizeable reductions in the acoustic response.

7.8.3 Summed Velocity System

Although in the control design simulation the bandlimited passive LQG control design was the best performing. When this control design was implemented, spillover effects in the unpassified and more poorly modeled portion of the plant caused instability for all but a very low control gain of 8-10% of the nominal designed value. Iterative redesign was unable to improve on this stability result. Consequently the controller performed very poorly and the resultant peak response was not discernably affected (in fact the microphone response in the 500-700 Hz range was adversely affected. However the bandlimited control action of the passive resonant mode controllers meant that their application did not suffer from the same difficulties. It was expected that of these controllers the best performing would be those utlizing several clusterings in parallel. However in implementation this was not the case and the best performing controller was found to be one that only considered a summation based on mode one clustering and a parallel combination of resonant modes. These modes were located at 33 Hz (plate mode 1), 134 Hz (plate mode 4), and 170 (plate mode 6) Hz. There was also a RMC designed for the undetermined plate resonance at 333Hz. The relative gain of these modes to their original normalized value of one was 3.5:1 for 33Hz, 1.6:1 for 134, 2:1 for 170 Hz, and 2.5:1 for 333Hz. The overall gain of the parallel combination was set to 18.2. The experimental closed loop microphone response under this control design is depicted in figure 7.33. This response shows a notable 5 dB reduction in the peak of the closed

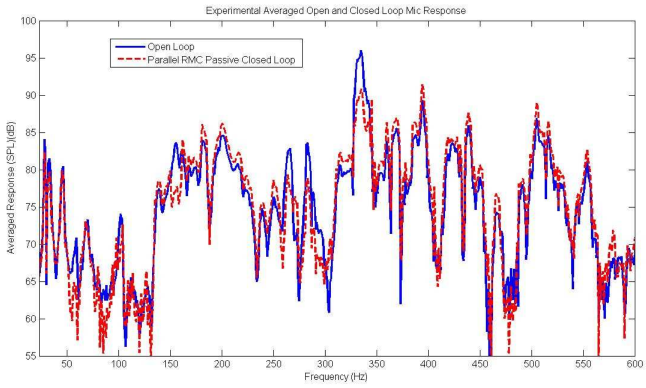

Figure 7.33 The open and closed loop speakers to microphones experimental response of the Summed SISO system with Passive Parallel RMC Clustering 1

loop microphone response, but significant increases elsewhere in the response (most notably at 390 Hz). In this case, this is most likely caused by the controller experiencing a mild amount of intermittent saturation rather than completely being due to the design of the controller and spillover effects into unmodeled dynamics.

7.9 Results Summary for 3-D Enclosures/Plate System

-table summary These results demonstrate the advantages of the control strategies emphasized in this thesis and the difficulty with more traditional MIMO based designs.

Table 7.3 Summarized Results for Considered Controllers

Controller Type	**Peak Microphone Response Reduction**	**Limiting Factor**
FULL MIMO		
Constant Acceleration Feedback	NONE	Stability
Constant Velocity Feedback	0.6 dB	Stability
LQG Design	1.0 dB	Stability
DECENTRALIZED	PASSIFIED	
Constant Velocity Feedback	1.9 dB	Stability
Mode 1 Clustered RMC 33Hz	3.1 dB	Saturation
Mode 5 Clustered RMC 161Hz	2.3 dB	Saturation
Mode 6 Clustered RMC 170Hz	1.7 dB	Saturation
Parallel RMC Control (31,161,170)Hz	4.75 dB	Saturation
SISO (CLUSTERED SUM)	PASSIFIED	
Constant Velocity Feedback	3.4 dB	Stability
LQG Passive	2.1 dB	Stability
Mode 1 Clustered RMC 33Hz	2.9 dB	Saturation
Mode 4 Clustered RMC 134Hz	1.1 dB	Saturation
Mode 5 Clustered RMC 161Hz	3.3 dB	Saturation
Mode 6 Clustered RMC 170Hz	2.7 dB	Saturation
Parallel RMC Control (31,134,170,333)Hz	5.3dB	Saturation
SISO (CLUSTERED SUM)	NOT PASSIFIED	
LQG	2.3	Stability

As a general rule of thumb the best control designs were those that utilized collocation, passivity, and bandlimited control action. These controller were able to regularly achieve peak noise reductions in the 4-5 dB range and with even more effort this could likely be significantly improved. It should be noted that this is not necessarily reflect the superiority of these controllers as much as a limitation of the modeling and implementation process. If better quality models could be developed for the MIMO system then there are numerous approaches that could likely yield a similar level of closed loop performance.

There were a number of practical issues that had to be considered, and problems solved in the modeling, design, and implementation of all of these controllers. In the experimental identification step of this process it was important to identify the system using swept sine response and the auto-ranging feature on the SRS analyzer. At first a white noise approach to system identification was attempted. However this approach was found to not resolve the peaks and troughs of the frf well and took a large number of averages. In modeling this inaccuracy (do to the fact that only one broadband input level is used) induced many spurious modes into the fits. The sweptsine approach with autoranging avoided this problem by looking at the response one tonal frequency at a time. Consequently if there was a low signal the magnitude of the source and the amplification of the measured signal could be automatically adjusted inside the analyzer to resolve the phase and magnitude with very high accuracy. Also important in this step was to identify the system with all analog conditioning electronics and digital filters in the loop. Otherwise the phase and magnitude discrepancies cause by neglecting these items would lead to instabilities when implementing controllers.

Many of the tribulations and pitfalls of modeling for control design have already been discussed in prior sections. However a constant theme in all control design is modeling. Without the accurate models controllers will suffer stability and performance limitations. In this work those controllers for which there was an accurate and concise model were both easier to design and implement. In general SISO responses of the collocated channels were found to be easier to fit control design models to. When preforming model reduction ,where those reduced order models will be utilized for passivity based designs, great care must be take to maintain the qualitative and quantitative properties of the system phase response.

Finally in discrete controller formulation and implementation, there were also a number of issues that were common. It was found to be much better to sample at a rate of 20,000 Hz or more. This helps prevent distortions in the 0-800 Hz range of the magnitude and phase responses of the digital compensators and filters used. It is critical to take full advantage of the ± 10 Volt input and output ranges of the D-Space A2D and D2A converters otherwise resolution errors start to introduce undesired noise and dynamics into your closed loop system. A saturation of at least ± 150mV is absolutely necessary to avoid damaging the actuators in the event of aggressive control action or instability. Actually in the experimentation process it is probably more correct to say it is not needed in the event of a stable system, since the outcome of the majority of experiments is an unstable controller. Along these same lines, it is always important to include a tunable gain that multiplies into the outside of all controllers designed. This is a quick way to deal with limitations on the controller gain imposed by uncertainty and noise without having to redesign and reload a brand new controller. Following these guidelines helps to eliminate many of the common problems with control implementation and enhances the likely hood of an eventual successful test.

8 Conclusions and Future Work

In this work two central questions were explored:

- Is it possible to develop a methodology for passive redesign of the plate structure that decreases acoustic-structure coupling and the sound level in the enclosure system?
- Is it possible to develop and *implement* MIMO controllers that ensure some robustness but still have the necessary performance for meaningful reductions of SPL in the destination enclosure?

In section 4 a methodology based on a parametrically defined FEM model, coupled to the acoustic model by the modal interaction model approach was put forth. Using FEMLAB^{TM}, a finite element toolbox for Matlab^{TM} , the model of the plate was developed and then exported as m-code for sensitivity studies and design optimization. The strength of this approach is that it allows the user explicit control over every aspect of the plate model from the node locations to the material properties on a spatial domain. It also does this in the Matlab^{TM} coding environment allowing for direct integration into control modeling, analysis, and design codes. Aside from writing a custom FEM code for the plate this method gives the highest level of interactivity with other functions and codes that would be necessary for solving the coupled active-passive control problem. Potential avenues of research to achieve this goal are discussed in section 8.2.

This modeling methodology was specifically adapted to target two different properties of the plate: 1) the mass distribution, and 2) the stiffness. Of these two approaches the mass redistribution was immediately the most effective, not because of its superiority but simply because the stiffness approach was flawed and needed additional constraints and interactive user input to allow the problem to be better posed. By redistributing the mass it was shown that passive reductions in simulated microphone response could be achieved. The exact resultant changes in the plate modal behavior were then explored to understand what had happened. What was indicated, was that rather than a redesign of mass distribution to decrease just sound power, or just volume velocity, the integration of this routine with the modal interaction model had a slightly different effect. At times it was found that the optimizer simply minimized the volume velocity of a particular mode, and other times it was found that the sound power was minimized, but in some cases a third result was achieved–the distribution of modal velocity was changed but not the volume velocity or square of velocity. In these cases the coupling coefficients linking these plate modes to the acoustic modes were notably reduced. In other words coupling the optimization routine with the acoustic enclosure by the modal interaction model has imposed a loose objective where by the acoustic structure coupling can be beneficially affected. These resultant improvements were then verified using limited experimental testing. Now for the second question.

- Is it possible to develop and *implement* MIMO controllers that ensure some robustness but still have the necessary performance for meaningful reductions of SPL in the destination enclosure?

In section 5 numerous control approaches were simulated and the analytical model of the 3-D enclosure system. These simulations amount to an exploration of different algorithms, controller structures, and system arrangements to determine what approaches are well suited to the ASAC problem. Furthermore, the simplicity, inherent robustness, and implementablity of these control approaches were important qualities for consideration. It is these same qualities which will aid future efforts in developing a combined active-passive approach. In such an approach fixing the structure of a control design will be a must, and it is important that the chosen structure meet these above mentioned criteria. The guiding principles are therefore:

1. Distribute the sensing and actuation to allow more uniform control over the plate than with a strict SISO system.

2. Locate the sensors and actuators where they will have excellent ability to both observe and control the plate modes.

3. Select sensor actuator pairs that are of the same "type" and then collocate them to enforce passive combinations at each pair.

4. Simplify the structure, the design process, and enhance the stability properties of the control by using a design that is based on passivity concepts.

5. Utilize controllers that are bandlimited in their control action to deal with systems with bandlimited passivity.

In the simulation section and the control implementation of section 7, the structures investigated and found to have significant potential included: CPPRMC's (clustered/parallel/passive resonant mode controllers); decentralized passification of the system and then application of a simple passive control technique like CPPRMC's velocity feedback, or even output feedback LQ regulators; signal summing, passification, and the use of CPPRMC's; and, lastly, signal summing passification and the application of a passive LQG approach. Of these approaches, the summed velocity signal CPPRMC's yielded the largest reduction in peak SPL in the destination enclosure, doing so in a fairly robust manner, and were simple enough that their design and structure could be easily implemented and utilized in a active-passive optimization routine. Another approach that is fairly well suited to optimization, although is less simple to implement in hardware, is the Passive LQ or Passive LQG structure of controller. One of the advantages of this more complicated structure is that its synthesis can be formulated in the context of a LMI problem, and this framework would permit different approaches to solving the combined passive-active problem. In fact, in this thesis a system of LMI's for the synthesis of passive LQG controllers was developed, implemented, and tested on a simple 1-D tube and plate apparatus. This effectively demonstrates the proof of concept of this approach, although further development of the implementation and exploration of its utility are needed.

8.1 Contributions

The following is a summary of the new contributions of this work to the existing body of work.

Modeling: The development of acoustic-structure models of a large two chamber 3-D enclosure wherein the structural model is parametrically defined and formulated for structural optimization.

Passive Control: 1) The exploration of an approach for mass redistribution with the goal of reducing acoustic structure coupling and transmitted noise; and 2) the formulation and exploration of a stiffening concept and optimization approach targeting the coupling of acoustics and structure.

Active Control: 1) The application of MIMO acoustic control to a two chamber 3-D acoustic-structure setup is a problem that has not previously been studied in great detail from either a simulation or a control implementation perspective; 2) The concept of using CPPRMC's has not previously been studied or implemented in hardware; 3) The targeting of plate modes (for control) that couple most strongly to the acoustic modes is a novel approach to the problem of structural controller design; 4) A demonstrated, implementable approach for a robust controller that produces sizable and spatially uniform (in an average sense) reductions in the acoustic response of the 3-D problem, and

5) an LMI based Passive LQG synthesis approach has been formulated, implemented, and tested in experiment.

Hardware: 1) An improvement of existing design approaches for a proof mass actuator to decrease nonlinearity, decrease overall weight, increase force, and maximize useful range of the actuator.

Together these contributions add to the existing breadth of work in passive and active noise control approaches, and lay the foundation for new avenues of research.

8.2 Future Avenues of Research

The following represent new questions or potential research topics raised in the course of this project. In the area of modeling it would be interesting to explore more complicated geometries of plate and enclosure. Likewise different boundary conditions for the plate and acoustic enclosure will allow the developed approaches to be vetted for a variety of acoustic enclosure-structure problems.

One exciting possibility raised in the course of this work involves a semiactive control concept using magneto-rheological (MR) fluids. For this idea a preliminary proof of concept prototype was created and tested, indicating some potential. In this concept a MR fluid could be "activated" as part of an active control strategy that directly controls structural material parameters themselves. This concept of direct active control over the material parameters is one that is a completely novel and new direction in the coupling of active and passive noise control techniques.

From a control theory point of view, efforts to design controllers in bandlimited passive sense raise questions about if this approach could be generalized. Specifically, could the approach of a bandlimited passivity be melded with H_∞ design methodology to produce a new LMI based multi-objective control problem? In the bandlimited passive regions of the plant, the synthesis of a bandlimited passive controller would assure stability and provide the opportunity for extremely high gain–something that a small gain based approach would not. In the unpassified regions of the plant a small gain based approach would ensure robust stability.

There are also several potential future avenues of research for using the passive-design approach (for which the groundwork has been set) to improve the performance of potential control designs in a synergistic manner. A few of these concepts will be briefly discussed. In all of these potential approaches an important area of investigation will be how to: 1) quickly and accurately generate state space matrices for a constrained change in the mass distribution (the forward problem studied in this dissertation), or 2) find the desired state space matrices and then solve the inverse problem for what the new structure needs to be.

For the forward problem, one possible approach is a computationally expensive method whereby the existing structural model (FEM) routine is called at each successive optimization step to generate new structural state space matrices (A,B,C,D). A second approach is to instead express the statespace system as a parameter varying system whereby the A,B,C,D matrices are expressed as functions of the mass values of domains 1-10. This problem will require much computational effort upfront to develop look-up tables or nonlinear functions for the design space of mass variables, but then the eventual passive optimization for many different controls could be greatly simplified. Yet another approach to the problem could be to directly construct the M and K matrices and incorporate symbolic perturbation variables (as many as desired) directly into these M and K matrices. Then, using a symbolic solver, directly propagate these terms into the formulation of the structural A,B,C,D matrices. Then the exact terms in the mass and stiffness matrices can be directly altered in the course of an optimization. For the inverse problem, one approach might be to determine the optimal values of the A,B,C,D matrices (and consequently the mode shape and/or modal frequencies necessary to achieve them) for a smaller number (10-20) of modes and modeshapes. Then using a very coarse mesh size the stiffness matrix could be fixed and the coarse mass matrix structure formulated as either an LMI problem or a least squares optimization for the lumped mass distribution. This low fidelity solution could then be utilized as the starting point for successive iterations of modeshape optimization and mass distribution.

Regardless of the method of structural solution (forward or inverse) there are a number of optimization objectives that could be formulated that would either allow the controller and the structure to be optimized together or would allow the structure to be optimized to meet an objective that makes the control easier. One such objective could be to meet a desired level of observability or controllability in the system. To do this an LMI not unlike that of 2.53 would be formulated and used in conjunction with the mass or stiffness (or mode and modeshape) optimization. Another objective that could be formulated might be to concentrate the vibrational energy of the plate either in frequency, or spatially. One possible idea for achieving this objective is to convolve the structural frequency response with one or more bandstop filters and then find mass or stiffness changes to the plate that minimize the H_2 norm of this convolved response. If effectively designed this should either have the effect of reducing the energy in the impulse response of the unweighted plant or have the effect of concentrating response energy in the frequency locations of the band stop. A similar approach could also be envisioned to concentrate response energy spatially. This might be accomplished by utilizing a highly uniform sensor field with spatial "holes" or weights in the sensor coverage (the spatial equivalent of a bandstop filter). The possibilities for control and structure optimization are seemingly limitless.

Bibliography

[1] Bardou, O., et. al., “Active power minimisation and power absorption in a plate with force and moment excitation”, *Journal of Sound and Vibration*, Vol. 208, No. 1, pp 111-152, 1997.

[2] Belegundu, A. D., and G. H. Koopmann, “A General Optimization Strategy for Sound Power Minimization”, *J. Structural Optimization*, Vol. 8, pp 113-119, 1994.

[3] Berkhoff, A. P., “Optimum sensoractuator distance for decentralized acoustic control”, *J. Acoust. Soc. Am.*, Vol. 110, No. 1, pp. 260-266, July 2001.

[4] Berkhoff, A. P., “Broadband radiation modes: Estimation and active control”, *J. Acoust. Soc. Am.*, Vol. 111, No. 3, pp. 1295-1305, March 2002.

[5] Bianchi, E., et. al., ”Smart panel with multiple decentralized units for the control of sound transmission. Part III: Control system implementation”, *Journal of Sound and Vibration*, Vol. 274, pp 215-232, 2004.

[6] Brebbia, C. A. and R. D. Ciskowski, *Boundary Element Methods in Acoustics.* Computational Mechanics Publications, Boston, MA,1991

[7] Burl, J., *Linear Optimal Control*, Addison-Wesley 1999.

[8] Cabell ,R. H. ,and G. P. Gibbs “Hybrid Active/Passive Control of Sound Radiation from panels with constrained layer damping and model predictive feedback control”, *Noise-Con 2000*, Newport Beach, CA, Dec. 3-5, 2000.

[9] Cazzolato, B. S., and C. H. Hansen, "Structural radiation mode sensing for active control of sound radiation into enclosed spaces", *J. Acoust. Soc. Am.*, Vol. 106, No. 6, pp. 3732-3735, Dec. 1999.

[10] Chen, C.T., *Linear System Theory and Design*,Oxford University Press, New York 1999.

[11] Chu, M. T., "Inverse Eigenvalue Problems", *SIAM Rev.*, Vol. 40, No. 1, pp 1-39, March 1998.

[12] Clark, R. L., and Cox, D. E., "Active control design for acoustic radiation using mixed-norm optimization", *J. Acoust. Soc. Am.*, Vol. 108, No. 3, pp. 1345-1348, Sept. 2002.

[13] Cobo, Pedro; et al., "Hybrid passiveactive absorption using microperforated panels", *J. Acoust. Soc. Am.*, Vol. 116, No. 4, Oct. 1998.

[14] Constans, E. W., et. al., "The Use of Modal Tailoring to Minimize the Radiated Sound Power of Vibrating Shells: Theory and Experiment", *Journal of Sound and Vibration*, Vol. 217, No. 2, 1998.

[15] Cunefare, K. A., "The radiation efficiency grouping of free-space acoustic radiation modes", *J. Acoust. Soc. Am.*, Vol. 109, No. 1, pp. 203-215, Jan 2001.

[16] Dehandschutter, W., et. al. "Active control of sound transmission loss through a single panel partition using distributed actuators. Part II : experiments", *International Conference on Noise and Vibration Engineering (ISMA23)*, pp 705-814, Leuven, Belgium, Sept. 16-18 1998.

[17] Dong, J., et. al., Design Optimization for Structural-Acoustic Problems Using FEA-BEA With Adjoint Variable Method. *ASME Journal of Mechanical Design*, Vol. 126, pp 527-533, May 2004.

[18] Dong, J., et. al., "Parametric design sensitivity analysis of high frequency structuralacoustic problems using the energy finite element method", *Proceedings of ASME 2003 Design Engineering Technical Conferences and Computere and Information in Engineering Conference*, Chicago, ILL, Sept. 2-6, 2003.

[19] Edoa, P. F., et. al., "A finite-element/boundary-element method for the modeling of piezotransducer radiation in fluids using a polynomial development of the Greens function", *J. Acoust. Soc. Am.*, Vol.115, No. 6, pp. 29472953, June 2004.

[20] Elliott, S. J., and L. Rees, "Reciprocity and the active control of distributed acoustic sources (L)", *J. Acoust. Soc. Am.*, Vol. 114, No. 1, pp. 52-54, July 2003.

[21] Elliott, S. J., et. al., "Active vibroacoustic control with multiple local feedback loops", *J. Acoust. Soc. Am.*, Vol. 111, No. 2, pp. 908-915, Feb 2002.

[22] Fahy, F., *Sound and Structural Vibration: Radiation, Transmission, and Response*, Academic Press, San Diego, CA, 1985.

[23] Finneran J. J. ,and M. C. Hastings, "Active impedance control within a cylindrical waveguide for generation of low-frequency, underwater plane traveling waves", *J. Acoust. Soc. Am.*, Vol. 105, No. 6, Jan. 1999.

[24] Fischer, M., and S. I. Hayek, "Active control of coupled structural-acoustic intensities in a fluid-loaded elastic plate", *J. Acoust. Soc. Am.*, Vol. 108, No. 5, pp. 2203-2210, Nov. 2000.

[25] Gardonio, P., and S. J. Elliott, "Active control of structure-borne and airborne sound transmission through double panel", *Journal of Aircraft*, Vol. 36, No. 6, pp 1023-1032, 1999.

[26] Gardonio, P., and S. J. Elliott, "A panel with matched polyvinylidene fluoride volume velocity sensor and uniform force actuator for the active control of sound

transmission", *Proceedings of the Institute of Mechanical Engineers, Journal of Aerospace Engineering*, Vol. 215 G, pp 187-206, 2001.

[27] Gardonio, P., and S. J. Elliott, "Smart panels with velocity feedback control systems using triangularly shaped strain actuators", *J. Acoust. Soc. Am.*, Vol. 117, No. 4, pp. 2046-2064, Dec. 2005.

[28] Gardonio, P., et. al., "Smart panels for active structural acoustic control", *Journal of Smart Materials and Structures*, Vol. 13, pp 1314-1336, 2004.

[29] Gardonio, P., et. al., "Smart panel with multiple decentralized units for the control of sound transmission. Part I: Theoretical predictions", *Journal of Sound and Vibration*, Vol. 274, pp 163-192, 2004.

[30] Gardonio, P., et. al., "Smart panel with multiple decentralized units for the control of sound transmission. Part II: Design of the decentralised control units", *Journal of Sound and Vibration*, Vol. 274, pp 193-213, 2004.

[31] Geng, H. C., et. al., "New modeling method and mechanism analyses for active control of interior noise in an irregular enclosure using piezoelectric actuators", *J. Acoust. Soc. Am.*, Vol. 113, No. 3, pp. 1439-1447, March 2003.

[32] Gibbs, G. P., et. al., "Radiation modal expansion: Application to active structural acoustic control", *J. Acoust. Soc. Am.*, Vol. 107, No. 1, pp. 332-339, Jan. 2000.

[33] Gosavi, S. V. and Kelkar,A. G. Passivity-based robust control of piezo-actuated flexible beam. In *Proceedings of the 2001 American Control Conference*, pages 2493–2497, Arlington, VA, June 25-27 2001.

[34] Griffin, S., et. al., "Feedback control of structurally radiated sound into enclosed spaces using structural sensing", *J. Acoust. Soc. Am.*, Vol. 106, No. 5, pp. 2621-2628, November 1999.

[35] Guo, Jingnan, and Jie Pan, "Increasing the insertion loss of noise barriers using an active-control system", *J. Acoust. Soc. Am.*, Vol. 104, No. 6, July 1998.

[36] Hac, A.; L. Liu, "Sensor and Actuator Location in Motion Control of Flexible Structures.", *Journal of Sound and Vibration.* Vol. 167, pp239-261, 1993.

[37] Haddad, W. M., Bernstein,D. S., and Wang Y. W., Dissipative H_2/H_∞ Controller Synthesis. *IEEE Trans. on Automatic Control*, vol. 39, No. 4, pp. 827-831, 1994.

[38] Halim, D.; S.O. Reza Moheimani, "An optimization approach to optimal placement of collocated piezoelectric actuators and sensor on a thin plate.", *Mechatronics.* Vol. 13 pp27-47, 2003.

[39] Henrioulle, K., et. al. "Active control of sound transmission loss through a single panel partition using distributed actuators. Part I : simulations", *International Conference on Noise and Vibration Engineering (ISMA23)*, pp 797-804, Leuven, Belgium, Sept. 16-18 1998.

[40] Henry, J. K., and R. L. Clark, "Noise transmission from a curved panel into a cylindrical enclosure: Analysis of structural acoustic coupling", *J. Acoust. Soc. Am.*, Vol. 109, No. 4, pp. 1456-1463, April 2001.

[41] Inman, D. J., *Engineering Vibration (2nd Ed.)*, Prentice Hall, Saddle River, NJ, 2001.

[42] ISURF Patent file #02045 *Method And System To Perform Energy-Extraction Based Active Noise Control*, Inventors: Atul G. Kelkar, Mechanical Engineering, ISU and Suresh M . Joshi, NASA LaRC.

[43] Johnson, M.E., and S. J. Elliott, "Active control of sound radiation from vibrating surfaces using arrays of discrete actuators", *Journal of Sound and Vibration*, Vol. 207, No. 5, pp 743-759, 1997.

[44] Johnson, B. F., and C. R. Fuller, "Broadband control of plate radiation using a piezoelectric, double-amplifier active-skin and structural acoustic sensing", *J. Acoust. Soc. Am.*, Vol. 107, No. 2, pp. 876-884, Feb 2000.

[45] Joshi, S. M. and Kelkar, A. G., Passivity-based robust control of systems with redundant sensors and actuators. *International Journal of Control*, 74(5):474–481, March 2001.

[46] Joshi, S. M. and Kelkar A. G., Robust passification via optimal sensor blending and control allocation. In *Proceedings of the American Control Conference*, San Diego, CA, June 2–4 1999.

[47] S. M. Joshi and S. Gupta, "On a Class of Marginally Stable Positive-Real Systems", *IEEE Trans. Automat. Contr.*, vol. 41, No. 1, January 1996, pp. 152-155.

[48] Joshi, S. M., *Control of large flexible space structures*, Springer-Verlag 1989.

[49] Kaiser, O. J., "Active Control of Sound Transmission through a Double Wall Structure", *Dissertation submitted to Swiss Federal Institute of Technology (ETH)*, Diss. ETH No. 14109, 2001.

[50] Kelkar, A. G. and Joshi, S. M., Control of elastic systems via passivity-based methods. *Journal of Vibration and Control*, 2003, (accepted).

[51] Kelkar, A. G. and Pota, H. R., Robust broadband control of acoustic noise in ducts: a passvity-based approach. *International Journal of Noise Control Engineering*, 51(2):97–105, March-April 2003.

[52] Kelkar, A. G., Mao, Y., and Joshi, S. M., LMI-based passification for control of non-passive systems. In *2000 American Control Conference (invited paper)*, pages 1271–1275, Chicago, IL, June 28-30 2000.

[53] Kelkar, A. G. and Joshi, S. M., Robust passification and control of non-passive systems. In *Proceedings of the American Control Conference*, Philadelphia, PA, June 24-26 1998.

[54] Kelkar, A. G. and Joshi, S. M., Robust control of non-passive systems via passification. In *Proceedings of the American Control Conference*, Albuquerque, NM, June 4–6 1997.

[55] Kelkar, A. G. and Joshi, S. M., *Control of Nonlinear Multibody Flexible Space Structures*, volume 221 of *Lecture Notes in Control and Information Sciences*. Springer-Verlag, 1996.

[56] Kessissoglou, N. J., "Active control of the plate energy transmission in a semi-infinite ribbed plate", *J. Acoust. Soc. Am.*, Vol. 107, No. 1, pp. 324-331, Jan. 2000.

[57] Kessissoglou, N. J., and J. Pan, "Active structural acoustic control of an infinite ribbed plate under light fluid loading", *J. Acoust. Soc. Am.*, Vol. 104, No. 6, pp. 324-331, Dec. 1998

[58] Kim,Jaehwan, and Joon-Hyoung Kim "Multimode shunt damping of piezoelectric smart panel for noise reduction", *J. Acoust. Soc. Am.*, Vol. 116, No. 2, Aug. 2004.

[59] Koopman, G. H. and J. B. Fahnline, *Designing Quiet Structures: A Sound Power Minimization Approach*, Academic Press, Sad Diego, CA, 1997.

[60] Cunefare, K. A. and G. H. Koopman. A boundary element approach to optimization of active noise control sources on three dimensional structures. *Journal of Vibration and Acoustics*, 113):387-394, 1991.

[61] Cunefare, K. A. and G. H. Koopman. Acoustic design sensitivity for structural radiators. *Transactions of the ASME*, 114):178-186, 1992.

[62] Kruger, D., "Minimizing the radiated sound power with minimal structural modification", *Doctoral Disseration, Iowa State Universtity*, Ames, IA, 1995.

[63] Kwon, Y. W., and H. Bang, *The Finite Element Method using MATLAB*, CRC Press, New York, NY, 1997.

[64] Lai, E., and G. K. Ananthasuresh, "On the design of bars and beam for desired Mode Shapes", *Journal of Sound and Vibration*, Vol. 254, No. 2, pp 393-406, 2002.

[65] Laplante, W., et al., "Active Control of Vibration and Noise Radiation from Fluid-Loaded Cylinder using Active Constrained Layer Damping", *Journal of Vibration and Control*, Vol. 8, pp 877902, 2002.

[66] Lau, S. K., and S. K. Tang, "Sound fields in a rectangular enclosure under active sound transmission control", *J. Acoust. Soc. Am.*, Vol. 110, No. 2, pp. 925-938, Aug. 2001.

[67] Leboucher, E., et. al., "A stability analysis of a decentralized adaptive feedback active control system of sinusoidal sound in free space", *J. Acoust. Soc. Am.*, Vol. 111, No. 1, pp. 189-199, Jan 2002.

[68] Lee, Y. S., et. al., "Volume velocity vibration control of a smart panel using a uniform force actuator and an accelerometer array", *Smart Materials and Structures*, Vol. 11, pp 863873, 2002.

[69] Lee, Joong-Kuen; et al., "Noise reduction of passive and active hybrid panels", *Smart Mater. Struct.*, Vol. 11, pp 940-946, 2002.

[70] Leishman, T. W., and Jiri Tichy, "On the significance of reflection coefficients produced by active surfaces bounding one-dimensional sound fields", *J. Acoust. Soc. Am.*, Vol. 113, No. 3, March 2003.

[71] Li Li and F. Paganini., LMI Relaxation to Riccati Equations in structured H_2 control. In *Proceedings of the 2006 American Control Conference*, pages 644–649, Minneapolis, Minnesota, USA, June 14-16 2006.

[72] Lin, Z., et al., "Active control of radiation from a piston set in a rigid sphere", *J. Acoust. Soc. Am.*, Vol. 115, No. 6, June 2004.

[73] Liu, F., Fang, B., and Kelkar, A. G., "LQG-Based Robust Broadband Control of Acoustic-Structure Interaction in 3-D Enclosure" In *American Control Conference*, Adam's Mark Hotel, Denver, CO, June 4-6 2003

[74] Lozano, R. and Joshi, S. M., On the Design of Dissipative LQG-Type Controllers. *Recent Advances in Robust Control* (P. Dorato and R. Yedavalli, Eds.), IEEE Press, 1990.

[75] Lozano-Leal, R. and Joshi, S. M., Strictly Positive Real Functions Revisited, *IEEE Trans. Automat. Contr.*, vol. 35, November 1990, pp. 1243-1245.

[76] Luo, J., and H. C. Gea, "Optimal Stiffener Design for Interior Sound Reduction Using a Topology Optimization Based Approach", *ASME J. Vibration and Acoustics*, Vol. 125, pp 267-273, July 2003.

[77] Maciejowski, J.M., *Multivariable Feedback Design*, Addison-Wesley 1989.

[78] Maury, C., et. al., "Active control of flow-induced noise transmitted through aircraft sidewalls", *J. Acoust. Soc. Am.*, Vol. 105, No. 2, 2003.

[79] Maury, C., et. al., "A wavenumber approach to modelling the response of a randomly excited panel Part I: General theory", *Journal of Sound and Vibration*, Vol. 252 No. 1, pp 83-113, 2002

[80] Maury, C., et. al., "A wavenumber approach to modelling the response of a randomly excited panel Part II: Application to aircraft panels excited by a turbulent boundary layer", *Journal of Sound and Vibration*, Vol. 252 No. 1, pp 115-139, 2002

[81] Moaveni, S., *Finite Element Analysis: Theory and Application with ANSYS*, Prentice Hall, Saddle River, NJ, 1999.

[82] Moheimani, S. O. R., et. al., *Spatial Control of Vibration: Theory and Experiments*, World Scientific Publishing Co., River Edge, NJ, 2003.

[83] Moser, M., *Engineering Acoustics: An Introduction to Noise Control*, Springer-Verlag, New York, NY, 2004.

[84] Nagaya, Kosuke "Silencer consisting of two-stage Helmholtz resonator with auto-tuning control", *J. Acoust. Soc. Am.*, Vol. 110, No. 1, July 2001.

[85] Naghshineh, K., et. al., "Use of Acoustic Basis Functions for Active Control of Sound Power Radiated from a Cylindrical Shell", *J. Acoust. Soc. Am.*, Vol. 103, No. 4, April 1998.

[86] Naghshineh, K., and G. H. Koopmann, "Active Control of Sound Power Using Acoustic Basis Functions as Surface Velocity Filters", *J. Acoust. Soc. Am.*, Vol. 93, No. 5, pp. 2740-2752, May 1993.

[87] Naghshineh, K., et. al., "Material Tailoring of Structures to Achieve a Minimum Radiation Condition", *J. Acoust. Soc. Am.*, Vol. 92, No. 2, pp. 841-855, August 1992.

[88] P. A. Nelson, and S. J. Elliot. *Active Control of Sound*, Academic Press, London, 1992

[89] Nylen, P., and F. Uhlig, "Inverse eigenvalue problem: existence of special spring-mass systems", *Inverse Problems*, Vol. 13, pp 10711081, 1997.

[90] Pan, J., et. al., “Analysis of low frequency acoustic response in a damped rectangular enclosure”, *Journal of Sound and Vibration*, Vol. 223 No. 4, pp 543-566, 1999.

[91] Parkins, J. W., et. al., “Narrowband and broadband active control in an enclosure using the acoustic energy density”, *J. Acoust. Soc. Am.*, Vol. 108, No. 1, pp. 192-203, July 2000.

[92] Petersen, I. R., James, M. R., and Dupuis, P., Minimax optimal control of stochastic uncertain systems with relative entropy constraints. *Proc. 36th IEEE Conference on Decision and Control*, San diego, CA, pp. 2248-2253, 1997.

[93] Pierce, A. D., *Acoustics: An Introduction to Its Physical Principles and Applications*, McGraw-Hill Book Co., New York, NY, 1981.

[94] Pota, H. R., Petersen, I. R., and Kelkar, A.G., Robust control of a 2d acoustic duct. In 15th World Congress of the IFAC, pages 1606–1611, Barcelona, Spain, July 21-26 2002.

[95] Pota, H. R., and Moheimani, S.O.R, and Smith, M., Resonant Controllers for Flexible Structures. *Proceedings of IEEE International Conference on Decision and Control*, Phoenix, Arizona, 1999.

[96] Preumont, A., *Vibration Control of Active Structures:An Introduction (2nd Ed.)*, Kluwer Academic Publishers, Norwell, MA, 2002.

[97] Quanlu, L., “Research into an integrated intelligent structure A new actuator combining piezoelectric ceramic and electrorheological fluid”, *J. Acoust. Soc. Am.*, Vol. 111, No. 2, pp. 856-860, Feb 2002.

[98] Remington, P. J., et al., “A hybrid activepassive exhaust noise control system for locomotives”, *J. Acoust. Soc. Am.*, Vol. 117, No. 1, Jan. 2005.

[99] Samejima,Toshiya, "A state feedback electro-acoustic transducer for active control of acoustic impedance", *J. Acoust. Soc. Am.*, Vol. 113, No. 3, March 2003.

[100] Samejima, T., "Modifying modal characteristics of sound fields by state feedback control", *J. Acoust. Soc. Am.*, Vol. 110, No. 3, pp. 1408-1414, Sept. 2001.

[101] Sampath, A., and B. Balachandran, "Active control of multiple tones in an enclosure", *J. Acoust. Soc. Am.*, Vol. 106, No. 1, pp. 211-225, July 1999.

[102] Skogestad, S.; I. Postlethwaite, *Multivariable Feedback Control Analysis and Design*, John Wiley and Sons 1996.

[103] Smith, J. P., et al., "A broadband passiveactive sound absorption system", *J. Acoust. Soc. Am.*, Vol. 106, No. 5, Nov. 1999.

[104] Sommerfeldt, S. D., and T. O. Samuels, "Incorporation of loudness measures in active noise control", *J. Acoust. Soc. Am.*, Vol. 109, No. 2, pp. 591-599, Feb. 2001.

[105] Sors, T. C., and Elliott, S. J., "Volume velocity estimation with accelerometer arrays for active structural acoustic control", *Journal of Sound and Vibration*, Vol. 258, No. 5, pp 867-83, 2002.

[106] Sors, T. C., and S. J. Elliott, "Modelling and feedback control of sound radiation from a vibrating panel", *Smart Mater. Struct.*, Vol. 8, pp. 301-314, 1999.

[107] St. Pierre, R. L., and G. H. Koopmann, "A Design Method for Minimizing the Sound Power Radiated From Plates by Adding Optimally Sized, Discrete Masses", *ASME J. Vibration and Acoustics*, 1995 Anniversary Issue of the Design Division, 1995.

[108] Tanaka, N., and S. D. Snyder, "Cluster control of a distributed-parameter planar structure Middle authority control", *J. Acoust. Soc. Am.*, Vol. 112, No. 6, pp. 2798-2807, Dec. 2002.

[109] Tseng, W. K., et. al., "Combined feedbackfeedforward active control of sound in a room", *J. Acoust. Soc. Am.*, Vol. 104, No. 6, pp. 34173425, Dec 1998.

[110] Williams, E. G., *Fourier Acoustics*, Acedemic Press, San Diego, CA, 1999.

[111] Wu, T. W., *Boundary Element Acoustics: Fundamentals and Computer Codes.* WIT Press, Ashyrst, Southampton, UK ,2000

[112] Yuan, Jing, "Causal impedance matching for broadband hybrid noise absorption", *J. Acoust. Soc. Am. (6), June 2003*, Vol. 113, No. 6, June 2003.

[113] Yuan, J., "Global damping of noise or vibration fields with locally synthesized controllers", *J. Acoust. Soc. Am.*, Vol. 111, No. 4, pp. 908-915, April 2002.

[114] Yaun, J., "A relaxed condition for perfect cancellation of broadband noise in 3D enclosures", *J. Acoust. Soc. Am.*, Vol. 107, No. 6, pp. 211-225, June 2000.

[115] Yaun, J., "Improving robustness of active noise control in ducts", *J. Acoust. Soc. Am.*, Vol. 114, No. 1, pp. 210-217, July 2003.

[116] Zhu, H., et al., "Active control of acoustic reflection, absorption, and transmission using thin panel speakers", *J. Acoust. Soc. Am.*, Vol. 113, No. 2, Feb. 2003.

[117] Zhu, Y., et. al., "Simultaneous Structural-control Optimization of a Coupled Structural-acoustic Enclosure", *Journal of intelligent material systems and structures*, Vol. 14, pp. 287-296, April-May 2003.